DISSERTATION

STEADY-STATE AND TIME RESOLVED SPECTROSCOPY TO PROBE THE EFFECTS OF CONFINEMENT ON CY3 AND THE DYNAMICS OF AOT/ISO-OCTANE REVERSE MICELLES

Submitted by

Jeffrey Todd McPhee

Department of Chemistry

In partial fulfillment of the requirements

For the Degree of Doctor of Philosophy

Colorado State University

Fort Collins, Colorado

Fall 2010

Doctoral Committee:

Department Chair: Ellen Fisher

Advisor: Alan Van Orden

Nancy E. Levinger
B. George Barisas
Amy Prieto
Karolin Luger

ABSTRACT

STEADY-STATE AND TIME-RESOLVED SPECTROSCOPY TO PROBE THE EFFECTS OF CONFINEMENT ON CY3 AND THE DYNAMICS OF AOT/*ISO*-OCTANE REVERSE MICELLES

This dissertation describes the use of steady-state and time-resolved spectroscopy to probe the effects of localized confinement on the water soluble dye Cyanine-3 (Cy3) and the dynamics of intermicellar interactions using fluorescence correlation spectroscopy (FCS). The first set of experiments presents a wide range of steady-state and time-resolved spectroscopy data which indicate that the Cy3 molecules form H-aggregates at concentrations so dilute (nM) that this behavior is not observed in bulk aqueous solution. This unique behavior allowed for a series of FCS and dynamic light scattering measurements to be performed on the same system. These results indicate the formation of a transient reverse micelle dimer, whose lifetime has been identified to be on the order of 15 μs. Furthermore, preliminary experiments are presented on the same reverse micelle system containing the Rhodamine 6G and the results are consistent with those obtained for Cy3 in the reverse micelles. Lastly, fluorescence resonance energy transfer within the reverse micelles was investigated using Cy3 and Cy5. The preliminary results suggest that FRET may be occurring within this extremely confined environment. The work as a whole provides insight into the nature of confinement as well as the dynamics occurring within the world of reverse micelles.

ACKNOWLEDGEMENTS

I would like to thank the National Science Foundation for providing a majority of my funding through this process.

I would like to thank my fellow group members throughout my time working on this dissertation: Jaemyeong Jung, Ming Yu, Keir Fogarty, Jon Gerding, Raj Nayak, Doug Shepherd and Kevin Whitcomb as well as any others I may have missed.

I would like thank Stephen Lathrop and Harit Vora for moral support throughout my graduate career.

I would also like to thank my parents and siblings for helping to shape who I am today and giving me the tools and motivation to succeed in this endeavor.

I would like to thank Nancy Levinger for her guidance throughout a majority of this work.

I also thank my advisor, Alan Van Orden, for providing me with the opportunity to succeed in my graduate career and for all of his help and support throughout this process.

Finally, I would like to thank my beautiful wife Kelly for all her moral support and understanding throughout this long process and for bringing our beautiful daughter Lila Grace into this world, I love you both very much.

TABLE OF CONTENTS

Chapter 1: Introduction

1.1. History, Structure and Properties of Reverse Micelles

The term "microemulsion" was first introduced in 1959 by the English chemist J.H. Shulman[1]. However, it was years earlier, in 1943, when he first discovered the properties of a solution composed of oil and water. During this time, he discovered that the mixed solution transitioned from one that was oil-rich to one that was water-rich and that both were stable. Since his discovery, these systems have been widely studied. This includes studies on this system and studies that have looked at the behavior of other molecules confined within. Furthermore, microemulsions have found a place in industry, due to their widespread applications. In order to better understand their applications and the interest scientists have in them, it is necessary to understand their composition and properties.

Shulman observed that when an organic liquid is mixed with an aqueous liquid, a cloudy solution is formed. This suggested that these two liquids are immiscible. After some time, these two phases separate from each other, leaving two distinct phases. One of the phases is organic while the other phase is aqueous. The novel discovery in Shulman's experiments was that he could induce these two phases to come together and form an optically transparent solution. By adding an alcohol to the mixture, the two phases came together to form a thermodynamically stable and optically transparent solution. As a result of these experiments, the term "microemulsion" was born, and the characterization of these systems began. Figure 1.1[1] shows a typical phase diagram for water, oil and a nonionic amphiphile as a function of both the

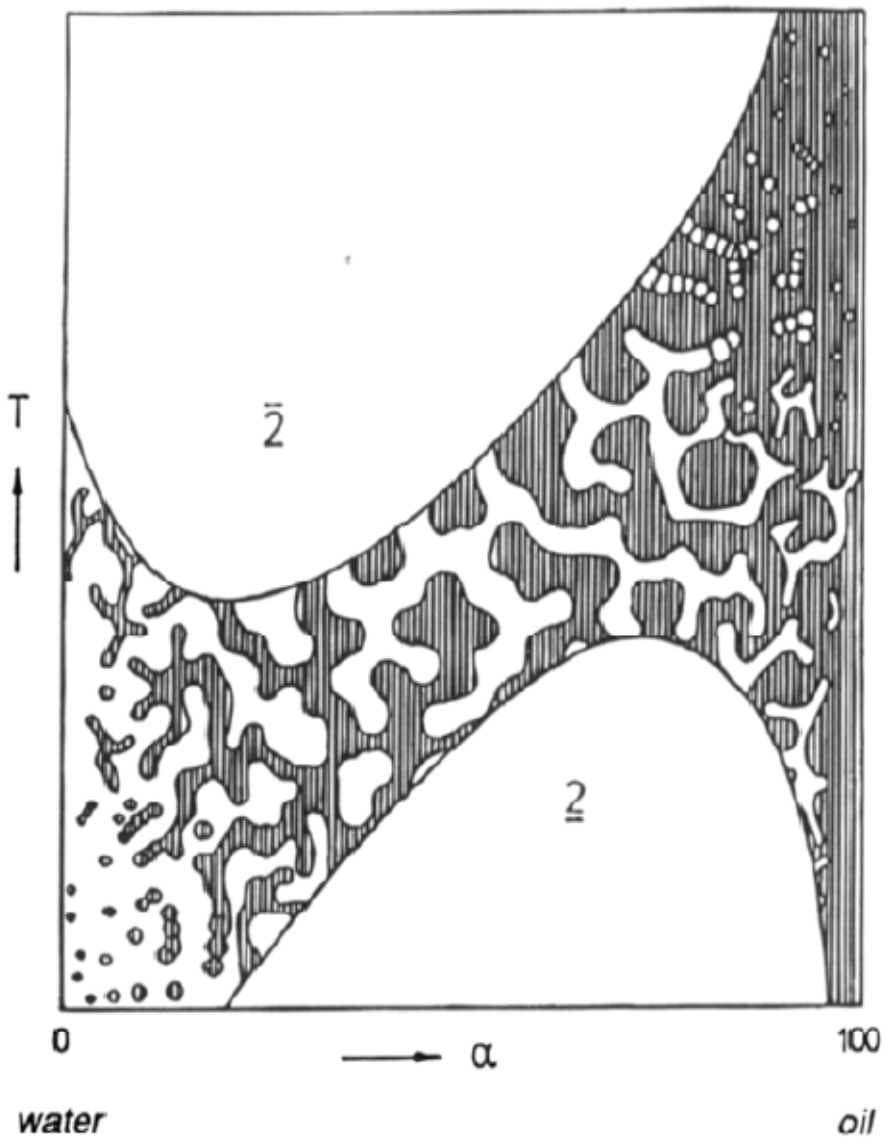

Figure 1.1: Typical phase diagram for water, oil and a nonionic amphiphile as a function of both the temperature and the weight fraction of oil in the system, defined as α. Figure taken from De, T. K.; Maitra, A., Solution Behavior of Aerosol OT In Nonpolar-Solvents. *Advances In Colloid And Interface Science* **1995,** 59, 95-193.

temperature and the weight fraction of oil in the system, defined as α. There are three important regions in this figure, the water rich side (left portion), the oil rich side (right portion), and the region in between. In the water rich region, and at constant amphiphile concentration, the mixture forms a stable dispersion of oil in water, which begins to coagulate at increasing temperatures. On the other side of the figure, when the mixture is rich in oil, the mixture forms a stable dispersion of water in oil, which begins to coagulate as the temperature decreases. In the middle part of the figure, the mixture takes on a sponge-like structure. The interesting and advantageous property of this system is the fact that it contains both a polar (water) and non-polar component (oil). Thus, a variety of molecules can be solubilized by this system. Numerous studies have been performed on microemulsions to better understand their phase behavior[1]. The experiments discussed in this chapter involved AOT (sodium- bis-2-ethyl-hexyl sulfosuccinate) in *iso*-octane reverse micelles. Thus, the discussion below will focus on the properties of this specific reverse micelle system.

AOT reverse micelles have found widespread use in the past 30 years, although the first discovery of AOT's use in the context of microemulsions was made in 1949. Matton and co-workers discovered that adding AOT to a mixture of oil and water produced reverse micelles and a cosurfactant was not required[1]. Furthermore, it was discovered that AOT can dissolve large amounts of water to form discrete droplets. Since many microemulsions require the use of four or five components, including a co-surfactant, it is clear that AOT reverse micelles have advantages over traditional microemulsion systems. Figure 1.2[1] shows the structure of AOT, which contains both non-polar groups and charged polar groups. A typical AOT reverse micelle solution consists of three components; AOT, water and *iso*-octane. Although reverse micelles will form by using other hydrocarbons, the experiments discussed later have only used *iso*-

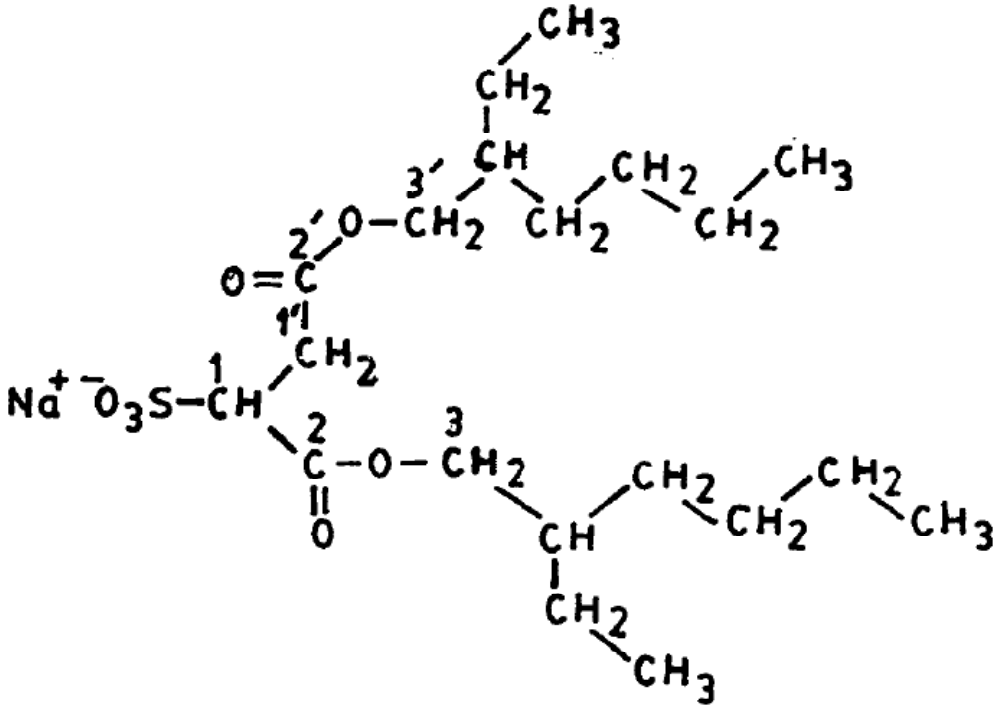

Figure 1.2: Structure of AOT molecule. Note the nonpolar hydrocarbon tails and the polar sulfonate headgroup. Figure taken from De, T. K.; Maitra, A., Solution Behavior of Aerosol OT In Nonpolar-Solvents. *Advances In Colloid And Interface Science* **1995,** 59, 95-193.

octane. Figure 1.3[1] shows the phase diagram for an AOT/*iso*-octane reverse micelle system. The diagram shows a rather large region where reverse micelles can be formed, mainly on the oil rich side. If there is not enough oil or too little water, the reverse micelles will not form. Moreover, if AOT is not added to the solution, then no reverse micelles will form. Thus, the correct combination of these three components allows the reverse micelles to form. Schematically, a reverse micelle consists of a well defined interior water pool that is surrounded by surfactant molecules (AOT). Recall from Figure 1.2 that AOT has both non-polar groups (hydrocarbons) and polar groups (SO_3). As the charged head groups surround the polar aqueous core, the hydrophobic tails protrude outwards where they surrounded by the non-polar organic phase (i.e. *iso*-octane). An illustration of a typical AOT/*iso*-octane reverse micelle is shown in Figure 1.4. The fact that reverse micelles possess three different layers, including both a polar and non-polar region, makes them an attractive system to study the effect of confinement and can be used as an analogue to a biological system. As a result, much research has been done to better understand the properties of AOT/*iso*-octane reverse micelles and molecules confined within

Early studies performed on AOT reverse micelles focused on their physical and chemical properties[1-14]. Specifically, there has been much interest in understanding the aggregation properties of AOT in non-polar solvents, such as cyclohexane and *iso*-octane. It has been reported that AOT molecules tend to form aggregates[1, 8]. It is suggested that this aggregation process is controlled by the polar head groups of the AOT molecule. The sulfonated head groups will move to the interior of the reverse micelles, where they are shielded from interactions with the bulk non-polar solvent. Furthermore, the stability of reverse micelles in nonpolar solvents is due to hydrogen bonding, dipole-dipole interactions, dipole-induced dipole interactions and dispersion forces. Many studies have been published regarding the aggregation number of AOT

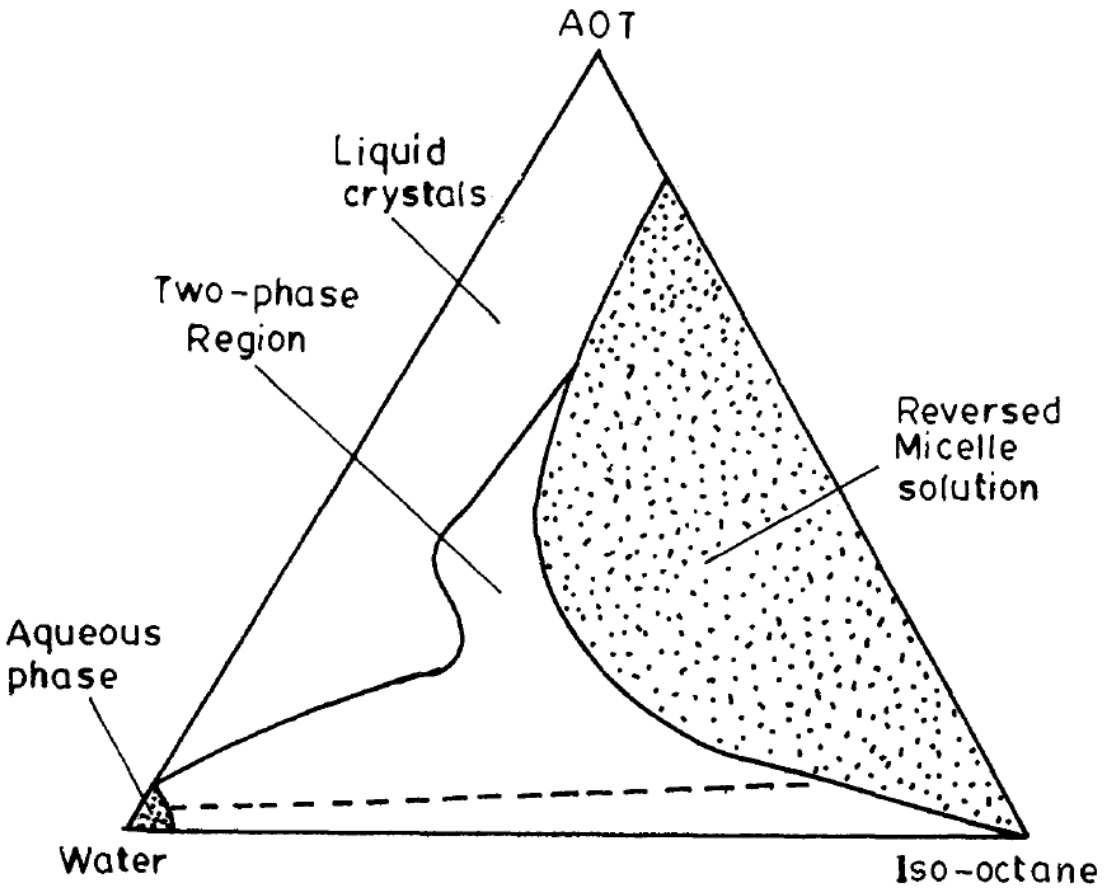

Figure 1.3: Phase diagram for an AOT/*iso*-octane reverse micelle system. Figure taken from De, T. K.; Maitra, A., Solution Behavior of Aerosol OT In Nonpolar-Solvents. *Advances In Colloid And Interface Science* **1995,** 59, 95-193.

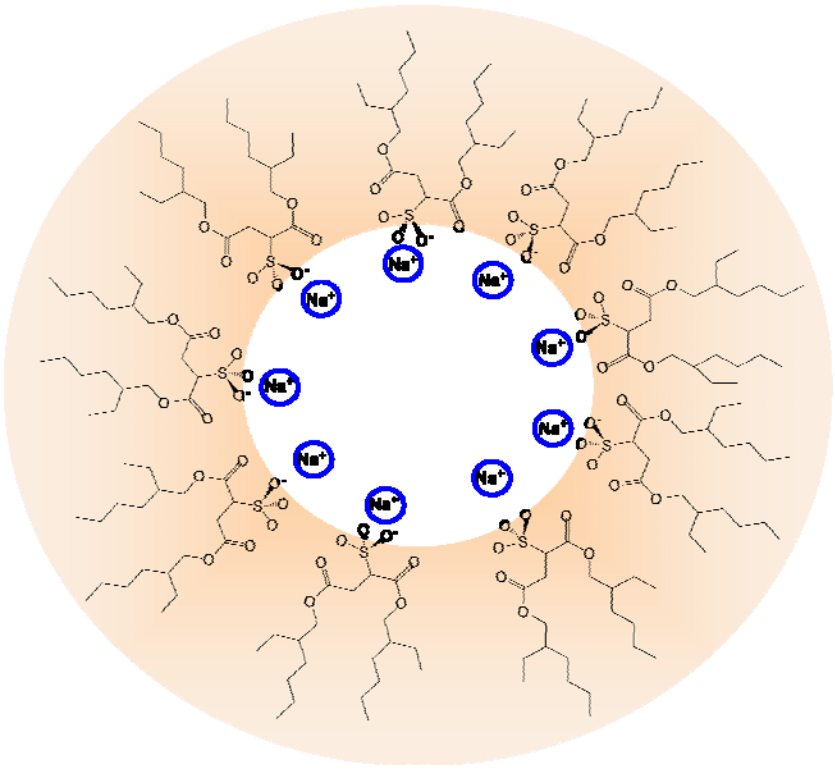

Figure 1.4: Illustration of an AOT/Iso-Octane Reverse Micelle. Note this figure is not drawn to scale. Figure used with permission from Professor Nancy E. Levinger.

in different solvents[1, 8]. The aggregation number is the number of molecules that are associated together to form a reverse micelle after the critical micelle concentration, or CMC, has been reached. The CMC is the concentration of surfactant above which reverse micelles spontaneously form. The results of these studies shows that the CMC and the aggregation number both depend on the temperature of the solution and the solvent used to prepare the reverse micelles.

Interestingly, water molecules tend to behave differently in reverse micelles than in bulk solution. It has been reported that the tiny droplets of water promote the aggregation of the surfactant around the interior water pool[1, 8, 14-17]. In the case of AOT reverse micelles, water is a driving force in the formation these particles. However, there are certain surfactants for which water actually hinders the process of forming reverse micelles, such as with the surfactant NaDEHP[1]. Not only does water play a critical role in the formation of the AOT reverse micelles, it also determined their size parameter, $w_{0,}$ of these spherical particles. This important size parameter is defined as[18]:

$$w_0 = \frac{[H_2O]}{[AOT]} \qquad (1.1)$$

where $[H_2O]$ and [AOT] are the molar concentrations of water and AOT, respectively. Thus, the size of the reverse micelles can be carefully controlled by adjusting the concentration of water and/or surfactant within the system. Furthermore, the hydrodynamic radius of the reverse micelles, can be estimated using the equation[18]:

$$R_H(nm) = 0.175w_0 + 1.5 \qquad (1.2)$$

which shows that as the reverse micelles become larger (increasing w_0), their hydrodynamic radius increases. Eventually, the radius becomes large enough that the water molecules behave as they do in bulk solution. There is some debate as to when this transition occurs, with some

groups reporting this happens at w_0 = 40, while others have reported this transition occurs at w_0=20[1].

An interesting property of reverse micelles is the effect that salt has on this system. Water uptake for a reverse micelle is inhibited by the addition of salt to the system. One possible explanation for this has been presented by Leodids and co-workers, who in 1989, proposed the inner surface model[19]. This model is based on the idea that an electrical double layer is formed inside the reverse micelle and that the surfactant groups are not rigid, but rather are flexible molecules within the system. As a result of this flexibility, both water molecules and ionic molecules can penetrate into the head groups, leading to a charge distribution over a small interfacial shell, which is on the order of 0.5 nm. This finding is interesting because counter ions are often used in AOT reverse micelles. Thus, when preparing solutions for which molecules confined within the water pool of the reverse micelle will be analyzed, it is important to choose a counter ion that will have minimal interactions with the head groups of the surfactant. This will ensure that the molecule of interest is confined within the interior water pool of the reverse micelle.

The type of nonpolar organic solvent used can affect the size of the reverse micelles. Hou and co-workers reported that increasing the chain length of the nonpolar solvent will result in an increase in the amount of solubilized water within the system[20, 21]. However, for alkyl chain lengths greater than seven, the size of the water pool will begin to decrease. In general, when performing studies on molecules confined within reverse micelles, it is important to choose a nonpolar solvent that will not solubilize the molecule. This will ensure that the molecule is confined within the interior water pool of the reverse micelle and not in the exterior nonpolar solvent.

Another important parameter of reverse micelle solutions is the degree of polydispersity that is present. Combining water, surfactant and a non polar solvent, results in the formation of spherical particles that are not all the same size. The polydispersity of reverse micelles depends on such factors as; size (w_0), temperature and pressure[14]. However, under ambient conditions, the amount of polydispersity is generally low[14]. Zulauf and Eicke presented a number of experimental and theoretical studies and concluded that the polydispersity of reverse micelles is dependent on their size. Their results suggests that an increase in w_0 results in an increase in the degree of polydispersity[8, 9, 13, 14, 22, 23].

The thermodynamics of reverse micelles provides information as to why this stable reverse micelle system would form. The formation of the reverse micelle is interesting in that water, which is hydrophilic, is being added to a system containing hydrophobic solvents. The literature suggests that the formation of reverse micelles is an entropy driven process(ref). In AOT reverse micelles, water molecules added to the surfactant/solvent system begin to form clusters. This is followed by monomer surfactant molecules surrounding the clustered water molecules and creating a dispersion of nanoparticles. It has been proposed that the clustering process is endothermic and involves the solvent molecules around the water molecules being disrupted. This is followed by an exothermic process, which involves the association of water molecules with the surfactant. Furthermore, there is a continuous equilibrium within this system, which involves water molecules within the water pool, which are relatively free, and other water molecules that are closer to the interfacial region and are bound to the head groups of the AOT. Further studies were carried out to determine the thermodynamics as a function of the surfactant concentration and the size of the reverse micelles. In these experiments, calorimetric measurements were done as the concentration of AOT increased. The experiments revealed that

as the concentration of AOT increases, the molar enthalpy change decreases. Moreover, the molar enthalpies decreased as the size of a reverse micelle increased, and the AOT concentration was held constant. Perhaps most revealing is that the molar enthalpies measured were positive indicating that the insertion of water into the reverse micelle core is not favorable from an enthalpy standpoint. Thus, the driving force for this insertion is likely to be driven by a favorable change in the entropy of the system. The positive change in the enthalpy can be justified when considering the hydrogen bond breaking that occurs as water is taken into the reverse micelle core and as the reverse micelles expand to accommodate the water. The water molecules prefer to be encapsulated within the interior water pool than to be stuck in the hydrophobic solvent layer. This is because the charged AOT head groups provide a more compatible environment for the water molecules.

Interestingly, reverse micelles begin to spontaneously shed water when cooled to temperatures below zero. There have not been a lot of studies that have investigated the thermodynamics of subzero temperature reverse micelles. However, it can be inferred that the loss of water is an entropically driven process. Under conditions like these, the energy barrier that is normally present, due to hydrophobic interactions, begins to break down. One study reported investigated the stability of reverse micelles as a function of temperature[14]. These studies focused on the temperature range from roughly 0 °C to 60 °C. The results suggest that the reverse micelles are very stable in the range of room temperature. At higher temperatures, above 40 °C, the larger reverse micelles (w_0>15) deviate from there expected size and become larger. Moreover, the larger reverse micelles showed an increase in size as they were cooled below ≈ 15 °C.

1.2 Intermicellar Interactions

The kinetics and mechanism of intermicellar interactions is an interesting and not well understood area of research. Studies have shown reactions occurring within reverse micelles including catalysis, intermolecular charge transfer, FRET and enzyme catalysis[20, 21, 24-28]. However, little research has focused exclusively on the exchange mechanisms and the kinetics governing this process. One study by Fletcher and co-workers[18]explored the kinetics of intermicellar interactions using a stopped-flow kinetic technique. The work proposed a mechanism for the exchange reaction between two reverse micelles. The process involves the diffusion limited collision of two reverse micelles to form an encounter pair which then fuses together to form a transient dimer structure. These measurements did not provide the time resolution to directly observe the formation of the transient dimer but the authors hypothesize the lifetime to be on the order of tens of microseconds. Furthermore, the reaction is thought to be dependent on the size of the reverse micelles, w_0, and the number of carbons in the nonpolar solvent used to make the reverse micelles. It was shown that larger reverse micelles have slower exchange rates. Furthermore, increasing the number of carbons in the solvent resulted in an increased rate of exchange between two reverse micelles. Although this work provided some insight into the kinetics of exchange within reverse micelles as well as a possible mechanism, the lack of sufficient time resolution did not allow the proposed transient dimer to be probed directly. To date, little work has followed up on this research, perhaps due to the limited analytical methods to probe this behavior.

As will be discussed in later chapters, fluorescence correlation spectroscopy provides adequate time resolution to probe processes occurring on the microsecond timescale, this making this technique attractive for studying the dynamics of intermicellar exchange. Furthermore, the work discussed in herein has investigated the role of confinement on a fluorescent dye molecule,

Cyanine-3 (Cy3), whose unique behavior within AOT reverse micelles has provided the opportunity to probe the nature of intermicellar interactions. Also, the work presents preliminary data regarding the nature of Rhodamine 6G and fluorescence resonance energy transfer between Cy3 and Cy5 within this same reverse micelle environment. Reverse micelles have provided a stable environment in which to study these two main themes. The initial groundwork and studies regarding the physical and chemical properties of reverse micelles has provided the appropriate knowledge needed to be able to utilize this system for the work presented herein. Since reverse micelles are optically transparent, stable and their size can be carefully controlled, makes them an attractive system for this research.

1. De, T. K.; Maitra, A., Solution Behavior of Aerosol OT In Nonpolar-Solvents. *Advances In Colloid And Interface Science* **1995,** 59, 95-193.

2. Balasubramanian, D., Water Inside Reverse Micelles. *Journal of the Indian Chemical Society* **1981,** 58, (7), 633-639.

3. Christen, H.; Eicke, H. F., Monte-Carlo Model Of Micelle Formation. *Journal of Physical Chemistry* **1974,** 78, (14), 1423-1427.

4. Eicke, H. F., Stabilization Of Micelles In Apolar Solvents By Solubilized Ions And Polar Liquids. *Journal of Colloid and Interface Science* **1975,** 52, (1), 65-76.

5. Eicke, H. F., Micelles - Formation, Stability, and Background For Possible Applications. *Chimia* **1977,** 31, (7), 265-267.

6. Eicke, H. F., Thermodynamical And Statistical Considerations On Some Microemulsion Phenomena. *Journal of Colloid and Interface Science* **1977,** 59, (2), 308-318.

7. Eicke, H. F., Cosurfactant Concept. *Journal of Colloid and Interface Science* **1979,** 68, (3), 440-450.

8. Eicke, H. F., Aggregation in Surfactant Solutions - Formation and Properties Of Micelles And Micro-Emulsions. *Pure and Applied Chemistry* **1980,** 52, (5), 1349-1357.

9. Eicke, H. F., Physical Investigation of the Formation and Properties of Aqueous Microphases. *Pharmaceutica Acta Helvetiae* **1982,** 57, (12), 322-329.

10. Eicke, H. F., Self-Organization of Amphiphilic Molecules - Micelles and Micro-Phases. *Chimia* **1982,** 36, (6), 241-246.

11. Eicke, H. F.; Christen, H., Stability of Micelles in Apolar Media. *Journal of Colloid and Interface Science* **1974,** 46, (3), 417-436.

12. Eicke, H. F.; Christen, H., Is Water Critical to Formation of Micelles in Apolar Media. *Helvetica Chimica Acta* **1978,** 61, (6), 2258-2263.

13. Eicke, H. F.; Rehak, J., Formation of Water-Oil-Microemulsions. *Helvetica Chimica Acta* **1976,** 59, (8), 2883-2891.

14. Zulauf, M.; Eicke, H. F., Inverted Micelles and Microemulsions in the Ternary-System H_2O-Aerosol-Ot-Isooctane As Studied By Photon Correlation Spectroscopy. *Journal of Physical Chemistry* **1979,** 83, (4), 480-486.

15. Fletcher, P. D. I.; Robinson, B. H., Dynamic Processes in Water-In-Oil Micro-Emulsions. *Berichte Der Bunsen-Gesellschaft-Physical Chemistry Chemical Physics* **1981,** 85, (10), 863-867.

16. Rouviere, J.; Couret, J. M.; Lindheimer, A.; Lindheimer, M.; Brun, B., Structure of AOT Reverse Aggregates.2. Salt Effects upon AOT Reverse Micelles. *Journal De Chimie Physique Et De Physico-Chimie Biologique* **1979,** 76, (3), 297-301.

17. Rouviere, J.; Couret, J. M.; Lindheimer, M.; Dejardin, J. L.; Marrony, R., Structure of AOT Reverse Aggregates.1. Shape And Size Of AOT Micelles. *Journal De Chimie Physique Et De Physico-Chimie Biologique* **1979,** 76, (3), 289-296.

18. Fletcher, P. D. I.; Howe, A. M.; Robinson, B. H., The Kinetics of Solubilisate Exchange Between Water Droplets of a Water-In-Oil Microemulsion. *Journal of The Chemical Society-Faraday Transactions I* **1987,** 83, 985-1006.

19. Leodidis, E. B.; Hatton, T. A., Specific Ion Effects in Electrical Double-Layers - Selective Solubilization of Cations in Aerosol-Ot Reversed Micelles. *Langmuir* **1989,** 5, (3), 741-753.

20. Hou, M. J.; Kim, M.; Shah, D. O., A Light-Scattering Study on the Droplet Size And Interdroplet Interaction in Microemulsions of Aot-Oil-Water System. *Journal of Colloid and Interface Science* **1988,** 123, (2), 398-412.

21. Hou, M. J.; Shah, D. O., Effects of the Molecular-Structure of the Interface and Continuous Phase of Solubilization of Water in Water Oil Microemulsions. *Langmuir* **1987,** 3, (6), 1086-1096.

22. Eicke, H. F.; Kubik, R., Optical Matching Phenomenon in Water-Oil Microemulsions. *Berichte Der Bunsen-Gesellschaft-Physical Chemistry Chemical Physics* **1980,** 84, (1), 36-41.

23. Eicke, H. F.; Kubik, R., Concentrated Dispersions of Aqueous Polyelectrolyte-Like Microphases in Non-Polar Hydrocarbons. *Faraday Discussions* **1983,** 76, 305-315.

24. Correa, N. M.; Zorzan, D. H.; Chiarini, M.; Cerichelli, G., Reverse Micellar Aggregates: Effect on Ketone Reduction. I. Substrate Role. *Journal of Organic Chemistry* **2004,** 69, (24), 8224-8230.

25. Correa, N. M.; Zorzan, D. H.; D'Anteo, L.; Lasta, E.; Chiarini, M.; Cerichelli, G., Reverse Micellar Aggregates: Effect On Ketone Reduction. 2. Surfactant Role. *Journal of Organic Chemistry* **2004,** 69, (24), 8231-8238.

26. Durfor, C. N.; Bolin, R. J.; Sugasawara, R. J.; Massey, R. J.; Jacobs, J. W.; Schultz, P. G., Antibody Catalysis in Reverse Micelles. *Journal Of The American Chemical Society* **1988,** 110, (26), 8713-8714.

27. Falcone, R. D.; Correa, N. M.; Biasutti, M. A.; Silber, J. J., Acid-Base and Aggregation Processes of Acridine Orange Base in N-Heptane/AOT/Water Reverse Micelles. *Langmuir* **2002,** 18, (6), 2039-2047.

28. Menger, F. M.; Yamada, K., Enzyme Catalysis in Water Pools. *Journal Of The American Chemical Society* **1979,** 101, (22), 6731-6734.

Chapter 2

Steady-State Fluorescence Spectroscopy and Fluorescence Correlation Spectroscopy: History, Theory and Applications

2.1 Introduction

The work presented in this dissertation has utilized steady-state and time-resolved fluorescence spectroscopy and fluorescence correlation spectroscopy to better understand the fluorescence properties and dynamics of different systems. The three main areas of research have been to understand the effects of confinement on the dye Cyanine-3 (Cy3), to probe intermicellar interactions between reverse micelles and to investigate the role of Joule heating in fluorescence correlation spectroscopy coupled with capillary electrophoresis (CE). Each project has its own dedicated chapter, where the details of the experiments and results are presented. Since each project has relied on fluorescence spectroscopy, it is important to lay the ground work for the general fundamentals of fluorescence, its history, and its utility as a sensitive technique to better understand complex systems[1-18].

2.2 Theory of Fluorescence

Fluorescence spectroscopy dates back to 1852, when Sir G.G stokes described the mechanism of the absorption and emission process[19]. Thus, the observation and development of fluorescence spectroscopy has a history that dates far back in time. The technique relies on the interaction between light and matter, which can be described by the equation[19]:

$$E = h\nu = \frac{hc}{\nu} \qquad (2.1)$$

where, E is the energy, h is Planck's constant, ν is the frequency and c is the speed of light, respectively. Equation 2.1 shows that there is a relationship between energy and frequency. Moreover, the frequency is related to the wavelength of light by the equation[19]:

$$\nu = \frac{c}{\lambda} \qquad (2.2)$$

where, λ is the wavelength (expressed in nm). Figure 2.1 shows the relationship between the energy levels within a molecule. As shown, molecules contain a series of closely spaced energy levels. Furthermore, molecules can be excited from the ground state to higher excited states by absorbing a discrete quantum of light that is equal to the energy difference between the states. Moreover, the electronic states contain vibrational energy levels (Figure 2.1), which leads to one of the key features of fluorescence that will be discussed later. Once a molecule absorbs a specific energy of light it can relax via different radiative and nonradiative decay pathways. Figure 2.2 shows a Jablonski diagram, which illustrates the various processes that compete with fluorescence emission. The figure also depicts the ground and excited electronic state and their associated vibrational levels. Furthermore, Figure 2.2 shows a molecule absorbing to the first excited state. In general, molecules absorb light from the lowest vibrational level of the ground electronic state to a higher vibrational level in the first excited state. During the time that the electron is in this higher vibrational state, the energy in excess of the lowest

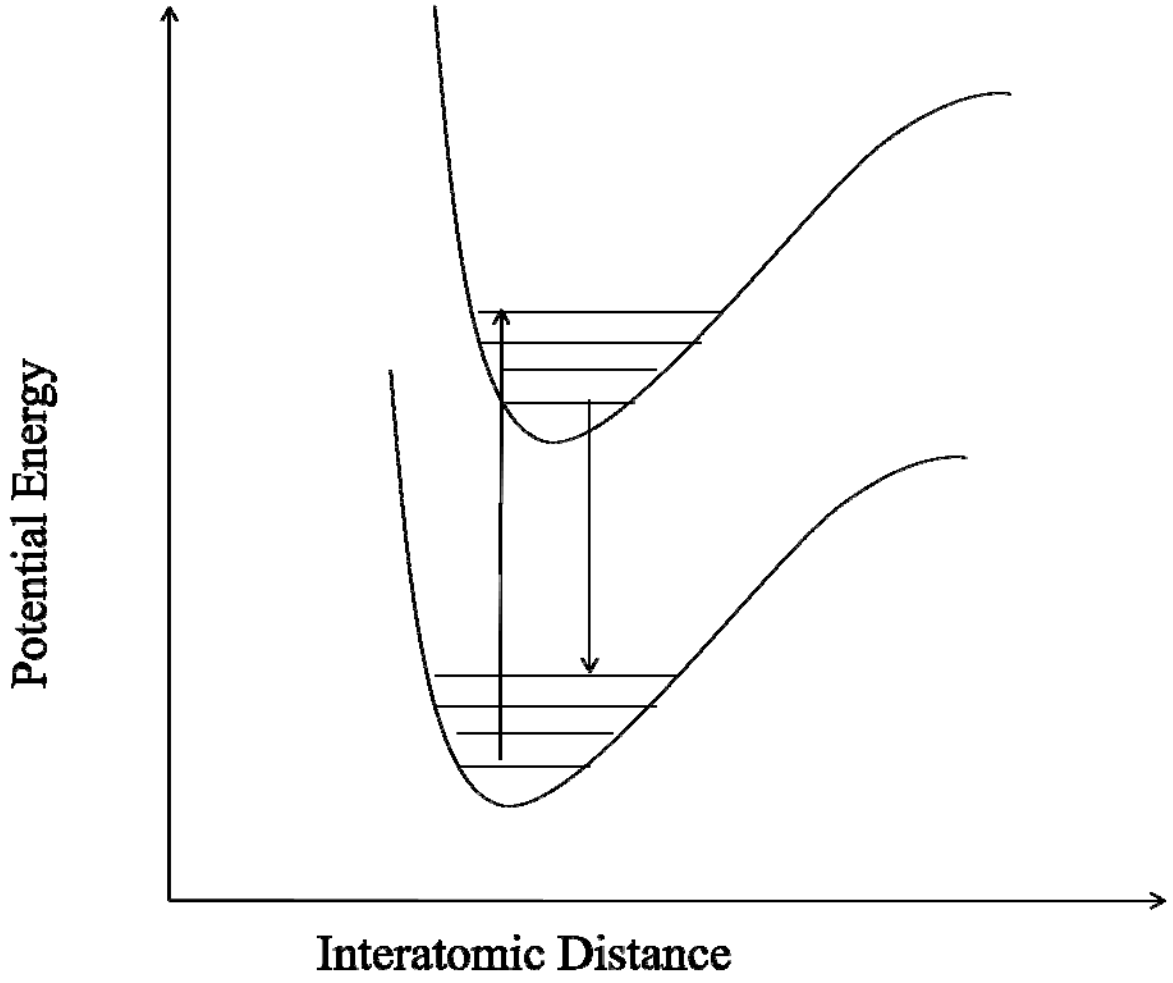

Figure 2.1: Potential energy diagram of a diatomic molecule showing the different electronic energy states and their associated vibrational energy levels. Figure adopted from Lakowicz, J. R., *Principles of Fluorescence Spectroscopy*. ed.; Kluwer Academic/Plenum: New York, 1999.

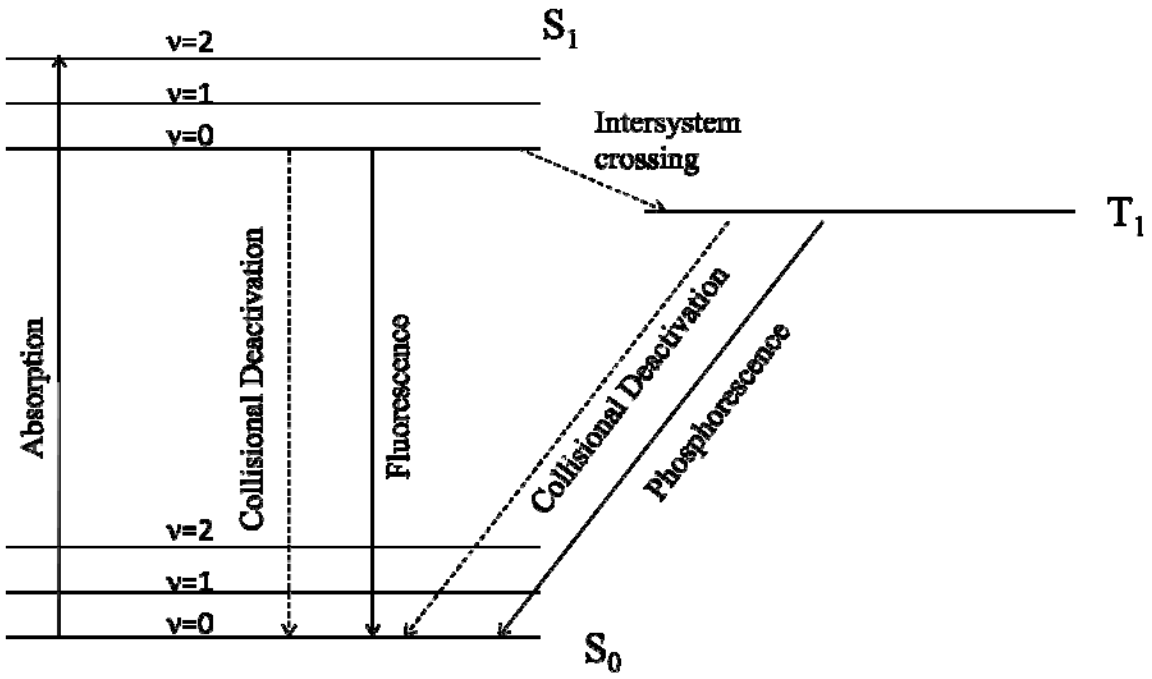

Figure 2.2: Jablonski diagram showing the different process occurring when a molecule interacts with light. Lakowicz, J. R., *Principles of Fluorescence Spectroscopy*. ed.; Kluwer Academic/Plenum: New York, 1999.

vibrational state is rapidly dissipated, causing the electron to relax from a higher vibrational level to the lowest vibrational level of the excited state (Figure 2.2). If the remaining energy is not further dissipated by non-radiative decay pathways, the electron

will return to the ground electronic state accompanied by the emission of energy (photons). Thus, the energy is seen in the form of light and this defines fluorescence. Figure 2.2 shows the triplet electronic energy state, which arises when unpaired electrons are present in the system. If all the electrons are paired, the multiplicity is zero, governed by the equation[19]:

$$M = 2S + 1 \qquad (2.3)$$

where, M is the multiplicity and S is the spin of the electrons, which is either +1/2 or -1/2. Thus, if all the electrons are paired, the spin value is equal to zero and the multiplicity is equal to one, which defines the singlet electronic state. In the case of the triplet state, where the electrons are unpaired, solving for equation 2.3 gives a multiplicity of 3 and hence the molecule is in the triplet electronic state.

Figure 2.2 also shows that there are many different decay pathways in which a molecule can relax to the ground electronic state including fluorescence, phosphorescence (emission from the triplet state, which will be discussed in more detail later), and collisional deactivation, which is caused by the molecules colliding.

Figure 2.3 represents the normalized absorption and fluorescence emission spectrum of the dye Cy3 in methanol[20]. Figure 2.3 shows that the fluorescence is shifted to longer wavelengths (lower energy) from the absorption. Recall that absorption of light typically occurs from the lowest vibrational level of the ground state to a higher vibrational level but that fluorescence takes place from the lowest vibrational level of the

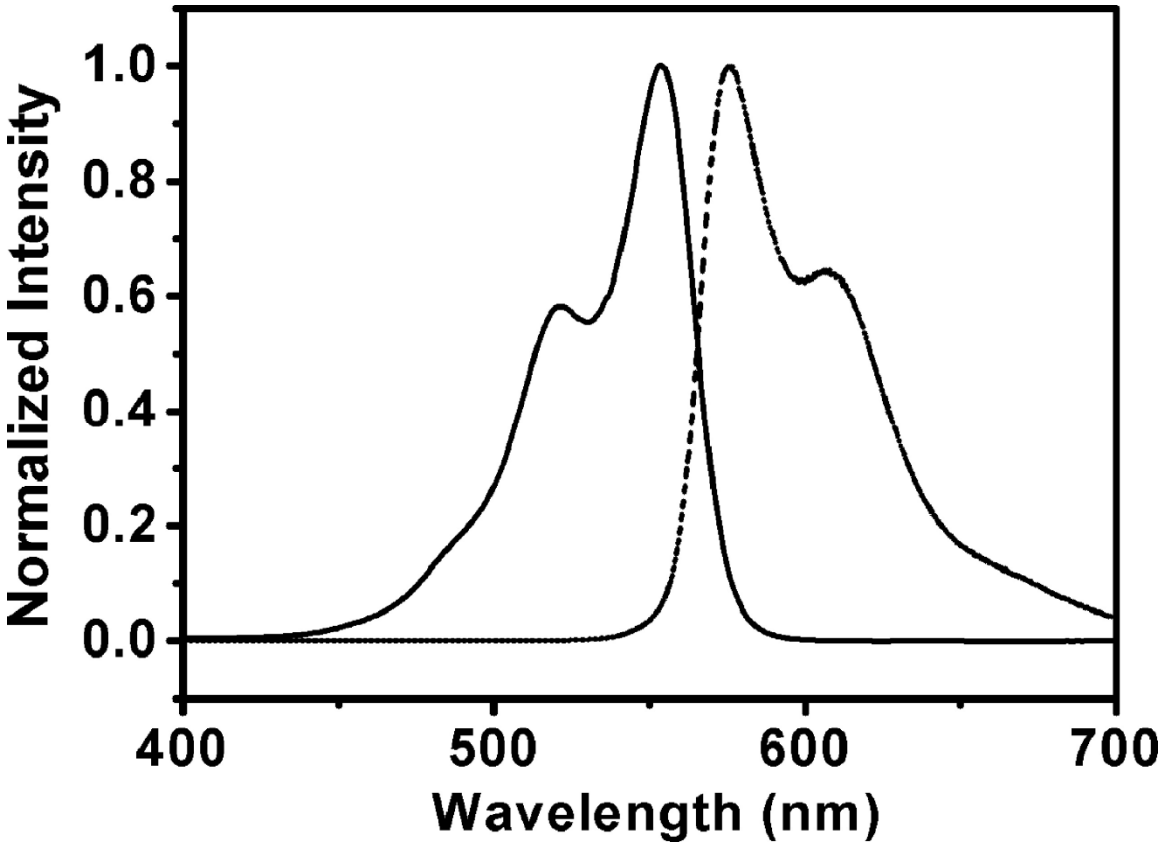

Figure 2.3: Normalized absorption and fluorescence emission of Cy3 in methanol. The concentration of Cy3 is on the order of μM. Figure taken from Jia, K.; Wan, Y.; Xia, A. D.; Li, S. Y.; Gong, F. B.; Yang, G. Q., Characterization of Photoinduced Isomerization And Intersystem Crossing of the Cyanine Dye Cy3. *Journal Of Physical Chemistry A* **2007,** 111, (9), 1593-1597.

first excited state. Thus, absorption occurs at a higher energy than the subsequent fluorescence. This phenomenon is known as the Stokes shift and is defined by the equation[19]

$$\text{Stokes shift} = 10^7\left(\frac{1}{\lambda_{ex}} - \frac{1}{\lambda_{em}}\right) \tag{2.4}$$

where, λ_{ex} and λ_{em} are the corrected maximum wavelengths for the excitation and emission wavelengths, respectively. These values are expressed in units of nm.

Every molecule has a characteristic property that quantitatively describes the molecules ability to fluoresce, which is known as the quantum yield (or quantum efficiency). The quantum yield is defined by the equation[19]:

$$\phi = \frac{number\ of\ photons\ emitted}{number\ of\ photons\ absorbed} \tag{2.5}$$

where, Φ is the quantum yield. Thus, the higher the quantum yield, the greater the fluorescence intensity. On the other hand, molecules that possess a quantum yield close to zero are basically non-fluorescent. These molecules still absorb light but have efficient non-radiative decay pathways to dissipate the energy (i.e. collisions). The quantum yield of a molecule can be determined experimentally using a known standard and the equation[19]:

$$\phi_{unk} = \phi_{std} * \frac{F_{unk}}{F_{std}} * \frac{q_{std}}{q_{unk}} * \frac{A_{std}}{A_{unk}} \tag{2.6}$$

where, F is the relative fluorescence, q is the relative photon output of the source and A is the absorbance. Thus, the quantum yield is an important property for fluorescence applications and can be determined experimentally.

Lastly, another important characteristic of molecules is their fluorescence lifetime. The fluorescence lifetime for dye molecules is generally on the order of nanoseconds. This parameter is a measure of the time a molecule spends in the excited state before relaxing to the

ground state. The general equation describing the fluorescence lifetime of a molecule is given by[21]:

$$I = I_0 e^{-t/\tau} \qquad (2.7)$$

where, I is the fluorescence intensity at time t, I_0 is the maximum fluorescence intensity during excitation and τ is the average lifetime of the excited state. Measurement of this property can give information as to what molecule is present, how the solvent environment affects the molecule as well as the presence of dye aggregates. Thus, this property of molecules is useful in the field of fluorescence and can be measured using time-correlated single photon counting techniques (TCSPC), which will be described more fully in later chapters.

2.3 Factors Affecting Fluorescence

There are many factors that can affect the fluorescence of a molecule. Typically, these factors can be broken into two sub-groups, those which are of a structural nature and those that have to do with the environment surrounding the molecule. Since the work presented in later chapters deals more with the effect of the environment on the fluorescence, this section will focus more on environmental factors that affect the fluorescence of a molecule. Structurally, it is worth noting that most unsubstituted aromatics exhibit an intense fluorescence in the UV-Visible range of the electromagnetic spectrum[19]. Moreover, as the conjugation increases, the fluorescence shifts to longer wavelengths (lower energy)[19].

Environmental effects encompass factors such as; solvent environment, the presence of "heavy" atoms, temperature, concentration and the rigidity of the environment (e.g. thin films). An example of solvent effects is the observed red shift in the fluorescence that is observed for polar molecules as the dielectric constant of the solvent increases. It is thought that the observed red shift is due to the fact that the excited electronic state of a polar molecule is more polar than

its ground state. Thus, as the solvent environment becomes more polar, it more effectively stabilizes the excited state. Thus, a shift to lower energy is observed.

Another significant environmental effect is the "heavy" atom effect, which promotes intersystem crossing. As a result, phosphorescence is the predominate form of emission (Figure 2.2). This effect results from the presence of heavy atoms, either as a substituent within the molecule or contained in the solvent. For example, the ratio of the phosphorescence to fluorescence in naphthalene is 48 times larger in an alcohol containing bromide than in the alcohol without bromide[19]. Furthermore, the presence of other heavy atoms, such as the halogens or oxygen, is thought to increase the rate of intersystem crossing.

The effect of temperature on the fluorescence emission of molecules has been studied extensively[19, 21] and it has been shown that the fluorescence decreases (as well as the quantum yield) with increasing temperature. One reason for this is the degradation of the fluorescence species at high temperatures. Furthermore, increases in fluorescence due to decreasing temperature can be rationalized by the fact that cooling down a solution increases the viscosity of the medium, thereby decreasing the rate of collisions. Thus, as the rate of collisions decreases, the propensity for energy to be dissipated via collisional deactivation is reduced. Moreover, other processes involving the excited singlet state, such as intermolecular bonding, tend to occur more slowly as the temperature decreases[19].

The rigidness of the media that a molecule is in can have a dramatic effect on the fluorescence emission. As the environment becomes more rigid, the viscosity increases, thereby causing a decrease in the rate of bimolecular collisions. As a result, a viable non-radiative pathway becomes less significant and the molecule is more likely to fluoresce than to undergo collisional deactivation. Furthermore, some aromatic molecules have conjugation that gives rise

to two different isomers, a trans- and a cis-isomer. For example, the dye molecule Cy3 has a fluorescent trans and a non-fluorescent cis form[20, 22]. In a rigid environment, the dye is less likely to isomerize to its non-fluorescent cis form and decay non-radiatively. Thus, the rigid environment leads to an increase in the fluorescence intensity of the molecule.

The concentration of fluorescent molecules has a significant effect on their fluorescence properties. The fluorescence emission is dependent on the power of the excitation beam, given by the equation[23]:

$$F = K'(P_0 - P) \tag{2.8}$$

where, F is the fluorescence, P_0 is the power of the incident beam, P is the power of the beam after it has transversed through the sample and K' is a constant that depends on the quantum yield of the system. The fluorescence intensity is related to the power of the beam by Beer's Law[23]:

$$\frac{P}{P_0} = 10^{-\varepsilon bc} \tag{2.9}$$

where, ε is the molar absorptivity, b is the pathlength and c is the concentration. Note that the absorbance is given[23]:

$$A = \varepsilon bc \tag{2.10}$$

Substituting equation 2.9 into equation 2.8 yields[23]:

$$F = K' P_0 \left(1 - 10^{-\varepsilon bc}\right) \tag{2.11}$$

Moreover, equation 2.11 can be expanded to a Maclaurin series to give the equation[23]:

$$F = K' P_0 \left[2.3\varepsilon bc - \frac{(2.3\varepsilon bc)^2}{2!} + \frac{(2.3\varepsilon bc)^3}{3!} \ldots \right] \tag{2.12}$$

If the exponential factor 2.3εbc is small, the subsequent terms in the series are small relative to the first. Thus, the equation can be approximated to[23]:

$$F = 2.3K'\varepsilon bcP_0 \qquad (2.13)$$

and at constant power, equation 2.13 simplifies to the equation[23]:

$$F = Kc \qquad (2.14)$$

Thus, at low concentration, the fluorescence emission as a function of concentration is linear. At higher concentrations, when the absorbance increases, the exponential terms in equation 2.12 start to dominate. Therefore, the fluorescence emission as a function of concentration deviates from a linear trend. At higher concentration the fluorescence typically begins to decrease. It is worth noting that self-quenching caused by increased collisions between molecules, thus increasing the rate of collisional deactivation, could explain the observed deviation from the linear trend. Furthermore, the increase in the concentration of the molecules can induce the molecule to form aggregates, which alters their spectroscopic properties. This aggregation phenomenon will be discussed more fully in the next section.

2.4 Aggregation of Fluorescent Molecules

Fluorescent molecules, such as dyes, are known to form aggregates that alter their spectroscopic properties. Two classes of aggregates are H- and J-aggregates. Figure 2.4 shows the energy level diagram for a monomer, a H- dimer and a J-dimer[24]. Note that a dimer is the simplest form of an aggregate and contains two molecules. H-aggregates form when two molecules have dipole moments that are in a stacked configuration (90° angle) whereas J-aggregates arise when the dipole moments of the molecules are positioned end to end (0° angle). Figure 2.4 shows that the energy needed to excite a H-aggregate is greater relative to the monomer and that the energy needed to excite a J-aggregate is lower relative to the monomer.

Thus, H-aggregates absorb at shorter wavelengths relative to the monomer (higher energy) and J-aggregates absorb at longer wavelengths to the red relative to the monomer (lower energy). As a result, spectroscopy can be used to identify the presence (or absence) of both H- and J-aggregates.

J-aggregates are typically highly fluorescent molecules, relative to the monomer whereas H-aggregates tend to be weakly or non-fluorescent[24]. It is suggested that J-aggregates have a highly allowed electronic transition between their ground and first excited state, leading to the observed enhancement in the fluorescence. On the other hand, the dipole-dipole interaction in H-aggregates suggests that the higher energy transition is allowed. As a result, an increase in phosphorescence (via intersystem crossing) is observed[25]. However, instances have been reported in which H-aggregates were highly fluorescent such as; in Langmuir-Blodgett layers, at low temperatures and in rigid environments[26]. Moreover, the formation of aggregates likely induces a change in the fluorescence lifetime. For example, Rosch and co-workers[26] measured the

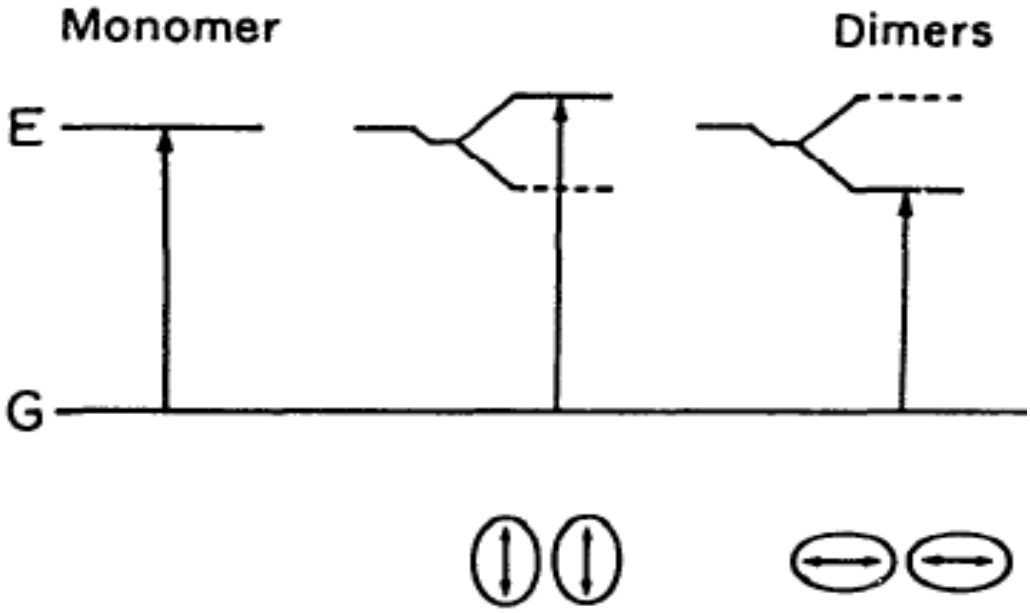

Figure 2.4: Energy level digram depicting the absoprtion of energy from the ground to first excited state for a dye monomer, H-aggregate (H-dimer) and J-agggregate (J-dimer). Herz, A. H., Aggregation Of Sensitizing Dyes In Solution And Their Adsorption Onto Silver-Halides.*Advances In Colloid And Interface Science* **1977,** 8, (4), 237-298.

fluorescence lifetime of H-aggregates of merocyanine dyes. These experiments determined that the fluorescence lifetime is at least 10 times greater than that observed for the monomer. Thus, changes in the fluorescence lifetime of molecules can be an indication that aggregation is occurring. Several factors that affect the process of aggregation include the solvent environment, the structure of the molecule, the temperature and the rigidness of the media that the molecules reside in[24, 25]. For example, it has been observed that the presence of salt solutions, e.g. KCl or NaCl, enhances the formation of aggregates[24, 25]. It is suggested that this results from an increase in the dielectric constant of the solvent. However, it should be noted that an increase in the dielectric constant is not a unique requirement for aggregation as it was reported that the presence of formamide, with a dielectric constant of 109, does not promote dye aggregation[25]. Furthermore, it has been observed that the presence of surfactants precludes aggregation. For example, studies were performed using normal micelles containing nonionic surfactants[24]. These studies showed that increasing the amount of surfactant decreased the amount of H-aggregation for cationic and anionic carbocyanines dyes. Furthermore, the addition of surfactant deaggregated a J-tetramer. It is suggested that the micelle provides a microenvironment in which the dielectric constant is low, thereby stabilizing the monomer form of the dye.

The structure of a molecule also affects the aggregation process. For example, "crowded" dyes are less likely to form aggregates compared to "compact" dyes[25]. Examples of compact dyes include planar cyanines and carbocyanines that typically contain aromatic groups joined by a methine bridge. Crowded dyes tend to have substituents present in the methine bridge. Furthermore, it was observed that an increase in chain length of the methine bridge, addition of chloro substituents as well as fused benzene rings increased the likelihood for dimerization (H-aggregation). In contrast, J-aggregates tend to be favored in structures that have

shorter chains. Another factor thought to enhance aggregation is an increase in hydrophobicity as has been reported for dyes containing longer N-akyl chains[24, 25].

Aggregation in solution has been reported to be a moderately exothermic process, with free energies reported in the range of a -2.8 to -22 kcal/mol for Rhodamine B and the general class of cyanines[25]. The free energy of the aggregation process has positive and negative contributions. Positive contributions include electrostatic forces and the formation of the aggregate, which in the case of a dimer results from two monomers converting into one dimer. West and Pearce suggested that negative contributions arise from the delocalization of electrons associated with the chromophore. This is thought to be a significant driving force in the aggregation process[27]. Furthermore, the relatively small free energy change within the system as a result of aggregation suggests that moderate changes to the parameters discussed previously, e.g. dielectric constant, ionic strength etc., would have a significant impact on the process of aggregation.

Lastly, the observed spectroscopic changes due to the formation of an aggregate makes this phenomenon important in the context of using dyes as fluorescent labels to study various bimolecular reactions and the kinetics of protein and DNA/RNA folding. Understanding the processes that alter the spectroscopy of the fluorescent label is critical to their applications. The aggregation process for different dyes can be interrogated since this process causes changes in the spectroscopy of the dye. Thus, steady-state and time-resolved fluorescence techniques can be used to probe this aggregation process as will be discussed in subsequent chapters.

Fluorescence Correlation Spectroscopy

A large portion of the work in this dissertation has used fluorescence correlation spectroscopy to probe dynamic processes occurring in a variety of systems. As such, it is important to discuss the theory and development of this powerful technique.

2.5 Development of FCS

The development of fluorescence correlation spectroscopy (FCS) has allowed for dynamic processes within molecules to be studied. This includes those that are inherently fluorescent, e.g. dyes, and those that are easily labeled with a fluorophore such as proteins, DNA and RNA. In order to understand the theory and experimental design concept behind this technique, it is important to discuss its foundation, which is the technique of dynamic light scattering (DLS).

Dating back to the late 1960s and early 1970s, DLS provided a new and important experimental technique to study microscopic molecules[28, 29]. DLS relies on the simple concept that when molecules are irradiate by a laser beam, some of the laser light is elastically scattered at angles that differ from the angle of incidence. Since laser light is coherent, interference patterns develop and this results in an intensity profile of the scattered light. The intensity profile is a function of the scattering angle of the laser light. Furthermore, the differences in the intensity of the scattered light result from the motion of the particles in the sample. The motion of the particles causes fluctuations in the local concentration, thereby causing changes in the intensity profile. In practice, DLS is used to monitor the intensity fluctuations of the scattered light at a particular angle. From these measurements, the data can be transformed into a

meaningful result using a statistical analysis technique known as autocorrelation. This mathematical treatment of the data allows the intensity fluctuations as a function of time to be characterized. Thus, insight into the dynamic processes that are occurring is obtained. This includes information about the diffusion and flow properties of molecules. DLS provided a foundation for the technique of FCS, which relies on fluctuations in the fluorescence signal as a function of time.

In the early 1970s, Magde, Elson and Webb, first reported on a series of experiments in which the diffusion and dynamics of DNA and an intercalating drug were measured[30-32]. The technique was similar to DLS, in that it involved measuring fluctuations in the signal brought about by molecules in the sample. However, in contrast to DLS, the experiments recorded fluctuations in the fluorescence intensity. This difference is important, as fluorescence is inherently more sensitive and selective than light scattering. Moreover, DLS has its limitations, in that the molecules of interest have to be big enough to produce a detectable scattering profile. However, fluorescence can be detected from both small and large molecules, thus giving FCS a more dynamic range than DLS. This allows for the study of a variety of molecules, both macroscopic and microscopic. Furthermore, FCS has the ability to monitor chemical reactions, which makes it an attractive alternative to DLS. In general, chemical reactions do not produce a large enough change in the scattering profile to be measured by DLS, whereas the fluctuations that arise in the fluorescence signal detected in FCS are usually large enough. Thus, FCS can be used to monitor these reactions. Lastly, DLS is only sensitive to the bulk diffusion properties of the sample. On the other hand, FCS is sensitive to molecules that are fluorescent and therefore can be used to study dynamics that may be occurring in a small sub-population of the bulk sample.

Unfortunately, the theoretical concepts behind FCS in the 1970s were difficult to implement experimentally. The technology available at the time was not where it is today and implementing FCS systems was not an easy endeavor. For one, FCS relies on the ability to have a small detection volume in order to probe fluorescence intensity fluctuations in individual molecules. If the detection volume is too large, i.e. picoliters or greater, the backscattering of the laser light overwhelms the fluorescence intensity fluctuations of the individual fluorophores, thus leading to large levels of noise and difficulty in performing the experiments. The backscattered light is proportional to the size of the detection volume. Thus, a smaller detection volume results in less noise being introduced into the system. Unfortunately, the detection volumes in the early days of FCS were much too large. Furthermore, the technology behind the detection of the fluorescence signal was not nearly where it is currently. In order to successfully implement an FCS system, the collection of the fluorescence and the detector efficiency has to be sufficient enough to detect the fluorescence emission from a single fluorophore. With the large detection volumes at the time, the backscattered laser light would overwhelm this fluorescence intensity fluctuation[33]. As a result, FCS was subject to long data acquisition times, on the order of minutes to hours, in order to detect any minute variations in the fluorescence signal. Although the technique showed a lot of promise, it sat relatively dormant until new advances in the technology of both optical systems and detectors occurred in the early 1990s.

In 1990, Shera and co-workers[34] successively demonstrated the ability to detect fluorescence from single molecules, which generated a renewed interest in FCS. Furthermore, in the mid 1990s, Rigler and co-workers[35, 36] and Zare and co-workers[37, 38] demonstrated that confocal microscopy could be used to detect single molecules as they diffused through a small detection volume. The use of confocal microscopy meant that the lengthy data acquisition times

required in the early days of FCS were no longer needed, as small changes in the fluorescence intensity could now be detected due to the deceased size of the focal volume.

Confocal microscopy has long been used as an imaging technique, but in the realm of FCS, it provided a way to greatly reduce the detection volume and thus was a great advancement for FCS experiments. In practice, a high numerical aperture (NA) microscope objective is used to focus the excitation laser beam to a diffraction limited spot. This means that only a few fluorophores will be in the detection volume at one time, leading to greater signal to noise ratios and reduced data acquisition times, as compared to the early days of FCS. The same objective is used to collect the resulting fluorescence, which is known as epi-illumination. In order to ensure that the fluorescence that is detected is only from the focal volume, a pinhole(s) is placed in front of the detector(s). The pinhole(s) spatially filter the emitted fluorescence. Thus, only fluorescence originating from the focal volume will be imaged onto the detector(s). The detection volume in a confocal microscopy experiment can be estimated by assuming that the detection volume is cylindrical in shape. The detection volume has a radius, defined as ω_0, and a height, which is defined as $2z_0$, where z_0 is the axial radius of the focal volume (Figure 2.5). These parameters can be calculated using the equations[33]:

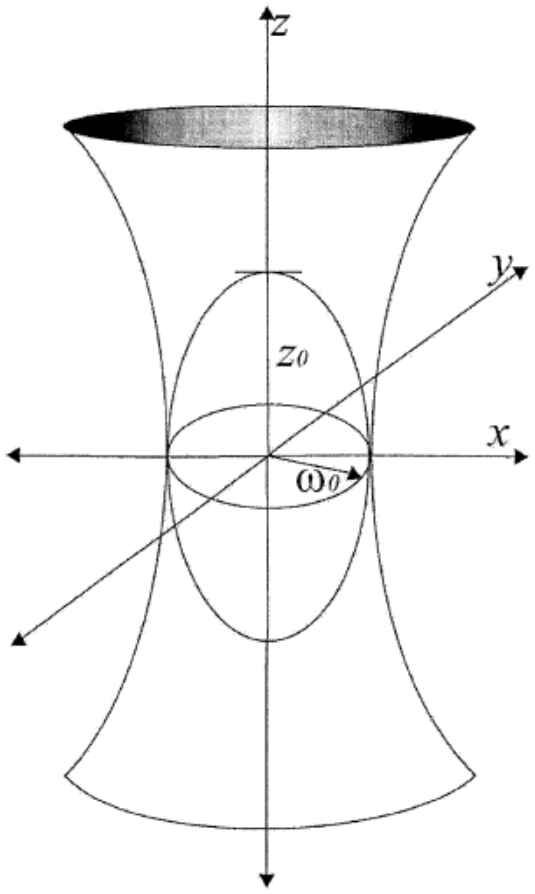

Figure 2.5: A schematic showing the optical probe region in an FCS experiment showing the radial (ω_0) and axial dimensions (z_0). The edge of the optical probe region is defined by the point in which the laser intensity decays to $1/e^2$ the intensity at the center. Van Orden, A.; Fogarty, K.; Jung, J., Fluorescence Fluctuation Spectroscopy: A Coming of Age Story. *Applied Spectroscopy* **2004,** 58, (5), 122A-137A.

$$\omega_0 = \frac{1.22\lambda}{2NA} \qquad z_0 = \frac{2n\lambda}{(NA)^2} \qquad (2.15)$$

where, λ is the excitation wavelength and NA is the numerical aperture of the microscope objective. For the experiments described in later chapters, where a 1.3 NA objective is used with an excitation wavelength of 514.5 nm to probe a molecule in an aqueous environment (n ~ 1.33), the resulting focal volume is on the order of 0.3 femtoliters, which is much less than the focal volumes attainable in the 1970s (picoliters or greater). This result is important as it allows for FCS experiments to be carried out successfully. The extremely small focal volume suppresses the backscattered light from the excitation laser beam, while allowing for low laser powers to be used(< 1 mW). Moreover, the number of fluorophores being probed at any given time is low, which enhances the signal to noise ratio. Lastly, confocal microscopy allows researchers to use a very small amount of sample (i.e. sub-microliters).

Although confocal microscopy coupled with FCS has provided a great step forward, the development of highly sensitive detectors was crucial for the technique to work. The use of single-photon counting avalanche photo-diode detectors (APD) has become the standard in FCS experiments. These detectors are capable of detecting visible photons with 30-70 % quantum efficiency. As a result, today's FCS experiments have high collection efficiency's asthey combine confocal microscopy with these highly sensitive detectors. Thus, the early development of the principles behind FCS, recent advances in technology and the use of confocal microscopy have made this technique very powerful for studying the dynamic processes occurring in various systems.

2.6 Theory of FCS

For most experiments performed herein, there was one fluorescent species of interest that was in a single excitation region. As a result, this discussion will begin by focusing on the theory behind the autocorrelation function. Later in the chapter, the theory behind cross-correlation analysis will be discussed, as this is a useful application of FCS. Moreover, part of my work involved performing two-beam fluorescence cross correlation experiments, which is discussed in the addendum to this dissertation. As a result, I was able to contribute to a publication in the January 2009 issue of *Analytical Chemistry*[39].

2.6.1 The Autocorrelation Function

Autocorrelation analysis is used when probing a single fluorescent species of interest within an excitation volume. Conformational changes or simple diffusion of a molecule(s) in and out of the probe volume produce fluorescence intensity fluctuations. These fluctuations are measured to produce an autocorrelation function. In order to derive the autocorrelation function, it is useful to first define the concentration correlation function. The concentration correlation function is defined as $\Phi_{jl}(r,r',\tau)$, which compares the size of the concentration fluctuation of the j^{th} component at one position and time to the fluctuation of the i^{th} component at a second position and time. Here, that second time is defined as τ. Considering only component j, the concentration of this component at position r and time t can be expressed as $C_j(r,t)$. The concentration fluctuation of this component can be expressed as[31]:

$$\partial C_j(r,t) = C_j(r,t) - \overline{C_j} \qquad (2.16)$$

where, $\overline{C_j}$ is the mean thermodynamic concentration of the jth component. Note that $\overline{C_j}$ is independent of time and position and is defined mathematically as[31]:

$$\overline{C_j}\left\langle C_j(r,t)\right\rangle \tag{2.17}$$

from these relationships, the concentration correlation function can be defined as[31]:

$$\Phi_{jl}(r,r',\tau)=\left\langle \partial C_j(r,t)\partial C_j(r,t+\tau)\right\rangle \tag{2.18}$$

Two situations can arise from this relationship; one in which the τ's are short compared to the diffusion and reaction of the system and the second, in which the τ's are long compared to these processes. In the first situation, the following is true[31]:

$$\Phi_{jl}(r,r',\tau)\approx\Phi_{jl}(r,r',0) \tag{2.19}$$

Thus, Φ_{jl} (r,r',0) is independent of changes in the system. Therefore, the diffusion and reaction times can be determined from the equilibrium properties of the system. In the second situation, the following relationship is true.

$$\Phi_{jl}(r,r',\tau)\approx\Phi_{jl}(r,r',\infty)=0 \tag{2.20}$$

Thus, the rate at which Φ_{jl} (r,r',τ) decays to zero with increasing τ allows one to measure how diffusion and chemical reactions change the system. The concentration correlation function can be expressed in terms of experimentally measured fluorescence intensity fluctuations, given by the equation[31]:

$$i(t)=\kappa\sum\varepsilon_j Q_j\int I(r)C_j(r,t)d^3r \tag{2.21}$$

where, κ is the percentage of fluorescent photons that are converted into photon counts, which accounts for losses due to the optics in the system and the quantum efficiency of the detector, ε_j is the extinction coefficient of the jth component, Q_j is the fluorescence quantum efficiency of component j, and I(r) is the laser intensity at position r. I(r) can be expressed as[31]:

$$I(r)=I_0\exp\left[-2\frac{x^2+y^2}{\omega_0^2}-2\frac{z^2}{z_0^2}\right] \tag{2.22}$$

where, x, y and z refer to the position of the incident beam relative to the center position of the laser focus. Note that the laser intensity at any point is dependent on the distance from the center position of its focus. An expression for the fluctuations in the photon counts can be expressed as[31]:

$$\partial i(t) = i(t) - \langle i \rangle \tag{2.23}$$

where, <i> is the average fluorescence intensity over the measurement. These intensity fluctuations can be used to calculate the temporal autocorrelation of the photon counts using the equation[31]:

$$G(\tau) = \frac{\langle \partial i(t) \partial i(t+\tau) \rangle}{\langle i \rangle^2} \tag{2.24}$$

The assumption is made that only one species is contributing to fluctuations in the fluorescence intensity. With this assumption, the sample is considered to be ideal as it only contains one fluorescent species and thus one diffusion coefficient. This assumption is generally valid as FCS requires sample concentrations that are ≈ 10 nM. As a result, equation 2.24 can be simplified to[31]:

$$G(\tau) = \frac{\sum_j (\varepsilon_j Q_j)^2 \iint I(r) I(r') \Phi_{jj}(r, r', \tau) d^3 r d^3 r'}{(I_0 \pi^{3/2}) \omega_0^2 z_0 \sum_j \varepsilon_j Q_j \overline{C_j})^2} \tag{2.25}$$

The denominator in equation 2.25 can be simplified into one term, $\langle i \rangle^2$, which yields[31]:

$$G(\tau) = \frac{1}{N} \left(\frac{1}{1 + \tau / \tau_d} \right) \left(\frac{1}{1 + (\kappa_0^2 * \tau / \tau_d} \right)^{1/2} \tag{2.26}$$

where, $N = \pi^{3/2} \omega_0^2 z_0 \overline{C}_j$ and is the average number of fluorescent molecules occupying the probe volume. Thus, the amplitude of the autocorrelation function is inversely proportional to N and

yields information about the number of fluorescent molecules in the probe region. This is illustrated in Figure 2.6, which shows the measured autocorrelation function for a 25 nM and a 50 nM sample of aqueous Cyanine-3. Furthermore, κ_0 is the ratio of ω_0 to z_0 and τ_d represents the average time the molecule, with diffusion coefficient D, resides in the probe region. The relationship between the diffusion coefficient, the radius of the probe volume and the diffusion time of the molecule through the probe volume can be expressed mathematically as[31, 33]:

$$\tau_d = \frac{\omega_0^2}{4D} \tag{2.27}$$

Thus, the autocorrelation function yields information about both the FCS experimental setup and the diffusion properties of the fluorescent molecules within the system. For example, measuring the autocorrelation function for a standard fluorescent molecule with a known diffusion time yields information about the size of the focal volume. On the other hand, knowing the size of the focal volume and measuring the autocorrelation function of a fluorescent molecule with an unknown diffusion coefficient yields information about its diffusion properties.

2.6.2 The Cross-Correlation Function

Fluorescence cross-correlation spectroscopy uses two spatially offset laser beams. This results in two detection volumes, defined as V_1 and V_2. A molecule traverses

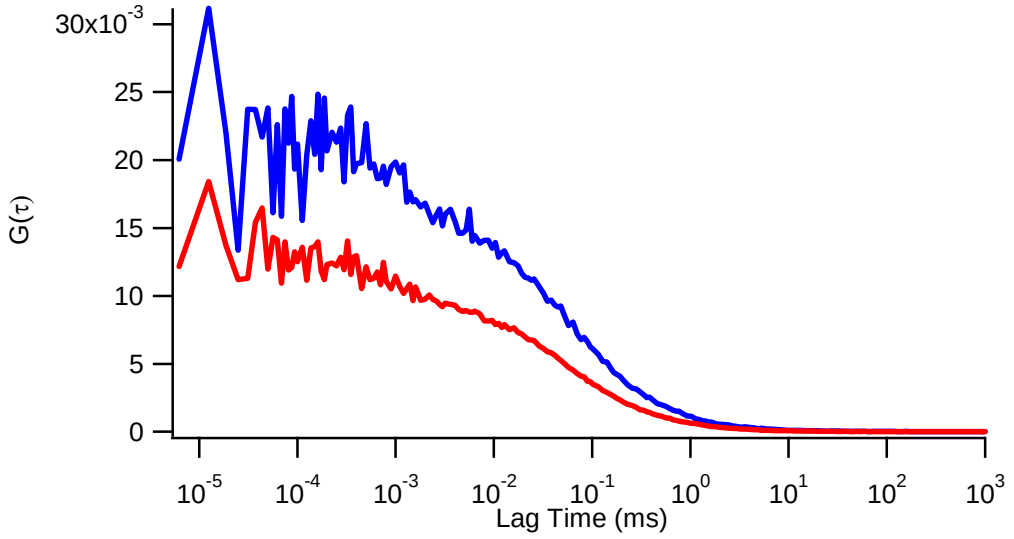

Figure 2.6: Measured autocorrelation functions for a 25 nM (blue) and 50 nM (red) aqueous Cyanine-3 samples. Note that the amplitude of the autocorrelation function for the 50 nM sample is roughly half as large as the 25 nM sample, consistent with equation 2.12.

through the detection volumes and fluorescence intensity fluctuations are observed within each probe region. The fluctuations that occur within the two detection volumes, V_1 and V_2, are then correlated. The distance between the two detection volumes is defined as R. A schematic representation showing the two spatially offset detection volumes is presented in Figure 2.7. The use of two detection volumes that are separated by the distance R implies that diffusion of molecules alone will not produce meaningful correlation data. This is in contrast to autocorrelation analysis, as described previously. To overcome this limitation, uniform flow is introduced by using pressure to flow the sample or by applying a voltage across the capillary.

In theory, the cross-correlation function mirrors the autocorrelation function. However, the difference is that it compares the fluorescent fluctuations from two spatially offset detection volumes. The cross-correlation function can be defined as[40, 41]:

$$G_{cc}(\tau) = \frac{\left\langle i_1\left(t, \vec{r}\right) i_2\left(t+\tau, \vec{r'}\right)\right\rangle}{\left\langle i_1\right\rangle\left\langle i_2\right\rangle} \qquad (2.28)$$

where, $i_1\left(t, \vec{r}\right)$ and $i_2\left(t, \vec{r}\right)$ represent the fluorescence intensities at the two detection volumes, V_1 and V_2 at time t and lag time $t + \tau$. Each detection volume has an x,y,z coordinate system, which is defined as r and r', respectively. Furthermore, because cross-correlation analysis involves flowing the molecules, the function can be expressed in the reverse direction, defined as[40, 41]:

$$G_{cc}(\tau) = \frac{\left\langle i_2\left(t, \vec{r}\right) i_1\left(t+\tau, \vec{r'}\right)\right\rangle}{\left\langle i_1\right\rangle\left\langle i_2\right\rangle} \qquad (2.29)$$

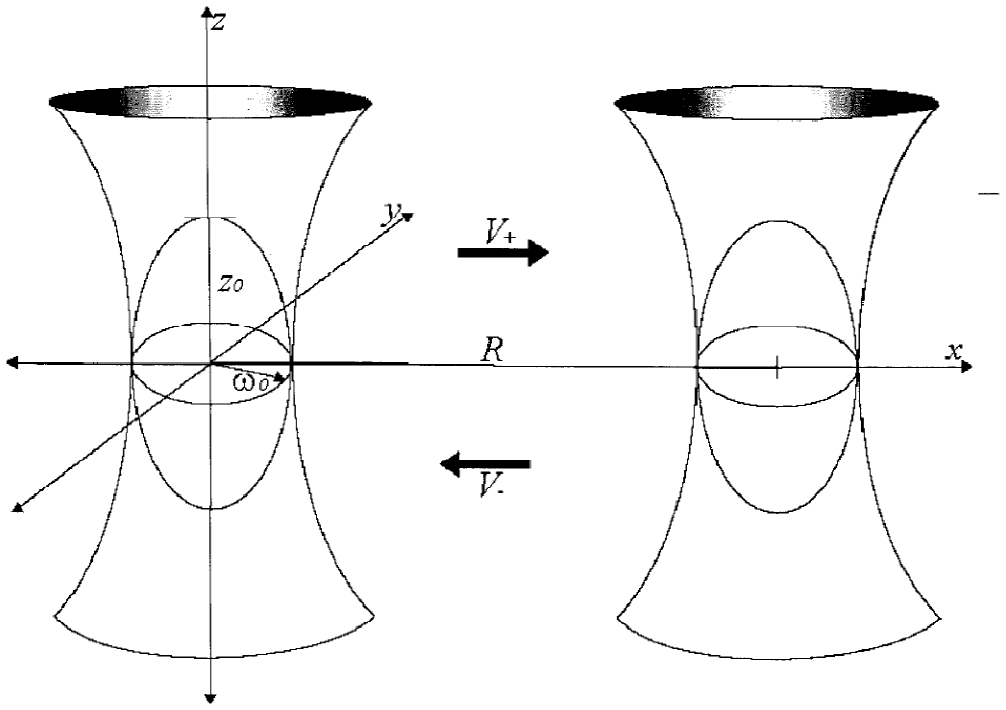

Figure 2.7: Schematic showing the two spatially offset optical probe regions in a fluorescence cross-correlation experiment. The radial (ω_0) and axial dimensions (z_0) are shown as is the distance separating the two optical probe regions, defined as R. Note that V_+ and V_- refer to the flow velocity in the forward and reverse direction, respectively. Van Orden, A.; Fogarty, K.; Jung, J., Fluorescence Fluctuation Spectroscopy: A Coming of Age Story. *Applied Spectroscopy* **2004,** 58, (5), 122A-137A.

The difference now being that detection volume 1 is monitored at a lag time, $t+\tau$. The fact that cross-correlation analysis can be performed in both directions gives rise to the term "forward" correlation, defined as $G_F(t)$, and "reverse" correlation, which is defined as $G_R(t)$. Equation 2.28 depicts the "forward" cross-correlation function and equation 2.29 depicts the "reverse" cross-correlation function. Furthermore, equation 2.28 can be expressed as[40, 41]:

$$G_F(\tau) = \frac{1}{N}\left(\frac{1}{1+\tau/\tau_d}\right)\left(\frac{1}{1+(\kappa_0^2 * \tau/\tau_d}\right)^{1/2} \exp\left[-\frac{\left(\vec{V}_\rho \tau - \vec{R}\right)^2}{\omega_0^2\left(1+\frac{\tau}{\tau_d}\right)} - \frac{V_z^2\tau^2}{z_0^2\left(1+\kappa_0^2\frac{\tau}{\tau_d}\right)}\right] \qquad (2.30)$$

where, $\vec{V}_\rho$ is the xy component of the flow, which transports the molecule from volume 1 to volume 2, and the term V_z represents the z component of the flow and $\vec{R}$ represents the distance between the two laser foci. In comparison to the autocorrelation function (equation 2.26), the cross-correlation function contains an exponential term. The exponential term accounts for the distance and flow between the two focal volumes, which is absent when performing autocorrelation analysis. In a cross-correlation experiment, the flow is confined along the x direction. Furthermore, the separation between the two probe volumes is confined to the x-axis. As a result, equation 2.16 can be simplified to[40, 41]:

$$G_F(\tau) = \frac{1}{N}\left(\frac{1}{1+\tau/\tau_d}\right)\left(\frac{1}{1+(\kappa_0^2 * \tau/\tau_d}\right)^{1/2} \exp\left[-\frac{R^2\left(1-\frac{\tau}{\tau_F}\right)^2}{\omega_0^2\left(1+\frac{\tau}{\tau_d}\right)}\right] \qquad (2.31)$$

where, R is the distance between the two detection volumes on the x-axis and τ_F is the time it takes for the molecule to flow between the detection volumes. The flow time depends on the flow velocity, V_x, and the spatial separation, R, by the equation[40, 41]:

$$\tau_F = \frac{R}{V_x} \tag{2.32}$$

Recall that the cross-correlation function can be expressed in terms of "forward" and "reverse". Thus, the reverse correlation function can be expressed as[40, 41]:

$$G_R(\tau) = \frac{1}{N}\left(\frac{1}{1+\tau/\tau_d}\right)\left(\frac{1}{1+(\kappa_0^2 * \tau/\tau_d}\right)^{1/2} \exp\left[\frac{R^2\left(1+\frac{\tau}{\tau_F}\right)^2}{\omega_0^2\left(1+\frac{\tau}{\tau_d}\right)}\right] \tag{2.33}$$

The difference between equation 2.31 and 2.33 is the sign in the exponential term, which is negative in the forward cross-correlation function and positive in the reverse cross-correlation function. The reason for this is the way that the flow velocity is defined, positive flow velocity in the forward direction and negative flow velocity in the reverse direction. Furthermore, the forward and reverse cross-correlation functions are independent of each other. The forward cross-correlation function is only sensitive to molecules moving from detection volume 1 to detection volume 2, and the reverse cross-correlation function is only sensitive to molecules moving from detection volume 2 to detection volume 1. Finally, the cross-correlation function will reach a maximum, defined as[40, 41]:

$$\tau_{\max} = -\left(\tau_d + \frac{\tau_F^2}{2\tau_d}\left(\frac{\omega_0}{R}\right)^2\right) + \left[\left(\tau_d + \frac{\tau_F^2}{2\tau_d}\left(\frac{\omega_0}{R}\right)^2\right)^2 + \tau_F^2\left(1+\left(\frac{\omega_0}{R}\right)^2\right) + 2\tau_d\tau_F\right]^{1/2} \tag{2.34}$$

The cross-correlation function rises to a maximum when $R >> \omega_0$ and $\tau_{max} \sim \tau_F$.

2.7 Measuring the Correlation Functions Experimentally

2.7.1 Autocorrelation Analysis

The autocorrelation function is obtained experimentally by accumulating single photons over a period of time. The photons are accumulated into "time bins", whose duration is defined as Δt. The fluorescence intensity at any given time is equal to the number of photons detected, n, divided by the time interval over which the photons were collected, Δt. This relationship can be expressed as t=iΔt. After a large number of time bins have been collected, the autocorrelation function, G(τ), can be expressed as[33]:

$$G(\tau) = \frac{(M-k)\sum_{i=1}^{M-k} n_i n_{i+k}}{\left(\sum_{i=1}^{M-k} n_1\right)^2} \qquad (2.35)$$

where, *M* is the total number of time bins and *k* is the time interval corresponding to lagtime τ=kΔt. In order for FCS to be sensitive to a wide range of timescales, e.g. nanoseconds to seconds, it is useful to allow the length of each successive time bin to vary. In this "multiple tau" approach, photons are initially collected in very short time bins, about a few nanoseconds in duration. Subsequent photons are collected into longer time bins that range from tens of nanoseconds to seconds. As a result, FCS is sensitive to a long range of timescales while not requiring excessively long data accumulation times.

2.3.1 Cross-Correlation Analysis

The cross correlation function, $G_F(\tau)$, can be expressed as[33, 40]:

$$G_F(\tau) = \frac{\frac{1}{M-k}\sum_{t=1}^{M-k} n_1(t) n_2(t+\tau)}{\left(\frac{1}{M-k}\right)^2 \sum_{t=1}^{M-k} n_1(t) \sum_{t=1}^{M-k} n_2(t+\tau)} \qquad (2.36)$$

where, n_1 is the photons detected by detector one, which is monitoring the first probe region, and n_2 is the photons collected by detector two, which is monitoring the second probe region. Recall that cross-correlation analysis uses two optical probe regions. Thus, equation 2.35, which describes the autocorrelation function with one optical probe region does not apply to cross-correlation analysis. Instead, additional terms need to be added to the equation. Note that equation 2.36 simplifies to equation 2.35 if both of the detectors are monitoring the same optical probe region.

2.8 Instrumentation

2.8.1 Optics and FCS Setup for Reverse Micelle Experiments

For the reverse micelle experiments described herein, the following instrumentation was used. The sample was placed on the stage of a Nikon Eclipse TE-2000-U microscope (Nikon Inc., Melville, NY, USA) and irradiated with a CW laser beam at either 514 nm (Ar ion laser, Melles-Griot, Carlsbad, CA, USA) or 532 nm (Nd:YAG laser, B & W Tek, Newark, DE, USA) using a 100X 1.3 numerical aperture microscope objective. The laser power was 0.05 mW, before entering the microscope. The resulting fluorescence and laser light was transmitted back through the microscope. Fluorescence was separated from the incident laser light with a dichroic mirror, which transmitted the fluorescent light out of the microscope at a 90 degree angle. Upon exiting the microscope, the fluorescence was split by a 50/50 beam splitter and imaged onto two 50 μm confocal pinholes. The resulting light was band-pass filtered and focused onto two single-photon-counting avalanche photodiode detectors (PerkinElmer Inc., Waltham, MA, USA). The resulting output of the detectors was recorded using the two channels of an ALV-5000E/EPP card (ALV, Langen, Germany) interfaced to a computer.

2.8.2 Optics and FCS Setup for DNA Hairpin Experiments

The optical setup for these experiments started with an air cooled, continuous wave, Argon-ion laser. The wavelength was set to 514.5 nm. The beam was expanded and then collimated using two telescoping lenses. After being re-collimated, the beam was split using a 50/50 beam splitter (Newport Inc., Irvine, CA, USA). The power of each beam was attenuated using the appropriate absorptive neutral density filters. The nearly parallel beams were then passed through a focusing lens with a focal length of 150 mm. Upon exiting the focusing lens, the beams hit a 530 nm dichroic mirror, which directs them into a 100x, 1.25 numerical aperture oil immersion objective (Edmund Industrial Optics, Barrington, NJ, USA). The objective focuses the beam into a glass window that has been burned into the fused silica capillary (Polymicrotechnologies, Phoenix, AZ, USA) used to deliver the sample. The size of the laser foci was controlled by carefully position the focusing lens such that it was 300 mm from the back of the microscope objective. The focusing lens was on a stage that can be adjusted in three directions, allowing for the beam size to be minimized ensuring a near ideal Gaussian beam profile. Pressure flow was used to rinse the capillaries, coat the capillaries and introduce the sample prior to taking measurements. To do so, a micro-centrifuge tube containing the appropriate solution was placed into a custom built pressure chamber that was attached to a tank of nitrogen gas. One end of the capillary, which is sealed inside the pressure chamber, was placed into the tube containing the solution. The pressure of nitrogen in the chamber was controlled by a pneumatic pressure regulator (Fairchild Model 81, Winston-Salem, NC, USA), which drove the solution through the capillary. For the experiments discussed in chapter 3, the capillary was filled with the sample and the microcentrifuge tubes containing the sample solution were placed at equal heights on each end of the capillary. A platinum wire, connected to a high

voltage power supply (Spellman, Plainview, NY, USA) was inserted into the sealed chamber and placed into the sample. At the other end of the capillary, a grounded platinum wire was placed into the sample. A voltage was applied across the capillary resulting in electrophoretic migration of the target molecules. The resulting fluorescence was collected through the objective described previously and passed back through the dichroic mirror, which rejects the laser light, and was split by a 50/50 beamsplitter cube (Thorlabs, Newton, NJ, USA). After being split, the fluorescence was spatially filtered using two 50 um pinholes (Thorlabs, Newton, NJ, USA) and subsequently filtered by two 535 long-pass filters, one for each detector. The filtered fluorescence was focused down onto the active area of two single photon counting avalanche photodiode detectors (PerkinElmer Optoelectronics, Wellesley, MA, USA) using aspheric lenses (Newport Inc., Irvine, CA, USA). The raw photon count data was digitized using a two channel, 800 MHz gated photon counter card (Becker and Hickl GmbH, Berlin, Germany) which was interfaced to a Pentium computer.

1. Woelfl, S.; Mages, M.; Ovari, M.; Geller, W., Determination of heavy metals in macrozoobenthos (chironomid larvae) from the river Tisza by total reflection X-ray fluorescence spectrometry. In *Metal Ions In Biology And Medicine,* ed.; 2004; Vol. 8, pgs. 330-333.

2. Tung, C. H.; Ho, N. H.; Zeng, Q.; Weissleder, R., In vivo imaging of thrombosis-associated enzyme using fluorescence peptide probes. In *Peptide Revolution: Genomics, Proteomics & Therapeutics*, ed.; 2004; pgs. 325-326.

3. Lee, J.; Govorov, A. O.; Kotov, N. A., Fluorescence enhancement and energy transport from bioconjugation between nanowires and nanoparticles. In *Physical Chemistry Of Interfaces And Nanomaterials Iii*, ed.; 2004;Vol. 5513, pgs.226-231.

4. Kitamatsu, M.; Saito, M.; Nakai, T.; Sisido, M., Fluorescence detection of conformationally-restricted oxy-peptide nucleic acids/DNA hybrids. In *Peptide Revolution: Genomics, Proteomics & Therapeutics*, ed.; 2004; pgs. 538-539.

5. Cha, A.; Zerangue, N.; Kavanaugh, M.; Bezanilla, F., Fluorescence techniques for studying cloned channels and transporters expressed in Xenopus Oocytes. In *Neurotransmitter Transporters*, ed.; 1998; Vol.296, pgs. 566-578.

6. Price, B. B.; Wright, J. C., Scanned Laser Fluorescence Line Narrowing Spectroscopy Of Photosensitive Organic Chromophores. *Analytical Chemistry* **1990,** 62, (18), 1989-1994.

7. Menezes, M. E.; Roepe, P. D.; Kaback, H. R., Design of a Membrane-Transport Protein For Fluorescence Spectroscopy. *Proceedings Of The National Academy Of Sciences Of The United States Of America* **1990,** 87, (5), 1638-1642.

8. Keller, M. A.; Saba, C. S., Monitoring of Polyphenyl Ether Lubricants Using Fluorescence Spectroscopy. *Applied Spectroscopy* **1990,** 44, (2), 266-268.

9. Bark, K. M.; Force, R. K., Analysis Of Polynuclear Aromatic Hydrocarbon Mixtures Desorbed From Particulate Matter In A Low-Temperature Matrix By Shpolskii Time-Resolved Fluorescence Spectroscopy. *Applied Spectroscopy* **1990,** 44, (8), 1373-1376.

10. Wong, A. L.; Harris, J. M., Quantitative Estimation of Component Amplitudes In Multiexponential Data - Application To Time-Resolved Fluorescence Spectroscopy. *Analytical Chemistry* **1989,** 61, (20), 2310-2315.

11. Schartner, K. H.; Lenz, P.; Mobus, B.; Schmoranzer, H.; Wildberger, M., Structures At The Xe 5s Threshold Studied By Photon-Induced Fluorescence Spectroscopy. *Journal of Physics B-Atomic Molecular And Optical Physics* **1989,** 22, (10), 1573-1581.

12. Johnson, P. A.; Barber, T. E.; Smith, B. W.; Winefordner, J. D., Ultralow Detection Limits For An Organic-Dye Determined By Fluorescence Spectroscopy With Laser Diode Excitation. *Analytical Chemistry* **1989,** 61, (8), 861-863.

13. Eng, J.; Lynch, R. M.; Balaban, R. S., Nicotinamide Adenine-Dinucleotide Fluorescence Spectroscopy and Imaging of Isolated Cardiac Myocytes. *Biophysical Journal* **1989,** 55, (4), 621-630.

14. Atkinson, G. H.; Blanchard, D.; Lemaire, H.; Brack, T. L.; Hayashi, H., Picosecond Time-Resolved Fluorescence Spectroscopy of K-590 In The Bacteriorhodopsin Photocycle *Biophysical Journal* **1989,** 55, (2), 263-274.

15. Yguerabi.J; Stryer, L., Fluorescence Spectroscopy Of An Oriented Model Membrane (Probes/Polarization/Oxidized Cholesterol Bilayer/Spherical Membranes). *Proceedings Of The National Academy Of Sciences Of The United States Of America* **1971,** 68, (6), 1217.

16. Benetti, P.; Omenetto, N.; Rossi, G., New Optical System For Flame Spectroscopy With Special Reference To Thermally Assisted Anti-Stokes Fluorescence Applications. *Applied Spectroscopy* **1971,** 25, (1), 57.

17. Wang, L.; Liu, R. T.; Chi, Z. X.; Yang, B. J.; Zhang, P. J.; Wang, M. J., Spectroscopic investigation on the toxic interactions of Ni2+ with bovine hemoglobin. *Spectrochimica Acta Part A-Molecular and Biomolecular Spectroscopy* 76, (2), 155-160.

18. Pully, V. V.; Lenferink, A.; Otto, C., Raman-Fluorescence Hybrid Microspectroscopy of Cell Nuclei. *Vibrational Spectroscopy* 53, (1), 12-18.

19. Guilbault, G. G., *Practical Fluorescence; Theory, Methods, and Techniques*. ed.; M. Dekker: New York, 1973.

20. Jia, K.; Wan, Y.; Xia, A. D.; Li, S. Y.; Gong, F. B.; Yang, G. Q., Characterization of Photoinduced Isomerization And Intersystem Crossing of the Cyanine Dye Cy3. *Journal Of Physical Chemistry A* **2007,** 111, (9), 1593-1597.

21. Lakowicz, J. R., *Principles of Fluorescence Spectroscopy*. ed.; Kluwer Academic/Plenum: New York, 1999.

22. Widengren, J.; Schwille, P., Characterization Of Photoinduced Isomerization And Back-Isomerization of the Cyanine Dye Cy5 by Fluorescence Correlation Spectroscopy. *Journal of Physical Chemistry A* **2000,** 104, (27), 6416-6428.

23. Skoog, D. A., Holler, F.J., *Principles of Instrumental Analysis*. 5th ed.; Saunders College Pub.: Philadelphia, 1998.

24. Herz, A. H., Aggregation Of Sensitizing Dyes In Solution And Their Adsorption Onto Silver-Halides.*Advances In Colloid And Interface Science* **1977,** 8, (4), 237-298.

25. James, T. H., *The Theory of the photographic process*. 4th ed.; Macmillan: New York, 1977.

26. Rosch, U.; Yao, S.; Wortmann, R.; Wurthner, F., Fluorescent H-Aggregates of Merocyanine Dyes. *Angewandte Chemie-International Edition* **2006,** 45, (42), 7026-7030.

27. West, W.; Pearce, S., Dimeric State of Cyanine Dyes. *Journal of Physical Chemistry* **1965,** 69, (6), 1894-&.

28. Berne, B., Pecora, R., *Dynamic Light Scattering With Applications to Chemistry, Biology and Physics*. ed.; Dover Publications Inc.: New York, 2000.

29. Schmitz, K. S., *An introduction to dynamic light scattering of macromolecules*. ed.; Academic Press Inc.: San Diego, 1990.

30. Magde, D.; Elson, E. L.; Webb, W. W., Fluorescence Correlation Spectroscopy .2. Experimental Realization. *Biopolymers* **1974,** 13, (1), 29-61.

31. Elson, E. L.; Magde, D., Fluorescence Correlation Spectroscopy .1. Conceptual Basis and Theory. *Biopolymers* **1974,** 13, (1), 1-27.

32. Magde, D.; Webb, W. W.; Elson, E., Thermodynamic Fluctuations In A Reacting System - Measurement By Fluorescence Correlation Spectroscopy. *Physical Review Letters* **1972,** 29, (11), 705-&.

33. Van Orden, A.; Fogarty, K.; Jung, J., Fluorescence Fluctuation Spectroscopy: A Coming of Age Story. *Applied Spectroscopy* **2004,** 58, (5), 122A-137A.

34. Shera, E. B.; Seitzinger, N. K.; Davis, L. M.; Keller, R. A.; Soper, S. A., Detection of Single Fluorescent Molecules. *Chemical Physics Letters* **1990,** 174, (6), 553-557.

35. Rigler, R., Fluorescence Correlations, Single-Molecule Detection And Large Number Screening - Applications In Biotechnology. *Journal Of Biotechnology* **1995,** 41, (2-3), 177-186.

36. Rigler, R.; Mets, U.; Widengren, J.; Kask, P., Fluorescence Correlation Spectroscopy with High Count Rate And Low-Background - Analysis Of Translational Diffusion. *European Biophysics Journal With Biophysics Letters* **1993,** 22, (3), 169-175.

37. Nie, S. M.; Chiu, D. T.; Zare, R. N., Real-Time Detection of Single-Molecules in Solution by Confocal Fluorescence Microscopy. *Analytical Chemistry* **1995,** 67, (17), 2849-2857.

38. Nie, S. M.; Chiu, D. T.; Zare, R. N., Probing Individual Molecules With Confocal Fluorescence Microscopy. *Science* **1994,** 266, (5187), 1018-1021.

39. Fogarty, K.; McPhee, J. T.; Scott, E.; Van Orden, A., Probing the Ionic Atmosphere of Single-Stranded DNA Using Continuous Flow Capillary Electrophoresis and Fluorescence Correlation Spectroscopy *Analytical Chemistry* **2009,** 81, (1), 465-472.

40. Magde, D.; Webb, W. W.; Elson, E. L., Fluorescence Correlation Spectroscopy .3. Uniform Translation and Laminar-Flow. *Biopolymers* **1978,** 17, (2), 361-376.

41. Brinkmeier, M. R., R., Two Beam Cross Correlation: A Method to Characterize Transport Phenomena in Micrometer-Sized Structures. *Exp. Techn. Phys.* **1995,** 41, (2), 205-210.

Chapter 3: Cy3 in AOT Reverse Micelles Studied By Steady-State and Time-Resolved Spectroscopy

This chapter discusses a number of steady-state and time-resolved fluorescence spectroscopy techniques that I used to study the photophysical properties of the dye Cyanine-3 (Cy3) inside AOT/*iso*-octane reverse micelles. The spectroscopic techniques utilized in this chapter are UV-Visible absorption spectroscopy, fluorescence emission spectroscopy, fluorescence excitation spectroscopy, and time-correlated single photon counting (TCSPC).

3.1 Introduction

The sensitivity and versatility of fluorescence has made it an exceptionally effective tool for a wide range of studies. Fluorescence spectroscopies are especially effective for studies of biological processes. By adding a fluorescent tag to a biomolecule, researchers can follow molecular recognition events, macromolecular folding, and more. As we introduce these fluorophores into increasingly confined environments in biological samples, understanding the effect of confinement on their basic photophysics becomes critical.

One model system providing significant and variable confinement is the reverse micelle[1]. Consisting of three different phases, these structures enable studies of the effects of spatial and orientational confinement on molecular processes. For example, at the appropriate concentrations, sodium di-2-ethylhexyl sulfosuccinate (AOT) in the presence of a non-polar organic solvent (i.e. *iso*-octane) and water forms reverse micelles that consist of a water pool, an interfacial region created by the polar headgroups and aliphatic tails of the surfactant, and the non-polar solvent[2-14]. Recall equation 4.1 which determines the size parameter of the reverse micelles. Thus, the size of these systems can be carefully controlled, making them attractive for studying the role of confined local environment on various processes, such as catalysis[15-18],

intermolecular charge transfer[19] and redox reactions[20, 21]. Here, we present a study that investigates the role of confinement in AOT reverse micelles on the behavior of water soluble organic cyanine dyes (i.e. Cy3).

The general class of cyanine dyes has a rich history of investigation in homogenous solutions[22-37]. As such, there have been many studies on the spectroscopic properties of these dyes. Typically, cyanine dyes have absorption bands in the visible spectrum consisting of a shoulder followed by an absorbance maximum[24, 25, 36, 38-44]. Generally speaking, cyanine dyes exist as monomers at lower concentrations (sub-μM) in aqueous solutions. However, as the concentration of the dye increases or the solvent environment changes, these dyes can form dimers and higher order aggregates that alter the spectroscopic properties of the dye. These aggregation processes have been studied extensively in bulk solutions[31, 32, 34, 39, 45-52]. In aqueous solution, cyanine dyes form both J- and H-aggregates, leading to shifts in their absorption maxima [31, 49, 53]. H-aggregates are characterized by a blue shift in the absorption spectrum, relative to the monomer peak, and exhibit weak fluorescence in non-confined media as compared to the monomer[48]. However, instances in which highly fluorescent H-aggregates of cyanine dyes have been reported in Langmuir-Blodgett layers, at low temperatures and in rigid environments[48, 54].

Cy3 has two forms, a fluorescent trans-isomer and its non-fluorescent cis-isomer. The trans-cis isomerization reaction has been studied extensively by a variety of techniques[23-26, 28, 35, 43, 44, 55-57]. Furthermore, Cy3 displays an absorption maximum at 550 nm and an emission maximum at 570 nm [41, 43, 55]. The dye exists in its monomer form at concentrations below 1 mM in aqueous solution. Cy3 exhibits a short fluorescence lifetime in aqueous solution, typically about 0.15 ns and has a low quantum yield (0.05)[41, 43, 55]. The short lifetime and corresponding

low quantum yield is thought to arise from the trans-cis isomerization reaction that the dye undergoes, which provides an efficient non-radiative decay pathway to compete with the radiative decay [41, 43, 55]. Studies of the cis-trans isomerization reaction show its sensitivity to changes in the solvent viscosity as well as weak influence of solvent polarity[43].

The working hypothesis that motivates this present study is that the confined environment within the reverse micelle can alter the kinetics and mechanism of trans-cis isomerization and aggregation of Cy3 confined within. Thus, Cy3 in reverse micelles can probe the effects of confinement on such processes. The results show an interesting, unexpected behavior of aqueous Cy3 inside AOT/*iso*-octane reverse micelles. The confined environment of the reverse micelles drives the formation of Cy3 aggregates at concentrations that are so low that this behavior is not observed in bulk water. This aggregation phenomenon has been studied and characterized using a variety of spectroscopic techniques; fluorescence emission, time-correlated single photon counting (TCSPC) and absorption measurements.

3.2 Experimental

3.2.1 Sample Preparation

Cy3 monoreactive dye pack was purchased from GE Life Science (Piscataway, NJ, USA). The solid dye was dissolved in Millipore water and the resulting solution stored under refrigeration. The reverse micelle solutions were prepared from AOT (sodium di-2-ethylhexyl sulfosuccinate, 99%, Sigma-Aldrich, St. Louis, MO), *iso*-octane (99.8%, Sigma-Aldrich, St. Louis, MO), and aqueous dye solution. The AOT undergoes a purification process, which has been described elsewhere[58]. Reverse micelles were prepared by dissolving AOT in *iso*-octane to form a 0.3 M stock solution to which aqueous dye solution and water were added. All samples were prepared using 2 ml of a 0.3 M AOT in *iso*-octane solution, 10.8 μL of an aqueous Cy3

solution, for which the concentration varied from 9.9 x 10^{-5} M to 9.9 x 10^{-6} M. The size (w_0) and concentration of the reverse micelles was then adjusted by adding an appropriate amount of *iso*-octane and water, totaling 1 ml, resulting in a reverse micelle sample with an overall AOT concentration of 0.2 M. For the experiments performed herein, the concentration of AOT in the final solution was 0.02 M, unless otherwise noted. To make these final samples, a 100 μL aliquot of a 0.2 M AOT sample was diluted into 900 μL of isooctane. The final dye concentration ranged from 3.6 x 10^{-8} M to 8.9 x 10^{-10} M. This yield occupation numbers for Cy3 molecules in the reverse micelles that range from 1 Cy3 molecule per 0.2 to 9 x 10^5 reverse micelles.

3.2.2 Steady-State and Time-Resolved Measurements

UV-Vis absorption spectroscopy was used to identify the absorption spectra of Cy3 in different sized reverse micelles. This was accomplished using a Cary 500 UV/Vis-NIR Spectrophotometer (Varian Inc., Walnut Creek, CA, USA). Spectra were collected using a 1 cm pathlength cuvette. Spectra were referenced to the spectrum of neat isooctane in the sample cuvette. Each sample was scanned a minimum of three times and the resulting spectra were averaged.

Steady-state fluorescence spectra were collected to identify changes in the emission wavelengths of Cy3 in the different size reverse micelles. The spectra were collected using a SPEX steady-state spectrofluorometer (HORIBA Jobin Yvon, Edison, NJ, USA) using a 1 cm pathlength cuvette. Spectra were collected by exciting at 514 and 532 nm, to capture emission characteristics of various features observed in absorption spectra.

Fluorescent lifetime measurements were performed to monitor any change in the fluorescence lifetime of Cy3 due to the surrounding environment. To do so, a Fluorocube

instrument (HORIBA Jobin Yvon, Edison, NJ, USA), which provides time-correlated single photon counting data, was used. The instrument response function was measured and the sample was subsequently loaded into the instrument. All samples were excited at a 514 nm wavelength of an Argon flash lamp selected by a monochromator. Subsequent fluorescence was detected at 560, 600 and 650 nm.

3.3 Results and Discussion

Figure 3.1 shows the normalized absorption spectra of Cy3 in water and in reverse micelles of varying size. In water, the Cy3 absorption spectrum matches reports in the literature[41] displaying a peak at 550 nm and a shoulder at 514 nm. The Cy3 absorption spectrum for the largest reverse micelle studied, w_0=30, is almost identical to that of Cy3 in water. This suggests that water molecules within the reverse micelle solvate the dye, which agrees with previous reports showing that water in reverse micelles take on the properties of bulk water for $w_0 \geq 15$[59]. As the environment becomes more confined, the peak at 550 nm gradually shifts to longer wavelength from w_0=15 to w_0=2. At the same time, the peak centered around 514 nm gradually becomes more intense as the size of the

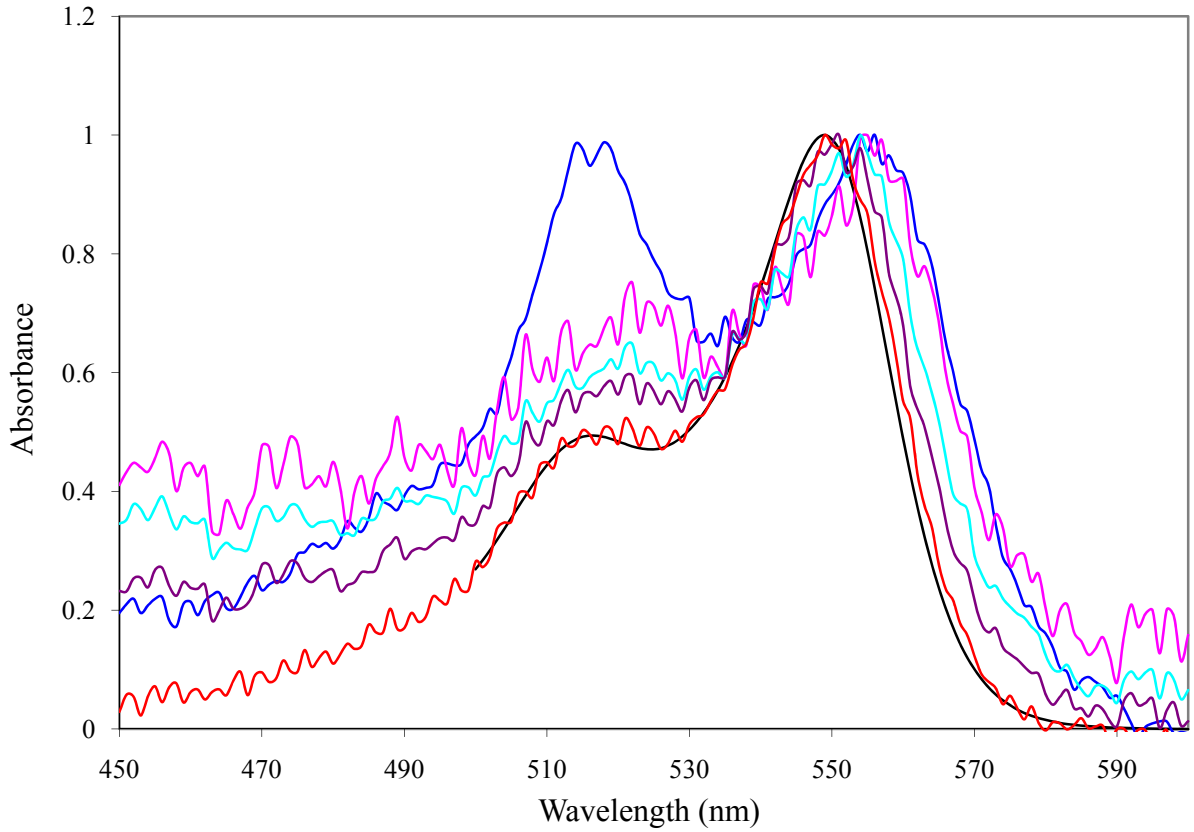

Figure 3.1: Normalized absorption spectra of Cy3 in a variety of environments; bulk water (black) and five different reverse micelle sizes, w_0=1 (blue), w_0=2 (pink), w_0=9 (turquoise), w_0=15 (purple) and w_0=30 (red). The concentration of Cy3 in the water sample is 9.9 x 10^{-5} M. In the five reverse micelle samples, the overall Cy3 concentration is held constant at 3.6 x 10^{-8} M. The concentration of AOT in the five reverse micelle samples is 0.02 M.

micelle becomes smaller. The most dramatic change occurs at w_0=1 where the spectrum shows that the peak shifts farther to the red than any other sample. Also, the peak at 514 nm now becomes as intense as the one shifted to the red. These spectra indicate that the dye in w_0=1 experiences a much different environment than when in bulk water.

Further spectroscopic changes appear in the normalized fluorescence emission spectra shown in Figure 3.2. For each spectrum, the overall Cy3 concentration is held constant at 3.6 x 10^{-8} M. Spectra displayed in the top panel (a) and the bottom panel (b) were excited at 532 nm and at 514 nm, respectively. Emission spectra shown for Cy3 in bulk water and in w_0=2-30 (Fig. 3.2a) do not vary significantly; the spectrum for Cy3 in w_0=1 broadens slightly and the primary peak at 570 nm is suppressed, consistent with the dye experiencing a more non-polar environment. However, fluorescence for Cy3 in the w_0=1 reverse micelle, shown in Figure 3.2b is fundamentally different than for all the other samples. The bottom panel shows that the fluorescence peaks at 600 nm. Furthermore, the inset panel shows a dramatic increase in the fluorescence intensity of Cy3 when in the extremely confined environment of the w_0=1 reverse micelle compared to the larger reverse micelles and aqueous solution. The quantum yield for Cy3 in a 0.2 w_0=1 reverse micelle sample for 514 nm and 532 nm excitation was calculated, referencing to an aqueous sample of Rhodamine 6G at the same overall dye concentration. Interestingly, the quantum yield for Cy3 in w_0=1 reverse micelles excited at 514 nm is ≈0.26 and at 532 nm is ≈ 0.48, both of which are a dramatic increase from the quantum yield of aqueous Cy3 (0.05). Moreover, this same calculation was carried out for Cy3 in a 0.2 M w_0=30 reverse micelle sample. This value was determined to be ≈

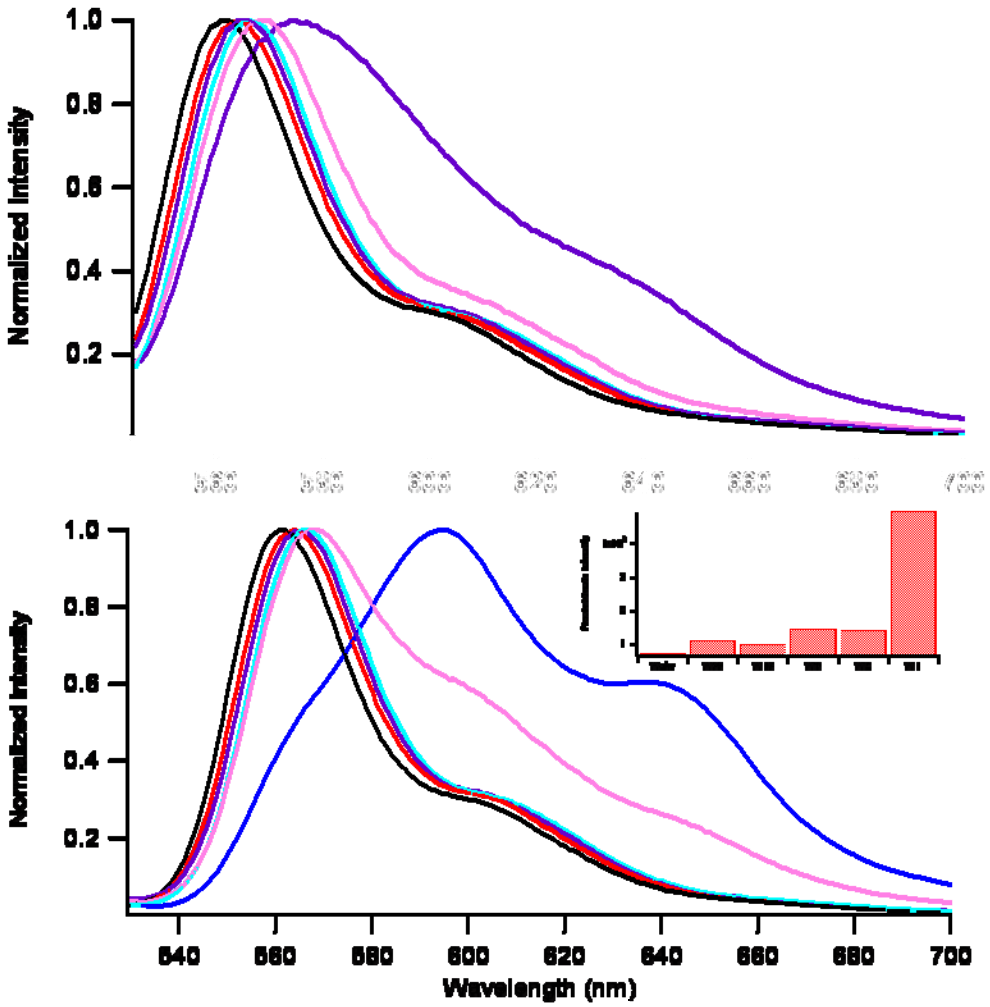

Figure 3.2: Normalized fluorescence emission spectra of Cy3 in different environments and at two different excitation wavelengths, 532 nm (top-a) and 514 nm (bottom-b). The different environments are as follows; bulk water (black) and five different reverse micelle sizes, w_0=1 (blue), w_0=2 (pink), w_0=9 (turquoise), w_0=15 (purple) and w_0=30 (red). Inset in the bottom panel shows the overall fluorescence intensity in each of the six samples, calculated from the area under the non-normalized emission curves. The concentration of Cy3 in all samples is 3.6 x 10^{-8} M and the concentration of AOT in the reverse micelle samples is 0.02 M.

0.09 at both the 514 nm and 532 nm excitation. The quantum yield in the w_0=30 is consistent with the quantum yield of aqueous Cy3. These data provide further evidence that a different form of the dye is present in the w_0=1 reverse micelle than from that observed in the larger reverse micelles and in bulk water.

Both absorption and fluorescence spectra of Cy3 suggest that the species probed in the w_0=1 reverse micelle is not a Cy3 monomer solvated in an aqueous environment. Various hypotheses could explain the observed spectra; despite the very low overall Cy3 concentration, it is hypothesized that the species observed is an H-aggregate of Cy3. The possibility that the reverse micelle environment stabilized the cis-form of the dye was considered. However, Jia and co-workers.[41] reported that the cis-isomer of Cy3 absorbs at 570 nm, much further to the red than the peak we observe at 514 nm in our absorption spectra eliminating this possibility. Also, a series of temperature dependent fluorescence emission experiments for Cy3 in w_0=1, w_0=2 and w_0=9 (Figures 3.3, 3.4 and 3.5) were performed. If the cis-isomer was being stabilized, we would expect to the fluorescence emission peaks at 600 nm and 650 nm decrease as the temperature decreased since a lower temperature should inhibit the rate of isomerization. The results show that the all three of the peaks increase with decreasing temperature for all three samples and thus the presence of the stabilized cis-isomer was ruled out.

The possibility that this species was a J-aggregate was also eliminated, because these aggregates absorb to the red (longer wavelengths) of the monomer peak[31, 60, 61]. The absorption spectra show an increased absorbance at shorter wavelength compared to the monomer peak, consistent with H-aggregation[48], The data also shows that the fluorescence intensity increases in the w_0=1 reverse micelle, which is consistent with the

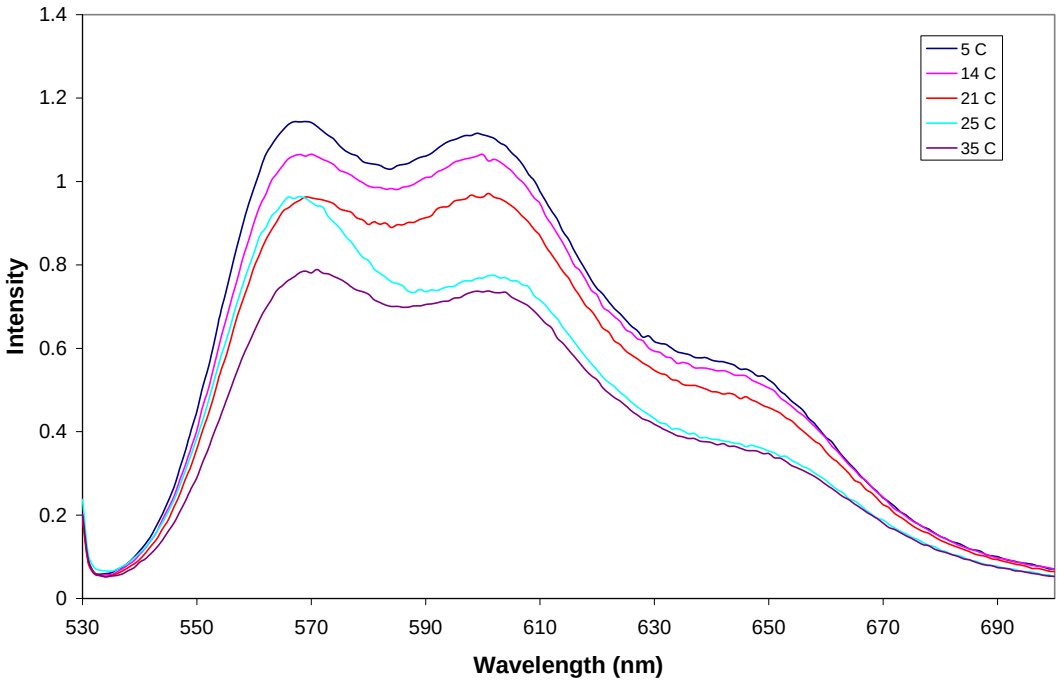

Figure 3.3: Temperature dependent fluorescence emission spectra for Cy3 in a w_0=1 reverse micelle performed at five different temperatures; 5 °C(blue), 14 °C (pink), 21°C (red), 25 °C and 35 °C(purple).

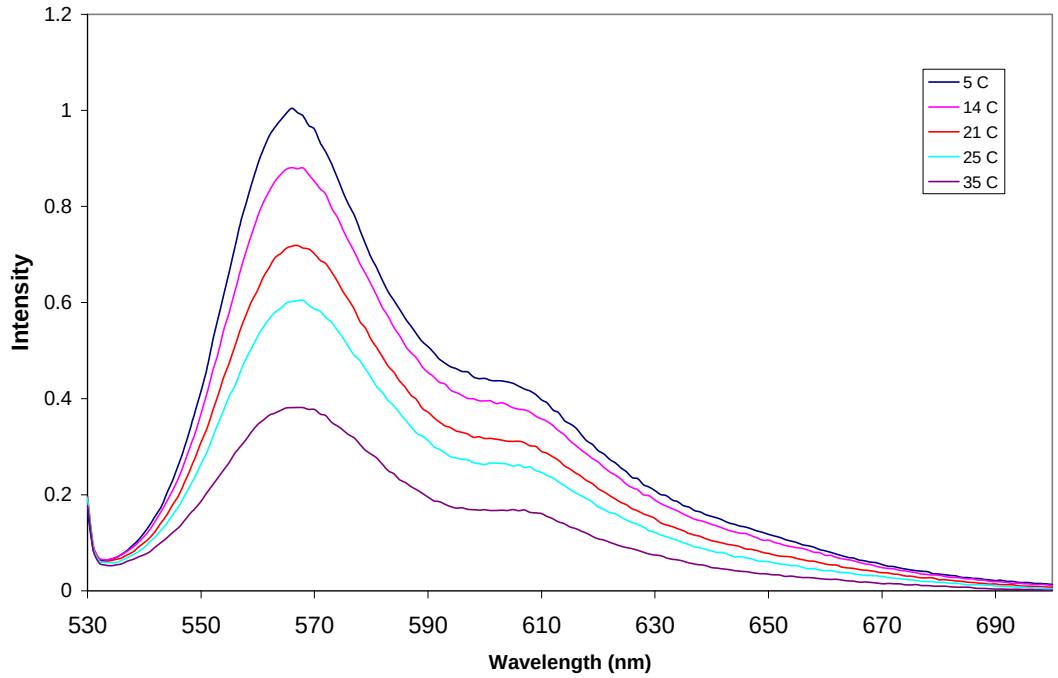

Figure 3.4: Temperature dependent fluorescence emission spectra for Cy3 in a w_0=2 reverse micelle performed at five different temperatures; 5 °C(blue), 14 °C (pink), 21°C (red), 25 °C and 35 °C(purple).

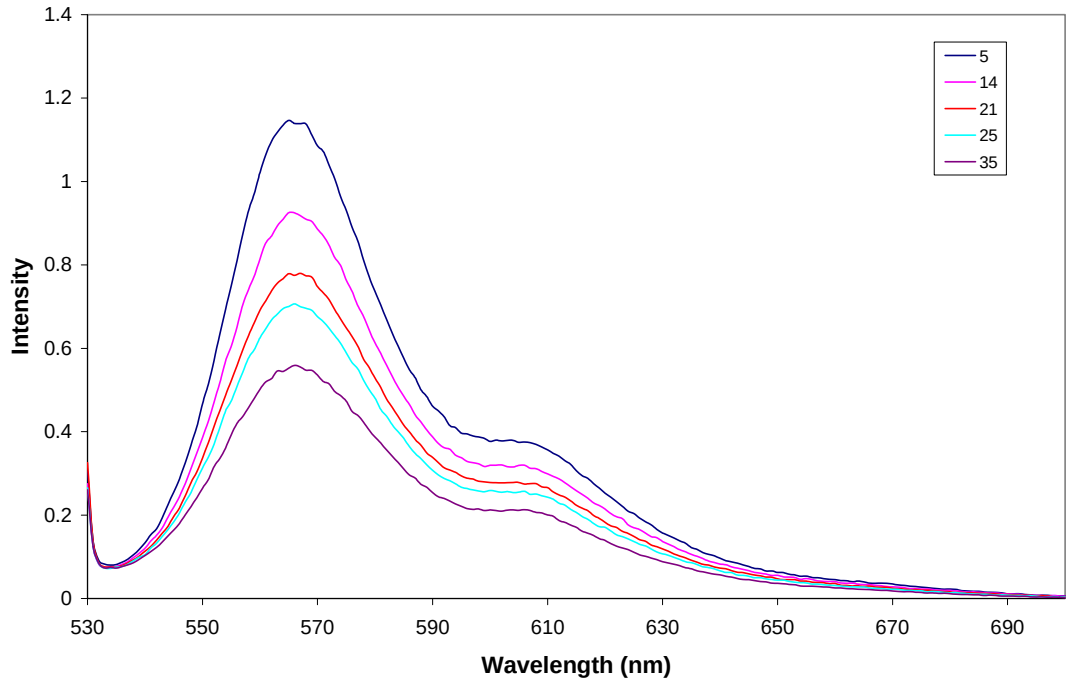

Figure 3.5: Temperature dependent fluorescence emission spectra for Cy3 in a w_0=9 reverse micelle performed at five different temperatures; 5 °C(blue), 14 °C (pink), 21°C (red), 25 °C and 35 °C(purple).

H-aggregate being in an extremely rigid and confined environment and thereby causing this species to be highly fluorescent[48]. Furthermore, the emission spectra show that th spectral features that arise are wavelength dependent. This indicates that the monomer form of the dye is also present in the w_0=1 as well as the H-aggregates and that we can selectively excite each form of the dye.

Further experiments investigated whether the new spectral features can be associated with a Cy3 aggregate. If this species is in fact an H-aggregate, the fluorescence spectra should depend on the overall Cy3 concentration inside the w_0=1 reverse micelle. Spectra of Cy3 in reverse micelles for different Cy3 concentrations are shown in Figure 3.6. At the lowest concentration, the spectral features closely resemble those seen for Cy3 in water and in larger reverse micelles. The emission maximum appears at 560 nm and with a shoulder at 600 nm. As the concentration increases, the emission maximum shifts to 600 nm and the peak at 560 nm decreases. Thus, as the concentration of Cy3 increases, the emission spectrum increasingly diverges from that seen in water and the larger micelles, indicating the presence of a new species at higher concentrations. The concentration dependence of this behavior suggests we are probing an H-aggregate in the w_0=1 reverse micelles.

If the spectral features observed arise due to H-aggregation, then the spectra should also depend on the overall AOT concentration. As the AOT concentration increases, the number of reverse micelles increases. With more reverse micelles in a sample, the probability of at least two Cy3 molecules coming in contact decreases and thus we expect to see less aggregation behavior as the concentration of AOT increases. To investigate this hypothesis, fluorescence emission experiments were carried out in

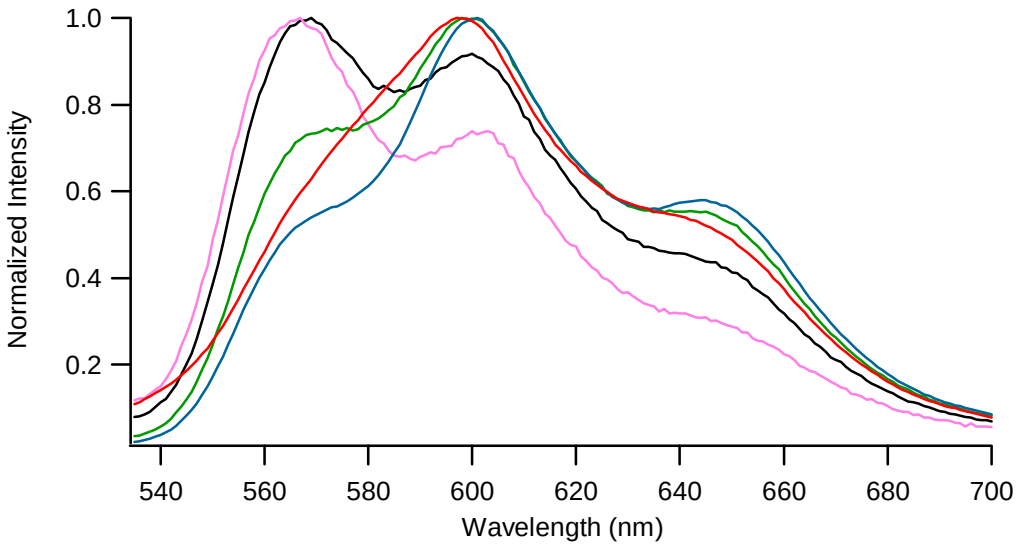

Figure 3.6: Normalized fluorescence emission spectra of Cy3 in a 0.02 M AOT w_0=1 reverse micelle sample at different overall concentrations of Cy3. The five concentrations analyzed are; 3.6 x10^{-8} M (red), 1.8 x10^{-8} M (blue), 8.9 x10^{-8} M (green), 3.6 x10^{-9} M (black) and 1.8 e-09 M (pink).

which the overall Cy3 concentration was held constant at 1.8 x 10^{-8} M and the reverse micelle size was fixed to w_0=1, but AOT concentration was varied. Figure 3.7 shows the spectra of Cy3 as a function of AOT concentration and at two different excitation wavelengths, 532 nm and 514 nm. The spectra at higher AOT concentration diverge less from the Cy3 spectrum in bulk water. This result further supports the hypothesis that this extremely confined environment drives the aggregation of the Cy3 molecules.

Another experiment to confirm the presence of H-aggregates measured the fluorescence lifetime of Cy3 in different environments. The lifetime of the H-aggregate is expected to be longer than that of the Cy3 monomer[48]. The data presented in Table 3.1 shows the fluorescence lifetime data for Cy3 in water, and in w_0=30 and w_0=1 reverse micelle samples. The data for Cy3 in water agrees with literature reports [55]. In the w_0=30 reverse micelle environment, the fluorescence decay displays two distinct components, consistent with the dye experiencing different environments over the course of its lifetime. The data is most interesting in the w_0=1, where not only is the decay biexponential, but the slower component gets significantly longer than in bulk water or larger reverse micelle sizes. To explore the nature of the longer component, the fluorescence lifetimes of Cy3 in the w_0=1, exciting it at 514 nm and collecting the emission at 561 nm, 600 nm and 650 nm, corresponding to the three peaks we observe in the emission spectrum was measured. Figure 3.8 shows the decays measured at 561 nm and 650 nm and results from biexponential fits are given in Table 3.2. The lifetimes measured are longer when monitoring the longer wavelength emission; this is attributed to the presence of H-aggregates, which is consistent with H-aggregates of other cyanine dyes[48].

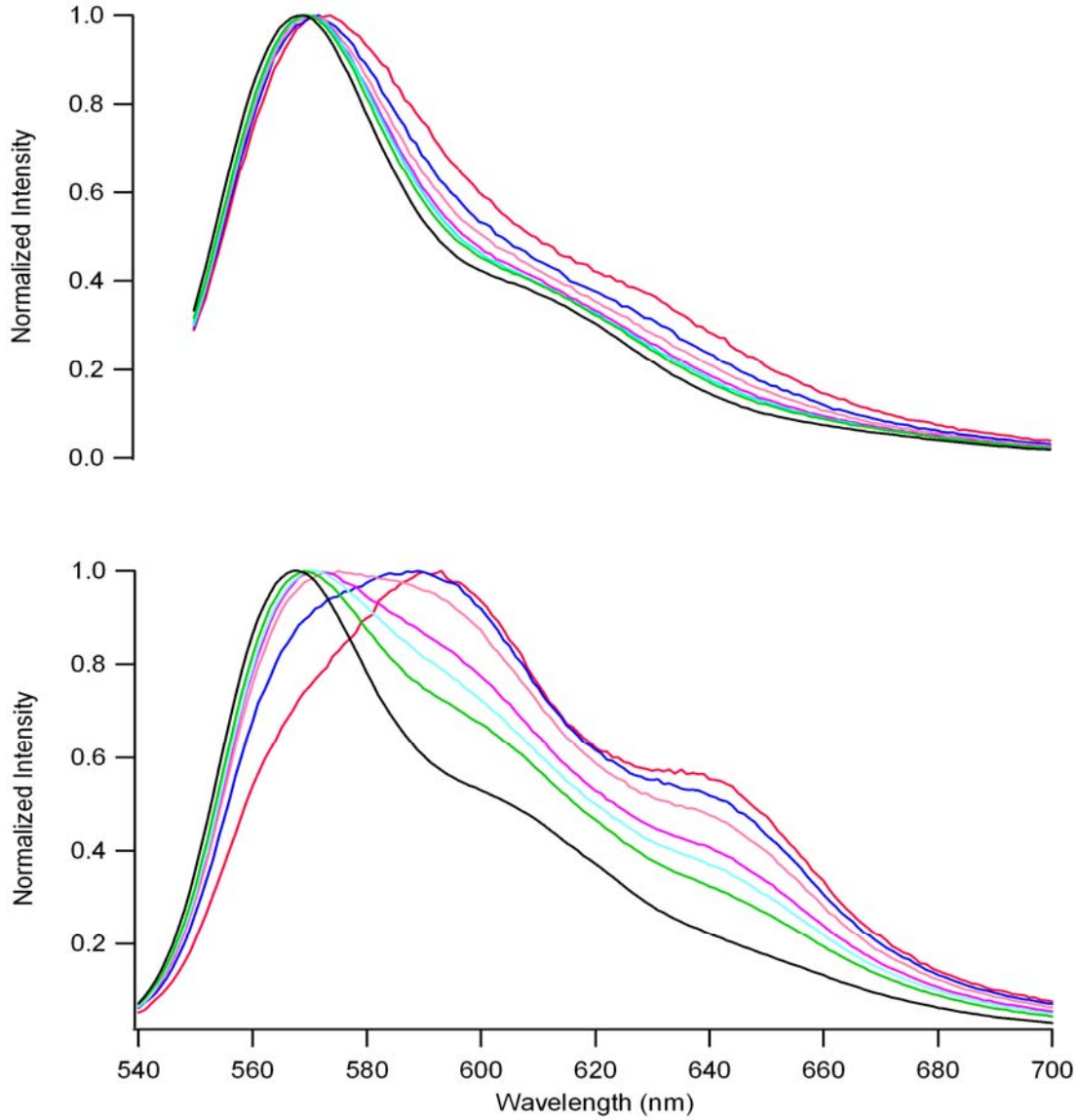

Figure 3.7: Normalized fluorescence emission spectra of Cy3 in w_0=1 reverse micelles as a function of AOT concentration and excitation wavelength, 532 nm (top) and 514 nm (bottom). The overall Cy3 concentration in all samples is 1.8 x10^{-8} M. The AOT concentration for each spectrum are as follows; 0.01 M (red), 0.02 M (blue), 0.04 M (pink), 0.06 M (purple), 0.08 M (turquoise), 0.1 M (green) and 0.2 M (black).

Sample	T_1 (%)	T_2 (%)
H_2O	0.284 ± 0.007 ns (100)	N/A
w_0=30	0.259 ± 0.010 ns (45)	3.02 ± 0.014 ns (55)
w_0=1	1.79 ± 0.017 ns (84)	6.88 ± 0.126 ns (14)

Table 3.1: Fluorescence lifetime data of Cy3 in three different environments; Water, w_0=30 and w_0=1. The samples were excited at 514 nm and the emission collected at 561 nm. The concentration of Cy3 is 3.6 x 10^{-8} M and the concentration of AOT in the reverse micelle sample is 0.02 M.

Wavelength	T_1 (%)	T_2 (%)
561 nm	1.79 ± 0.017 ns (84.09)	6.88 ± 0.126 ns (14.09)
600 nm	1.98 ± 0.018 ns (61.47)	10.4 ± 0.091 ns(38.53)
650 nm	1.73 ± 0.037 ns (60.21)	8.74 ± 0.161 ns (39.79)

Table 3.2: Fluorescence lifetime data of Cy3 in w_0=1. The samples were excited at 514 nm and the lifetime measured at three different wavelengths, 561 nm, 600 nm and 650 nm. The concentration of Cy3 is 3.6 x 10^{-8} M and the concentration of AOT is 0.02 M. Note the error bars represent the error in the fit of the data.

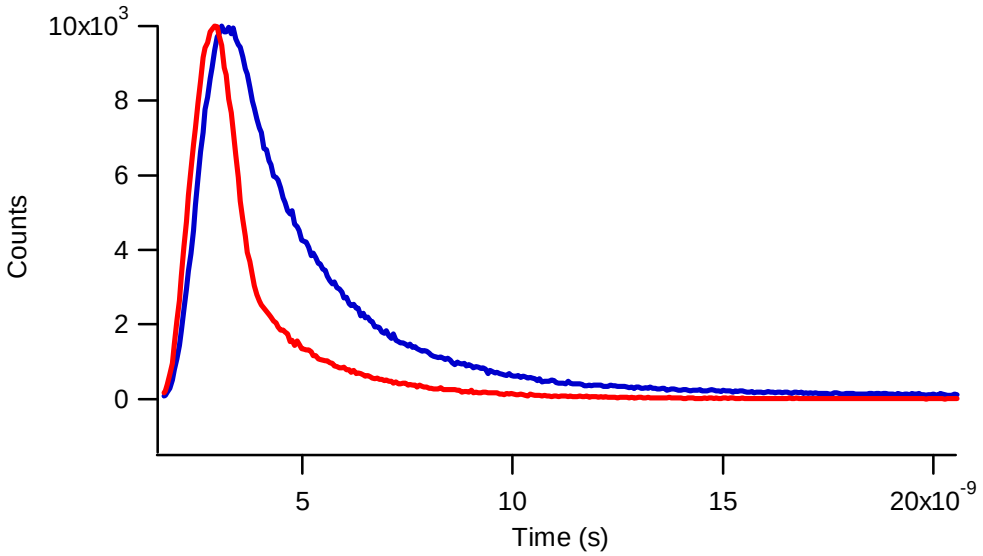

Figure 3.8: Fluorescence lifetime data of Cy3 inside a w_0=1 reverse micelle excited at 514 nm and collected at 561 nm (red) and 600 nm (blue). The concentration of Cy3 is 3.6 x 10^{-8} M and the concentration of AOT is 0.02 M.

If the species excited at 514 nm is the H-aggregate, then exciting the same samples at a longer wavelength should produce spectra that are consistent with the monomer Cy3 molecules that are also present in the system. This was confirmed by the fluorescence emission experiments shown in Figure 3.2, where different spectral features arise when exciting Cy3 in the w_0=1 at 514 nm and 532 nm. To further investigate, fluorescence excitation experiments were carried out at three different monitoring wavelengths, 561 nm, 600 nm and 650 nm. Figure 3.9 shows that emission at 600 and 650 nm correlates with absorption at a shorter wavelength compared to emission at 560 nm. Figures 3.10 and 3.11 show the results of the same fluorescence excitation experiment but for Cy3 in w_0=2 and w_0=9, respectively. The spectra show there is no correlation between the excitation wavelength and the resulting fluorescence spectra for w_0=2 and w_0=9. This indicates that only one form of the dye is present, consistent with our previous results. This data provides further evidence that two forms of the dye exist in our sample and that each form can be accessed by exciting the samples at different wavelengths.

The results show that the smallest reverse micelle provides a unique environment that drives Cy3 to undergo reactions that would otherwise not occur. The w_0=1 reverse micelles behave as nanoreactors that drive the formation of H-aggregates at extremely low overall dye concentrations. In the presence of larger reverse micelles, where the environment begins to resemble that of bulk water, this behavior is not seen. Yet, in the extremely confined environment of the smallest reverse micelles, there is a driving force, which causes these dye molecules to come together and form highly fluorescent H-aggregates. This result is highly unexpected, as the concentration of dye molecules is so

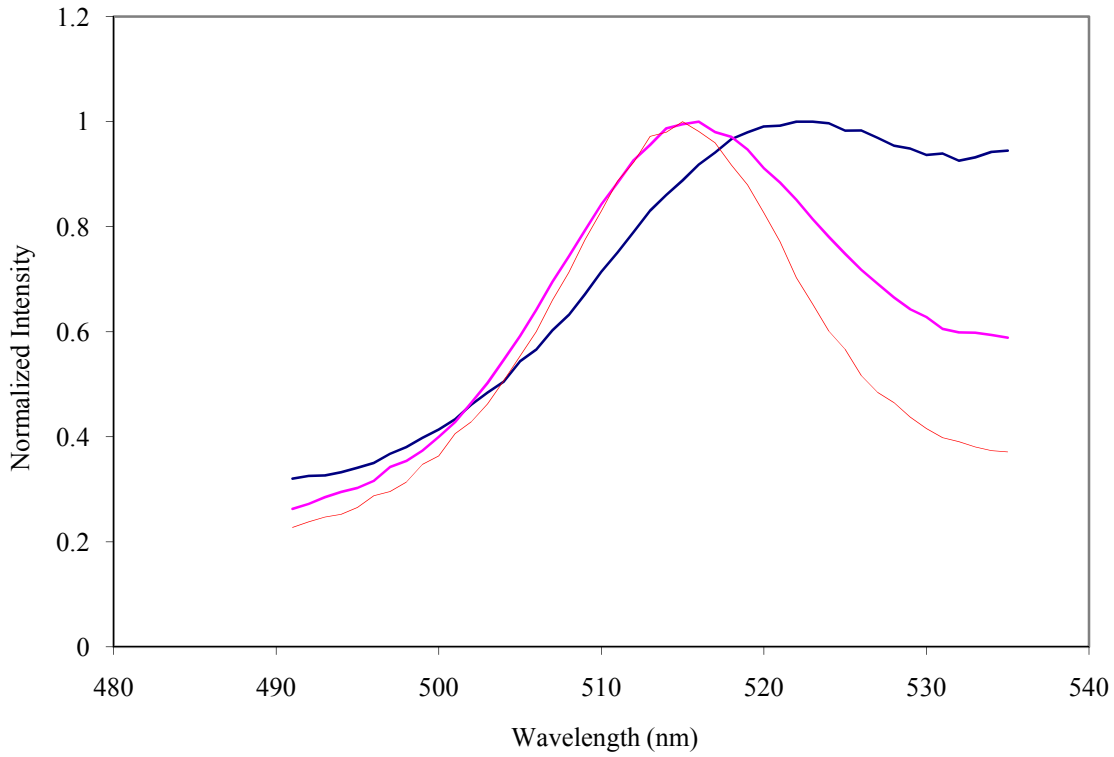

Figure 3.9: Normalized fluorescence excitation spectra for Cy3 in a 0.02 M AOT w_0=1 reverse micelle sample, monitored at three different emission wavelengths; 561 nm (blue), 600 nm (pink) and 650 nm (red). The concentration of Cy3 is 3.6 x 10^{-8} M.

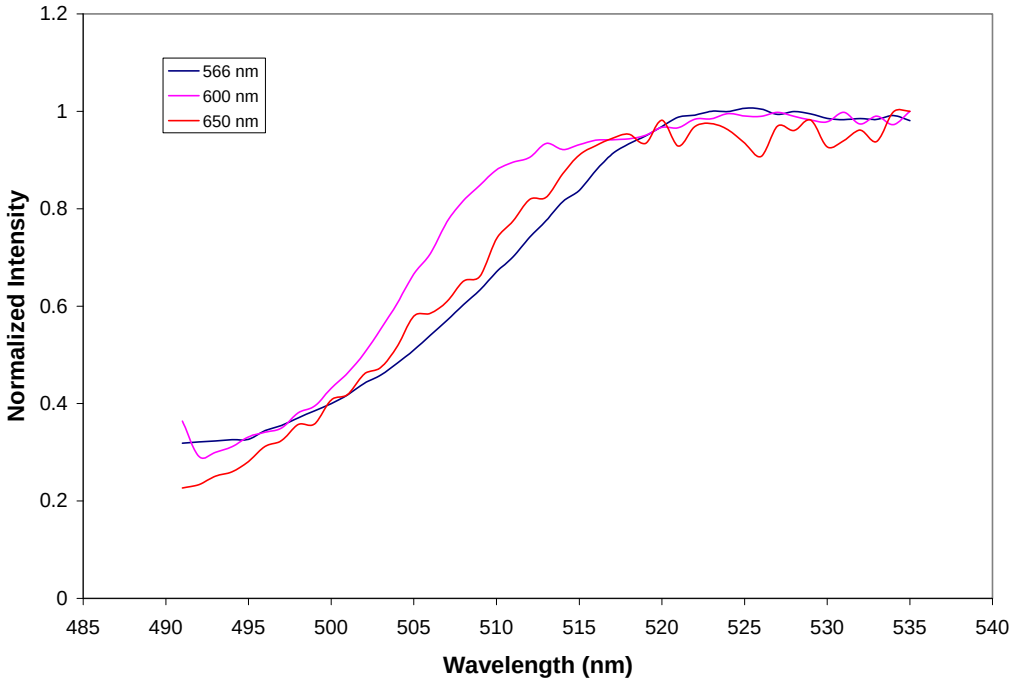

Figure 3.10: Fluorescence excitation spectra for Cy3 in a 0.02 M AOT w_0=2 reverse micelle sample as a function of the emission wavelength. The emission wavelength for each experiment was; 570 nm (blue), 600 nm (pink) and 650 nm (red). The concentration of Cy3 is 3.6 x 10^{-8} M.

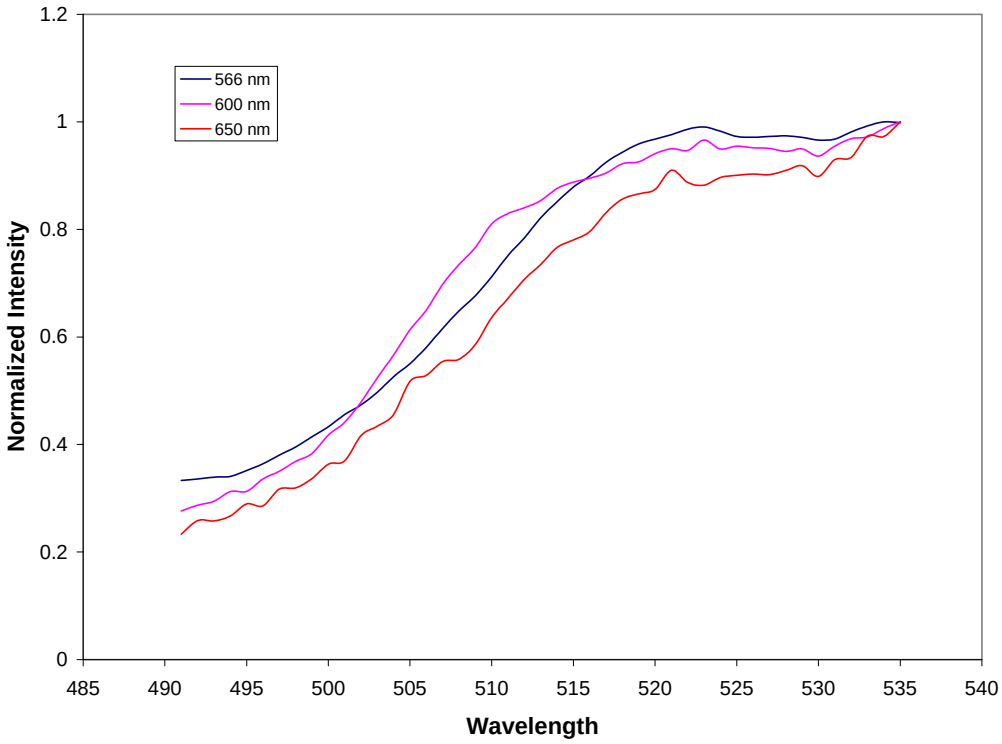

Figure 3.11: Fluorescence excitation spectra for Cy3 in a w_0=9 reverse micelle sample as a function of the emission wavelength. The emission wavelength for each experiment was; 570 nm (blue), 600 nm (pink) and 650 nm (red). The concentration of Cy3 is 3.6 x 10^{-8} M.

low compared to the concentration of reverse micelles that the occupation number for our system ranges from one Cy3 molecule per 20,000 to 900,000 reverse micelles.

A range of initial rates were calculated for the given concentrations for the reaction of two dye molecules, each contained within an individual reverse micelle, using the equation:

$$rate_0 = k_D [A_0]^2 \qquad (3.3)$$

where, k_D is the diffusion limited rate constant and A_0 is the initial Cy3 concentration. Solving for equation 3.2 gives an initial rate that ranges from 1.8×10^{-5} to 4.5×10^{-8}. Furthermore, the half-life, $\tau_{1/2}$, is given by the equation:

$$\tau_{1/2} = \frac{1}{k_D [A_0]} \qquad (3.4)$$

which ranges from ≈ 2 to 40 ms. Thus, although the occupation number for our system is extremely low, the rate of collisions between the reverse micelles is such that it is feasible for this aggregation to occur. It is hypothesized that as two individual reverse micelles come in contact, each containing a Cy3 molecule, the local concentration is so high that the reaction is favored toward the formation of the Cy3 aggregate. Changes observed in the spectroscopy of Cy3 in the w_0=2 reverse micelle (see Figures 3.4 and 3.5), indicating that this could be a point where the formation of H-aggregates starts to become possible.

A set of experiments to determine the overall equilibrium constant for the association/dissociation of the Cy3 aggregate were carried. The goal of these experiments was to obtain information about the relative concentrations of monomer and dimer in each sample. To do so, the fluorescence emission for varying concentrations of Cy3 in w_0=1 reverse micelles excited at 514 nm was measured. The results of this experiment are shown in Figure 3.12. Assuming that the predominant form of the H-aggregate is a Cy3 dimer, a series of equations were derived to analyze the data shown in Figure 3.12.

First, the mass balance equation for our system is:

$$[A_0] = [A] + 2[A_2] \tag{3.5}$$

where, A_0 is the overall Cy3 concentration, A is the concentration of Cy3 monomer and A_2 is the concentration of Cy3 dimer. The equilibrium constant governing the association/dissociation reaction is then given by:

$$K = \frac{[A_2]}{[A]^2} = \frac{[A_2]}{[A_0]^2 - 4[A_2][A_0] + 4[A_2]^2} \tag{3.6}$$

solving equation 7 for $[A_2]$ yields:

$$[A_2] = \left[\frac{(4KA_0 + 1) - \sqrt{8KA_0 + 1}}{8K} \right]. \tag{3.7}$$

Second, we assumed the fluorescence emission shown in Figure 3.7 is determined by the equation:

$$F = \varepsilon_m [A] + \varepsilon_d [A_2] \tag{3.8}$$

where, F is the total fluorescence emission, ε_m is the molecular brightness of the monomer and ε_d is the molecular brightness of the dimer. The molecular brightness is a quantity that depends on the absorption cross-section and quantum yield of the species being probed as well as the collection efficiency of the optical setup. Given the mass balance in equation 3.6, we obtain the following expression:

$$F = \varepsilon_m [A_0 - 2A_2] + \varepsilon_d [A_2] \tag{3.9}$$

and substituting equation 3.8 into equation 3.10 gives:

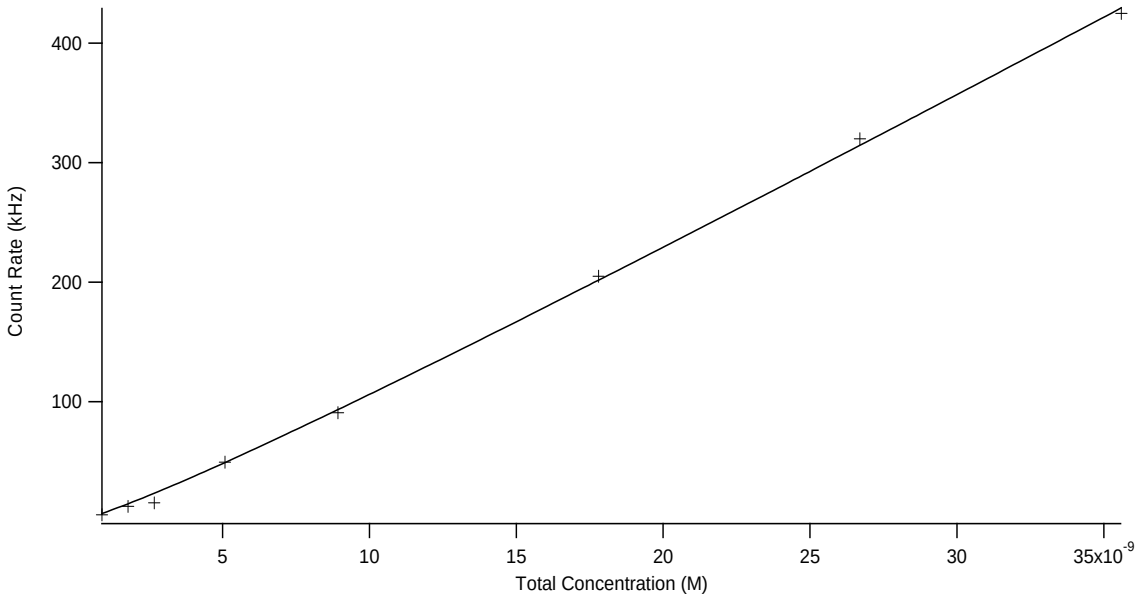

Figure 3.12: Total fluorescence for varying concentrations of Cy3 in 0.02 M AOT w_0=1 reverse micelle samples excited at 514 nm. The concentration of Cy3 ranges from 1.78 10^{-9} M to 3.56 x 10^{-8} M. The data was analyzed to equation 5 and the resulting fit line is shown.

$$F = \varepsilon_m A_0 - 2\varepsilon_m \left[\frac{(4KA_0 + 1) - \sqrt{8KA_0 + 1}}{8K} \right] + \varepsilon_d \left[\frac{(4KA_0 + 1) - \sqrt{8KA_0 + 1}}{8K} \right]. \quad (4.10)$$

The fluorescence intensity for varying Cy3 concentrations is shown in Figure 7. This data was fit to equation 11 using K and ε_d as adjustable parameters. To calculate ε_m, we assumed that the fluorescence emission at the lowest Cy3 concentration, 8.93 x 10^{-10} M, arose predominantly from the Cy3 monomer. This gives a value for $\varepsilon_m \approx 6 \times 10^9$ counts s^{-1} nM^{-1}. To provide an initial estimate for ε_d, we assumed that the fluorescence emission at the highest Cy3 concentration was predominantly from the Cy3 dimer. This gives a value for $\varepsilon_d \approx 2.4 \times 10^{10}$ counts s^{-1} nM^{-1}. From this analysis, we determined $K \approx (1.4 \pm 0.7) \times 10^8$ and $\varepsilon_d \approx (2.9 \pm 0.16) \times 10^{10}$ counts s^{-1} nM^{-1}.

In the following chapter, fluorescence correlation spectroscopy is used to investigate the kinetics of the Cy3 H-aggregation in reverse micelles. The results indicate that the formation of Cy3 H-aggregates is accompanied by the formation of a transient dimer complex between two reverse micelles. The equilibrium constant calculated here is used to determine the kinetic rate parameters of the Cy3 labeled reverse micelles.

3.4 Conclusion

Steady-state and time-resolved spectroscopy has been used to investigate the effect of reverse micelle environment on Cy3 dye molecules. We observed that the dye begins to aggregate under the extremely confined condition of the w_0=1 reverse micelle, which changes both the spectroscopy and the fluorescence lifetime compared to that of the monomer. Furthermore, it is possible to access each form of the dye, depending on the excitation wavelength. What is most interesting about these results is that this behavior is not seen at the same overall concentrations in bulk water or in the larger reverse micelles. This suggests that the w_0=1 reverse micelles provide a unique environment for the dye to undergo reactions that would

not occur in bulk solution. Moreover, this unexpected aggregation is very interesting considering that the occupation number of the reverse micelles ranges from 1 Cy3 molecule per 20,000 to 900,000 reverse micelles. Furthermore, this aggregation behavior is not observed in the larger reverse micelles and bulk water. The results of this study indicate that the reverse micelle environment can provide a catalyst to cause reactions to occur that would not occur under bulk solution conditions. These results are relevant for studying molecular behavior in extremely confined biological environments such as cells, organelles, and nucleotides.

1. De, T. K.; Maitra, A., Solution Behavior of Aerosol-OT in Non-polar Solvents Reverse Micelles. *Advances in Colloid and Interface Science* **1995,** 59, 95-193.

2. Eicke, H. F.; Christen, H., Stability of Micelles in Apolar Media. *Journal of Colloid and Interface Science* **1974,** 46, (3), 417-436.

3. Fletcher, P. D. I.; Howe, A. M.; Robinson, B. H., The Kinetics of Solubilisate Exchange Between Water Droplets of a Water-in-oil Microemulsion. *Journal of The Chemical Society-Faraday Transactions I* **1987,** 83, 985-1006.

4. Leodidis, E. B.; Hatton, T. A., Specific Ion Effects in Electrical Double Layers-Selective Solubilization of Cations in Aeresol-OT Reversed Micelles. *Langmuir* **1989,** 5, (3), 741-753.

5. Eicke, H. F., Aggregation in Surfactant Solutions - Formation and Properties of Micelles and Microemulsions. *Pure and Applied Chemistry* **1980,** 52, (5), 1349-1357.

6. Eicke, H. F., Physical Investigation of the Formation and Properties of Aqueous Microphases. *Pharmaceutica Acta Helvetiae* **1982,** 57, (12), 322-329.

7. Eicke, H. F.; Kubik, R., Optical Matching Phenomenon in Water-Oil Microemulsions. *Berichte Der Bunsen-Gesellschaft-Physical Chemistry Chemical Physics* **1980,** 84, (1), 36-41.

8. Eicke, H. F.; Kubik, R., Concentrated Dispersions of Aqueous Polyelectrolyte-Like Microphases in Non-polar Hydrocarbons. *Faraday Discussions* **1983,** 76, 305-315.

9. Eicke, H. F.; Rehak, J., Formation of Water-Oil-Microemulsions. *Helvetica Chimica Acta* **1976,** 59, (8), 2883-2891.

10. Zulauf, M.; Eicke, H. F., Inverted Micelles and Microemulsions in the Ternary-System H2O-Aerosol-OT-Isooctane as Studied by Photon Correlation Spectroscopy *Journal of Physical Chemistry* **1979,** 83, (4), 480-486.

11. Baruah, B.; Crans, D. C.; Levinger, N. E., Simple Oxovanadates as Multiparameter Probes of Reverse Micelles. *Langmuir* **2007,** 23, (12), 6510-6518.

12. Baruah, B.; Roden, J. M.; Sedgwick, M.; Correa, N. M.; Crans, D. C.; Levinger, N. E., When is Water not Water? Exploring Water Confined in Large Reverse Micelles Using a Highly Charged Inorganic Molecular Probe
Journal Of The American Chemical Society **2006,** 128, (39), 12758-12765.

13. Baruah, B.; Swafford, L. A.; Crans, D. C.; Levinger, N. E., Do Probe Molecules Influence Water in Confinement? *Journal Of Physical Chemistry B* **2008,** 112, (33), 10158-10164.

14. Correa, N. M.; Levinger, N. E., What Can You Learn from a Molecular Probe? New Insights on the Behavior of C343 in Homogeneous Solutions and AOT Reverse Micelles. *Journal Of Physical Chemistry B* **2006,** 110, (26), 13050-13061.

15. Crans, D. C.; Baruah, B.; Levinger, N. E., Oxovanadates: A Novel Probe for Studying Lipid-Water Interfaces. *Biomedicine & Pharmacotherapy* **2006,** 60, (4), 174-181.

16. Crans, D. C.; Rithner, C. D.; Baruah, B.; Gourley, B. L.; Levinger, N. E., Molecular Probe Location in Reverse Micelles Determined by NMR Dipolar Interactions. *Journal of the American Chemical Society* **2006,** 128, (13), 4437-4445.

17. Crans, D. C.; Trujillo, A. M.; Bonetti, S.; Rithner, C. D.; Baruah, B.; Levinger, N. E., Penetration of Negatively Charged Lipid Interfaces by the Doubly Deprotonated Dipicolinate. *Journal Of Organic Chemistry* **2008,** 73, (24), 9633-9640.

18. Falcone, R. D.; Correa, N. M.; Biasutti, M. A.; Silber, J. J., Properties of AOT Aqueous and Nonaqueous Microemulsions Sensed by Optical Molecular Probes. *Langmuir* **2000,** 16, (7), 3070-3076.

19. Harpham, M. R.; Ladanyi, B. M.; Levinger, N. E., The Effect of the Counterion on Water Mobility in Reverse Micelles Studied by Molecular Dynamics Simulations. *Journal Of Physical Chemistry B* **2005,** 109, (35), 16891-16900.

20. Harpham, M. R.; Levinger, N. E.; Ladanyi, B. M., An Investigation of Water Dynamics in Binary Mixtures of Water and Dimethyl Sulfoxide. *Journal Of Physical Chemistry B* **2008,** 112, (2), 283-293.

21. Moilanen, D. E.; Levinger, N. E.; Spry, D. B.; Fayer, M. D., Confinement or the Nature of the Interface? Dynamics of Nanoscopic Water. *Journal of the American Chemical Society* **2007,** 129, (46), 14311-14318.

22. Roess, D. A.; Smith, S. M. L.; Winter, P.; Zhou, J.; Dou, P.; Baruah, B.; Trujillo, A. M.; Levinger, N. E.; Yang, X. D.; Barisas, B. G.; Crans, D. C., Effects of Vanadium-Containing Compounds on Membrane Lipids and on Microdomains Used in Receptor-Mediated Signaling. *Chemistry & Biodiversity* **2008,** 5, (8), 1558-1570.

23. Tan, H. S.; Piletic, I. R.; Riter, R. E.; Levinger, N. E.; Fayer, M. D., Dynamics of Water Confined on a Nanometer Length Scale in Reverse Micelles: Ultrafast Infrared Vibrational Echo Spectroscopy. *Physical Review Letters* **2005,** 94, (5).

24. Abuin, E.; Lissi, E.; Solar, C., Effect of Urea on the Enzymatic Activity of a Lipase Entrapped in AOT-Heptane-Water Reverse Micellar Solutions. *Journal of Colloid and Interface Science* **2005,** 283, (1), 87-93.

25. Correa, N. M.; Durantini, E. N.; Silber, J. J., Catalysis in Micellar Media. Kinetics and Mechanism for the Reaction of 1-Fluoro-2,4-Dinitrobenzene with N-Butylamine and

Piperidine in N-Hexane and AOT/N-Hexane/Water Reverse Micelles . *Journal of Organic Chemistry* **1999,** 64, (16), 5757-5763.

26. Martinek, K.; Levashov, A. V.; Klyachko, N.; Khmelnitski, Y. L.; Berezin, I. V., Micellar Enzymology. *European Journal of Biochemistry* **1986,** 155, (3), 453-468.

27. Menger, F. M.; Yamada, K., Enzyme Catalysis In Water Pools. *Journal Of The American Chemical Society* **1979,** 101, (22), 6731-6734.

28. Novaira, M.; Moyano, F.; Biasutti, M. A.; Silber, J. J.; Correa, N. M., An Example of How to Use AOT Reverse Micelle Interfaces to Control a Photoinduced Intramolecular Charge-Transfer Process. *Langmuir* **2008,** 24, (9), 4637-4646.

29. Correa, N. M.; Zorzan, D. H.; Chiarini, M.; Cerichelli, G., Reverse Micellar Aggregates: Effect on Ketone Reduction. I. Substrate Role. *Journal of Organic Chemistry* **2004,** 69, (24), 8224-8230.

30. Correa, N. M.; Zorzan, D. H.; D'Anteo, L.; Lasta, E.; Chiarini, M.; Cerichelli, G., Reverse Micellar Aggregates: Effect on Ketone Reduction. 2. Surfactant Role. *Journal of Organic Chemistry* **2004,** 69, (24), 8231-8238.

31. Cherny, D. I.; Eperon, I. C.; Bagshaw, C. R., Probing Complexes With Single Fluorophores: Factors Contributing to Dispersion of FRET in DNA/RNA Duplexes. *European Biophysics Journal With Biophysics Letters* **2009,** 38, (4), 395-405.

32. Conley, N. R.; Biteen, J. S.; Moerner, W. E., Cy3-Cy5 Covalent Heterodimers for Single-Molecule Photoswitching. *Journal Of Physical Chemistry B* **2008,** 112, (38), 11878-11880.

33. Dempster, D. N.; Thompson, G. F.; Morrow, T.; Rankin, R., Photochemical Characteristics of Cyanine Dyes .1. 3,3'-Diethyloxadicarbocyanine Iodide. *Journal Of The Chemical Society-Faraday Transactions Ii* **1972,** 68, 1479-&.

34. Hoebeke, M.; Piette, J.; Vandevorst, A., Viscosity-Dependent Isomerization and Fluorescence Yields of Merocyanine 540. *Journal Of Photochemistry And Photobiology B-Biology* **1990,** 4, (3), 273-282.

35. Kuzmin, V. A.; Darmanyan, A. P., Study of Sterically Hindered Short-Lived Isomers of Polymethine Dyes By Laser Photolysis. *Chemical Physics Letters* **1978,** 54, (1), 159-163.

36. Luschtinetz, F.; Dosche, C.; Kumke, M. U., Influence of Streptavidin on the Absorption and Fluorescence Properties of Cyanine Dyes. *Bioconjugate Chemistry* **2009,** 20, (3), 576-582.

37. Momicchioli, F.; Baraldi, I.; Berthier, G., Theoretical-Study Of Trans Cis Photoisomerism In Polymethine Cyanines. *Chemical Physics* **1988,** 123, (1), 103-112.

38. Redmond, R. W.; Kochevar, I. E.; Krieg, M.; Smith, G.; McGimpsey, W. G., Excited State Relaxation In Cyanine Dyes: A Remarkably Efficient Reverse Intersystem Crossing From Upper Triplet Levels. *Journal Of Physical Chemistry A* **1997,** 101, (15), 2773-2777.

39. Rentsch, S. K.; Danielius, R. V.; Gadonas, R. A., Picosecond Time-Resolved Kinetic-Studies On The Formation of Short-Lived Pseudoisocyanine Iodide Photoisomers In Methanol And Ethylene-Glycol. *Chemical Physics Letters* **1981,** 84, (3), 450-453.

40. Rentsch, S. K.; Danielius, R. V.; Gadonas, R. A.; Piskarskas, A., Picosecond Kinetics and Transient Spectra of Pseudoisocyanine Monomers and J-Aggregates in Aqueous-Solution. *Chemical Physics Letters* **1981,** 84, (3), 446-449.

41. Rentsch, S. K.; Fassler, D.; Hampe, P.; Danielius, R.; Gadonas, R., Picosecond Time-Resolved Spectroscopic Studies of A Monomer Dimer System of 3,3'-Diethyl Thiacarbocyanine Iodide in Aqueous-Solution. *Chemical Physics Letters* **1982,** 89, (3), 249-253.

42. Rentsch, S. K.; Gadonas, R. A.; Piskarskas, A., Picosecond Spectroscopic Study of the Influence of the Solvent on the Photoisomerization and Relaxation of a Streptocyanine Dye. *Chemical Physics Letters* **1984,** 104, (2-3), 235-239.

43. Sun, Y. S.; Landry, J. P.; Fei, Y. Y.; Zhu, X. D., Effect of Fluorescently Labeling Protein Probes on Kinetics of Protein-Ligand Reactions. *Langmuir* **2008,** 24, (23), 13399-13405.

44. Sundstrom, V.; Gillbro, T.; Bergstrom, H., Picosecond Kinetics of Radiationless Relaxations of Triphenyl Methane Dyes - Evidence For A Rapid Excited-State Equilibrium Between States of Differing Geometry *Chemical Physics* **1982,** 73, (3), 439-458.

45. Velsko, S. P.; Fleming, G. R., Solvent Influence on Photochemical Isomerizations - Photophysics of DODCI. *Chemical Physics* **1982,** 65, (1), 59-70.

46. Volke, D.; Hoffmann, R., Quantitative proteomics by fluorescent labeling of cysteine residues using a set of two cyanine-based or three rhodamine-based dyes. *Electrophoresis* **2008,** 29, (22), 4516-4526.

47. Aramendia, P. F.; Duchowicz, R.; Scaffardi, L.; Tocho, J. O., Photophysical Characterization of a Photochromic System - The Case of Merocyanine-540. *Journal Of Physical Chemistry* **1990,** 94, (4), 1389-1392.

48. Bergmann, K.; Okonski, C. T., A Spectroscopic Study of Methylene Blue Monomer, Dimer, and Complexes With Montmorillonite. *Journal Of Physical Chemistry* **1963,** 67, (10), 2169-&.

49. Dipaolo, R. E.; Scaffardi, L. B.; Duchowicz, R.; Bilmes, G. M., Photoisomerization Dynamics and Spectroscopy of the Polymethine Dye DTCI. *Journal Of Physical Chemistry* **1995,** 99, (38), 13796-13799.

50. Jia, K.; Wan, Y.; Xia, A. D.; Li, S. Y.; Gong, F. B.; Yang, G. Q., Characterization of Photoinduced Isomerization and Intersystem Crossing of the Cyanine Dye Cy3. *Journal Of Physical Chemistry A* **2007,** 111, (9), 1593-1597.

51. West, W.; Pearce, S.; Grum, F., Steroisomerism in Cyanine Dyes-Meso-Substituted Thiacarbocyanines. *Journal Of Physical Chemistry* **1967,** 71, (5), 1316-&.

52. Widengren, J.; Schwille, P., Characterization of Photoinduced Isomerization and Back-Isomerization of the Cyanine Dye Cy5 by Fluorescence Correlation Spectroscopy. *Journal Of Physical Chemistry A* **2000,** 104, (27), 6416-6428.

53. Widengren, J.; Seidel, C. A. M., Manipulation and Characterization of Photo-Induced Transient States of Merocyanine 540 by Fluorescence Correlation Spectroscopy. *Physical Chemistry Chemical Physics* **2000,** 2, (15), 3435-3441.

54. Chambers, R. W.; Kajiwara, T.; Kearns, D. R., Effect of Dimer Formation of Electronic Absorption and Emission-Spectra of Ionic Dyes - Rhodamines and Other Common Dyes. *Journal Of Physical Chemistry* **1974,** 78, (4), 380-387.

55. Chibisov, A. K.; Zakharova, G. V.; Gorner, H., Photoprocesses in Dimers of Thiacarbocyanines. *Physical Chemistry Chemical Physics* **1999,** 1, (7), 1455-1460.

56. Cooper, W.; Liebert, N. B., Excimer and Related Emission in Cyanine Dyes at Low-Temperature. *Photographic Science And Engineering* **1972,** 16, (1), 25-&.

57. Rosch, U.; Yao, S.; Wortmann, R.; Wurthner, F. , Fluorescent H-Aggregates of Merocyanine Dyes. *Angewandte Chemie-International Edition* **2006,** 45, (42), 7026-7030.

58. Sundstrom, V.; Gillbro, T., Excited-State Dynamics And Photophysics Of Aggregated Dye Chromophores In Solution. *Journal Of Chemical Physics* **1985,** 83, (6), 2733-2743.

59. Vanderauweraer, M.; Biesmans, G.; Deschryver, F. C., On the Photophysical Properties of Aggregates Of 3-(2-Phenyl)-Indolocarbocyanines. *Chemical Physics* **1988,** 119, (2-3), 355-375.

60. Vanderauweraer, M.; Verschuere, B.; Deschryver, F. C., Absorption and Fluorescence Properties Of Rhodamine-B Derivatives Forming Langmuir-Blodgett Films. *Langmuir* **1988,** 4, (3), 583-588.

61. West, W.; Pearce, S., Dimeric State Of Cyanine Dyes. *Journal Of Physical Chemistry* **1965,** 69, (6), 1894-&.

62. Zhang, Y. Z.; Xiang, J. F.; Tang, Y. L.; Xu, G. Z.; Yan, W. P., Aggregation Behaviour of Two Thiacarbocyanine Dyes in Aqueous Solution. *Dyes and Pigments* **2008,** 76, (1), 88-93.

63. Mandal, A. K.; Pal, M. K., Strong Fluorescence Emissions by H-Aggregates of the Dye Thiacyanine in the Presence of the Surfactant Aerosol-OT. *Chemical Physics* **2000,** 253, (1), 115-124.

64. Sanborn, M. E.; Connolly, B. K.; Gurunathan, K.; Levitus, M., Fluorescence Properties and Photophysics of the Sulfoindocyanine Cy3 Linked Covalently To DNA. *Journal Of Physical Chemistry B* **2007,** 111, (37), 11064-11074.

65. Seret, A.; Hoebeke, M.; Vandevorst, A. , Triplet Yield Of Merocyanine 540 In Water Is Wavelength Dependent. *Photochemistry And Photobiology* **1990,** 52, (3), 601-604.

66. Sundstrom, V.; Gillbro, T., Viscosity-Dependent Isomerization Yields of Some Cyanine Dyes - A Picosecond Laser Spectroscopy Study. *Journal Of Physical Chemistry* **1982,** 86, (10), 1788-1794.

67. Stahla, M. L.; Baruah, B.; James, D. M.; Johnson, M. D.; Levinger, N. E.; Crans, D. C., H-1 NMR Studies of Aerosol-OT Reverse Micelles With Alkali and Magnesium Counterions: Preparation and Analysis of MAOTs. *Langmuir* **2008,** 24, (12), 6027-6035.

68. Gadde, S.; Batchelor, E. K.; Kaifer, A. E., Controlling The Formation Of Cyanine Dye H- And J-Aggregates With Cucurbituril Hosts In The Presence Of Anionic Polyelectrolytes. *Chemistry-a European Journal* **2009,** 15, (24), 6025-6031.

69. Nikolenko, L. M.; Ivanchihina, A. V.; Brichkin, S. B.; Razumov, V. F., Ternary AOT/Water/Hexane Systems As "Micellar Sieves" For Cyanine Dye J-Aggregates. *Journal of Colloid and Interface Science* **2009,** 332, (2), 366-372.

Chapter 4: Probing Intermicellar Interactions Using Fluorescence Correlation Spectroscopy and Dynamic Light Scattering

4.1 Introduction

The properties of sodium di-2-ethylhexyl sulfosuccinate (AOT) reverse micelles have a rich history of investigation[1]. This is largely due to their utility to probe the effects of confinement on various molecular processes such as catalysis[2-5], intermolecular charge transfer[6] and redox reactions[7, 8]. AOT reverse micelles form when the appropriate amounts of water, surfactant and a non-polar solvent are added together and consist of a water pool, surrounded by an interfacial region defined by the polar headgroups of the surfactant and the aliphatic tails that penetrate into the non-polar solvent[9-21]. The size of reverse micelles can be controlled by varying the concentration of water and surfactant in the system and is defined as w_0. This size parameter is governed by the equation[22]

$$w_0 = \frac{[H_2O]}{[AOT]} \tag{4.1}$$

where, [AOT] and [H_2O] are the molar concentrations of each species in the non-polar solvent. The hydrodynamic radius of AOT reverse micelles is on the order of nanometers and is defined by the equation[22]:

$$R_H(nm) = 0.175 w_0 + 1.5 \tag{4.2}$$

where, R_H is the hydrodynamic radius. Moreover, studies have shown that AOT reverse micelles are a dynamic system that consists on average of spherical particles[1]. These spherical particles have been characterized using light scattering techniques, which have determined both size and

diffusion properties[23]. These measurements have probed the ensemble average of reverse micelles in a bulk solution and are not sensitive to dynamic processes that may influence the molecular level interactions between the reverse micelles.

Only a few studies report the kinetics of intermicellar interactions. Fletcher and co-workers. investigated exchange reactions involving proton transfer, electron transfer and metal-ligand complexation[22]. Their investigation suggested the existence of a transient dimer that forms between the reverse micelles. This structure depends on the diffusion limited collision between two reverse micelles. Subsequently, an encounter pair is formed in which the two reverse micelles are in contact followed by coalescence of the reverse micelles to form the transient dimer. Although Fletcher and co-workers. predicted its existence, the limited time resolution precluded confirmation of the transient dimer. However, based on indirect observation the lifetime of the transient dimer was inferred to be on the order of 25 μs[22].

Fluorescence correlation spectroscopy allows for dynamic processes to be studied that occur on timescales that range from nanoseconds to milliseconds[24-31]. Thus, by labeling the reverse micelles with a fluorescent molecule, fluorescence correlation spectroscopy can be used to better understand the nature of intermicellar interactions. Measuring fluorescence fluctuations that are brought about by diffusion and other dynamic processes allows information about the kinetics of the system to be determined.

Chapter 3 reported the observation of Cy3 H-aggregates in AOT reverse micelles[32]. This unique behavior of the dye has provided the opportunity to probe intermicellar interactions that is reported here. The fluorescence correlation spectroscopy measurements suggest that the formation of the Cy3 H-aggregate also induces the formation of a transient reverse micelle dimer. In contrast to previous studies[22], the fluorescence correlation spectroscopy measurements

have sufficient time resolution to actively probe the formation of the transient reverse micelle dimer and allow us to characterize the kinetics of this process. Formation of the transient dimer causes the diffusion properties within the reverse micelle system to change, leading to a small subset of Cy3 labeled reverse micelles that possess anomalous diffusion occurring at a slower rate than the bulk solution. This chapter presents results from fluorescence correlation spectroscopy and dynamic light scattering measurements as well as a kinetic analysis describing the dimerization of the Cy3 dye and the reverse micelles.

4.2 Experimental Methods

4.2.1 Sample Preparation: Cy3 monoreactive dye pack was purchased from GE Life Science (Piscataway, NJ, USA). The solid dye was dissolved in Millipore water and the resulting solution stored under refrigeration. The reverse micelle solutions were prepared from AOT (sodium di-2-ethylhexyl sulfosuccinate, 99%, Sigma-Aldrich, St. Louis, MO), *iso*-octane (99.8%, Sigma-Aldrich, St. Louis, MO), and aqueous dye solution. The AOT undergoes a purification process, which has been described elsewhere[33]. Reverse micelles were prepared by dissolving AOT in *iso*-octane to form a 0.3 M stock solution to which aqueous dye solution and water were added. All samples were prepared using 2 ml of a 0.3 M AOT in *iso*-octane solution, 10.8 μL of an aqueous Cy3 solution, for which the concentration varied from 9.9×10^{-5} M to 9.9×10^{-6} M. The size (w_0) and concentration of the reverse micelles was then adjusted by adding an appropriate amount of *iso*-octane and water, totaling 1 ml, resulting in a reverse micelle sample with an overall AOT concentration of 0.2 M. For the experiments performed herein, the concentration of AOT in the final solution was 0.02 M, unless otherwise noted. To make these final samples, a 100 μL aliquot of a 0.2 M AOT sample was diluted into 900 μL of isooctane.

The final dye concentration ranged from 3.6 x 10^{-8} M to 8.9 x 10^{-10} M. This yields occupation numbers for Cy3 molecules in the reverse micelles that range from one Cy3 molecule per 20,000 to 900,000 reverse micelles.

4.2.2 Dynamic Light Scattering Measurements: Dynamic light scattering (DLS) measurements were performed to obtain the hydrodynamic radii of the reverse micelle samples. These values were obtained using a DynaPro Titan dynamic light scattering instrument (Wyatt Technology, Santa Barbara, CA, USA). Each sample underwent ten, 10-second scans.

4.2.3 Fluorescence Correlation Spectroscopy Measurements: Fluorescence correlation spectroscopy (FCS) was used to probe the dynamics occurring within the reverse micelles. The experimental procedure and setup for the FCS experiments have been reported previously[24, 34, 35]. Briefly, the sample was placed into a well-slide and covered with a microscope cover slide, which sealed to the well-slide to prevent evaporation. The well-slide was treated with Sigmacote (Sigma-Aldrich, St. Louis, MO, USA) to prevent the Cy3 molecules from sticking to the glass cover slide. Prior to FCS experiments, well-slides were stored overnight in Piranha solution to ensure cleanliness. Before use, the well-slides were rinsed with water and placed into an oven for 10 minutes and then cooled to room temperature. The sample was placed on the stage of a Nikon Eclipse TE-2000-U microscope (Nikon Inc., Melville, NY, USA) and irradiated with a CW laser beam at either 514 nm (Ar ion laser, Melles-Griot, Carlsbad, CA, USA) or 532 nm (Nd:YAG laser, B & W Tek, Newark, DE, USA) using a 100× 1.3 numerical aperture microscope objective. The laser power was 0.05 mW, before entering the microscope. The resulting fluorescence and laser light were transmitted back through the microscope. Fluorescence was separated from the incident laser light with a dichroic mirror, which transmitted the fluorescent light out of the microscope at a 90 degree angle. Upon exiting the

microscope, the fluorescence was split by a 50/50 beam splitter and imaged onto two 50 μm confocal pinholes. The resulting light was band-pass filtered and focused onto two single-photon-counting avalanche photodiode detectors (PerkinElmer Inc., Waltham, MA, USA). The resulting output of the detectors was recorded using the two channels of an ALV-5000E/EPP card (ALV, Langen, Germany) interfaced to a computer. Samples underwent ten, 200-hundred second scans. For data analysis, the scans were averaged and plotted in a graphical analysis program (Igor Pro version 5.03). The fitting routine was performed using this same data analysis program.

4.3 Results

In the preceding chapter, the presence of H-aggregates in the smallest reverse micelle, w_0=1, was reported using a variety of steady-state and time-resolved fluorescence techniques[32]. These results are critical to understanding of the dynamics of this system as studied using FCS.

FCS measures the fluorescence fluctuations of particles diffusing through an optical probe region created by focusing an excitation laser beam to a diffraction limited spot[25, 28, 36]. The fluctuations are analyzed to produce an autocorrelation function, which characterizes the time dependent properties of the fluctuations occurring on timescales ranging from nanoseconds to milliseconds. On the longest timescale, the autocorrelation function reflects the particle diffusion time, τ_d, which represents the average diffusion time of single particles through the optical probe region. Measurement of τ_d characterizes the diffusion properties of the particle and is governed by the equation[25]:

$$\tau_d = \frac{\omega_0^2}{4D} \qquad (4.3)$$

where, ω_0 is the radius of the laser beam at its focus and D is the diffusion coefficient of the particle. In our experiment ω_0 was determined through calibration measurements to be ≈ 0.241 ± 0.012 μm. The diffusion coefficient is determined by the equation[25]:

$$D = \frac{k_B T}{6\pi\eta R_H} \tag{4.4}$$

where, k_B is the Boltzmann constant, T is the temperature, η is the viscosity, and R_H is the hydrodynamic radius of the diffusing particle. In our experiments, the observed fluorescence is due to the Cy3 dye confined within the reverse micelle. Hence, the measured value of τ_d characterizes the diffusion of the reverse micelles.

Figure 4.1 shows the characteristic autocorrelation functions of Cy3 (Figure 4.2) in five differently sized reverse micelles excited at 514 nm. The largest Cy3 reverse micelle system shows an autocorrelation function consistent with diffusion of isolated reverse micelles on the sub-millisecond timescale. At the sub-microsecond timescale a dynamic process is observed that is consistent with previous FCS studies for Cy3 in aqueous solution[29]. As the reverse micelles become smaller, the width of the autocorrelation function decreases, consistent with faster diffusion of the micelles. The dynamics occurring at shorter timescales exhibit similar behavior for micelles ranging from w_0=30 to w_0=2. The autocorrelation functions were analyzed for w_0=30 to w_0=2 that are shown in Figure 4.1 using the equation:

$$G(\tau) = \left(\frac{A}{1 + \frac{\tau}{\tau_d}} \right) * \left(1 + B \exp\left(\frac{-\tau}{\tau_{rxn1}} \right) \right) \tag{4.5}$$

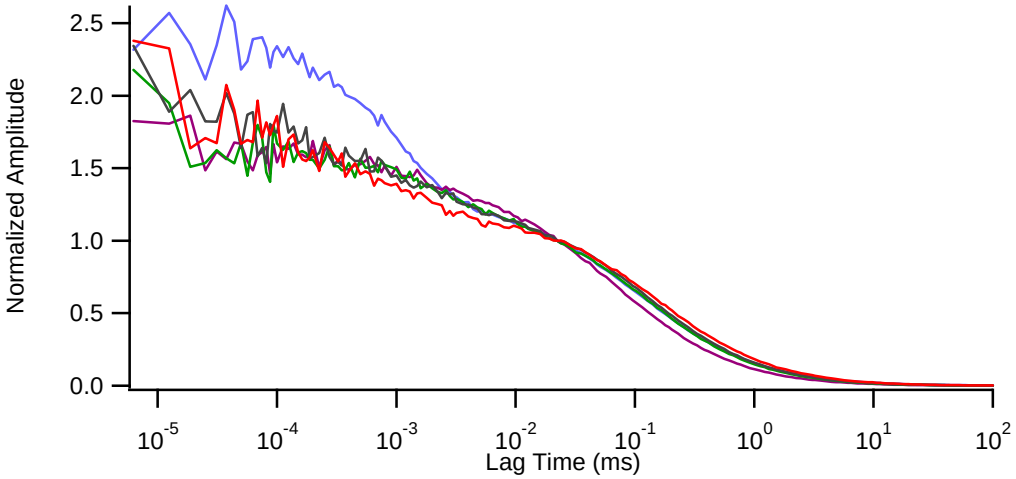

Figure 4.1: Autocorrelation curves of Cy3 from fluorescence correlation spectroscopy experiments in five different reverse micelle samples of varying size; w_0=1 (blue), w_0=2 (purple), w_0=9 (green), w_0=15 (black), and w_0=30 (red). The concentrations of Cy3 and AOT in all samples are 3.56×10^{-8} M and 0.02 M, respectively.

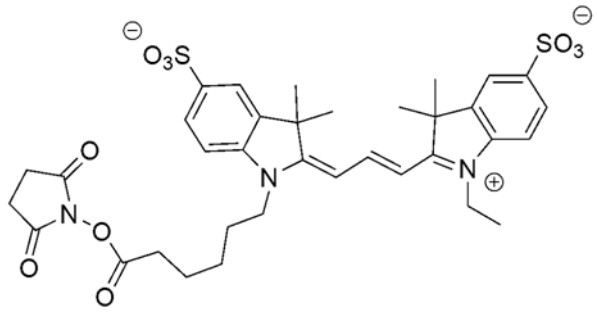

Figure 4.2: Structure of Cy3.

where, A is the amplitude of the autocorrelation function, B is the fraction of molecules undergoing dynamics on the shorter timescale, τ_{rxn1} is the time constant for the process occurring on the shorter timescale and τ_d is the diffusion time. Using equation 4.5, we calculated the diffusion coefficient for each reverse micelle sample was calculated and the hydrodynamic radius was determined using equation 4.4 (Table 4.1). The FCS results were corroborated using dynamic light scattering (DLS), which is also shown in Table 4.1. The results for both techniques are consistent for w_0=30 to w_0=2.

However, when the size of the reverse micelle is reduced to w_0=1, an abrupt change in the autocorrelation function occurs. First, a dramatic increase in the amplitude of the autocorrelation function is observed at the shorter time scales, which suggests a new dynamic process occurs on the sub-microsecond timescales in the w_0=1 reverse micelle. Various processes could be responsible for the reaction we observe occurring on the sub-microsecond timescale for Cy3 in w_0=1 reverse micelles excited at 514 nm. These include intersystem crossing, aggregation, or isomerization[27-31]. The previous chapter showed that trans-cis isomerization of the Cy3 monomer is suppressed in w_0=1 reverse micelles. Thus, isomerization as the source of the sub-μs process was eliminated. Two additional experiments were performed to investigate the possibility of triplet blinking or association/dissociation as the source of this observed process. If triplet blinking were responsible for the sub-microsecond process, then the feature should increase in intensity with increasing laser power[27, 29, 31]. Figure 4.3 shows the autocorrelation of FCS data

Table 4.1: Hydrodynamic radii of different size reverse micelle samples determined experimentally by fluorescence correlation spectroscopy (FCS) and dynamic light scattering (DLS) and estimated theoretically by equation 4.2. The concentration of Cy3 is 3.6 x 10^{-8} M and the concentration of AOT is 0.02 M.

Size (w_0)	FCS R_H (nm)	DLS R_H (nm)	Theoretical R_H (nm)
30	5.4 ± 0.6	7.4 ± 0.4	6.8
15	4.2 ± 0.5	3.7 ± 0.1	4.1
9	3.9 ± 0.4	2.8 ± 0.1	3.1
2	2.5 ± 0.3	2.1 ± 0.1	1.9
1	2.3 ± 0.3[1], 4.4 ± 0.3[2]	1.8 ± 0.3	1.7

[1]Hydrodynamic radius for w_0=1 reverse micelles measured at 532 nm excitation.

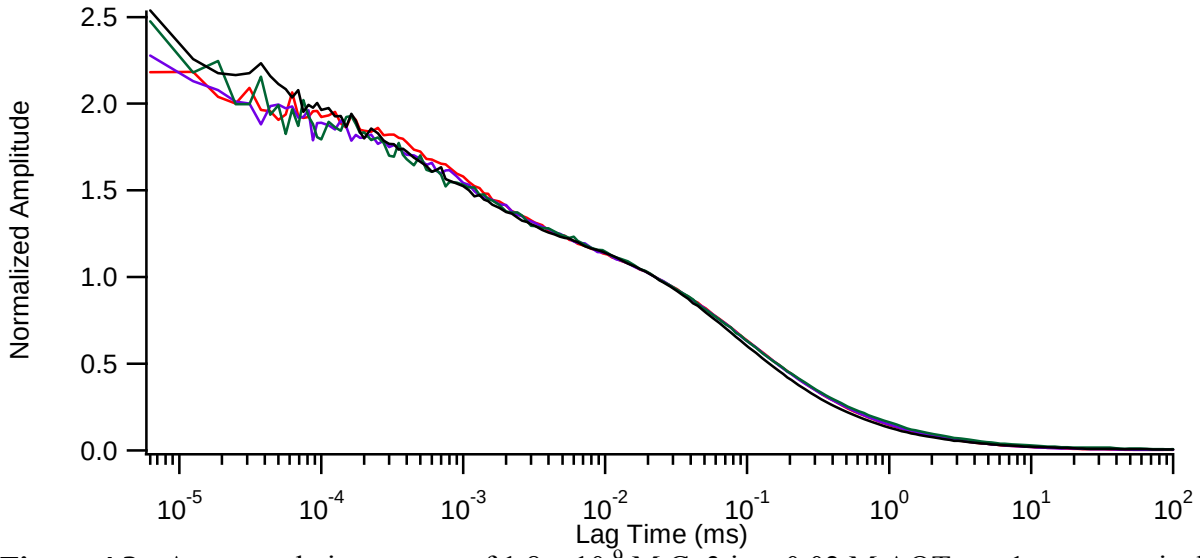

Figure 4.3: Autocorrelation curves of 1.8 x 10^{-9} M Cy3 in a 0.02 M AOT w_0=1 reverse micelle sample from fluorescence correlation spectroscopy experiments at four different laser excitation powers; 0.1 mW (red), 0.2 mW (blue), 0.9 mW (green) and 2.4 mW (black).

collected with varying the laser intensity and no measureable change in the amplitude of the sub-μs process with laser power was observed. This suggests that confinement in the w_0=1 reverse micelle does not enhance triplet blinking and that it is not responsible for the observed process.

A second experiment investigated whether the sub-μs fluctuation was caused by the association/dissociation of the Cy3 aggregate. From the previous results, it was deduced that emission at different wavelengths corresponds to monomer or aggregate forms of Cy3. If aggregation was occurring, then emission associated with the monomer form of the dye observed at 570 nm should correlate with emission at 600 or 650 nm as the aggregate dissociates to form the monomer. Using filters and separate detectors, we monitored three separate two-color fluorescence cross correlation functions: 570 nm and 600 nm; 570 nm and 650 nm; and 600 nm and 650 nm. Results shown in Figure 4.4 reveal that the amplitude of this process does not vary significantly with wavelength. The previous chapter showed a dramatic increase in the fluorescence emission at 600 nm and 650 nm associated with aggregate formation [32]. It is hypothesized that the sub-microsecond dynamic process is related to the aggregate form of the dye that occurs in the w_0=1 reverse micelle.

A comparison of the autocorrelation functions for w_0=1 and w_0=2 reveal that the w_0=1 reverse micelles diffuse more slowly than the w_0=2 reverse micelles. However, the DLS results for w_0=1 show the reverse micelles diffuse faster than the w_0=2 reverse micelles, in agreement with literature values[23]. Differences exist between the reverse micelles measured by FCS and those measured by DLS; specifically, FCS probes only a minute fraction of reverse micelles in solution, those containing the Cy3 dye, while DLS probes the entire ensemble. Thus, FCS experiments reveal anomalous diffusion for Cy3 containing reverse micelles compared to the bulk reverse micelles.

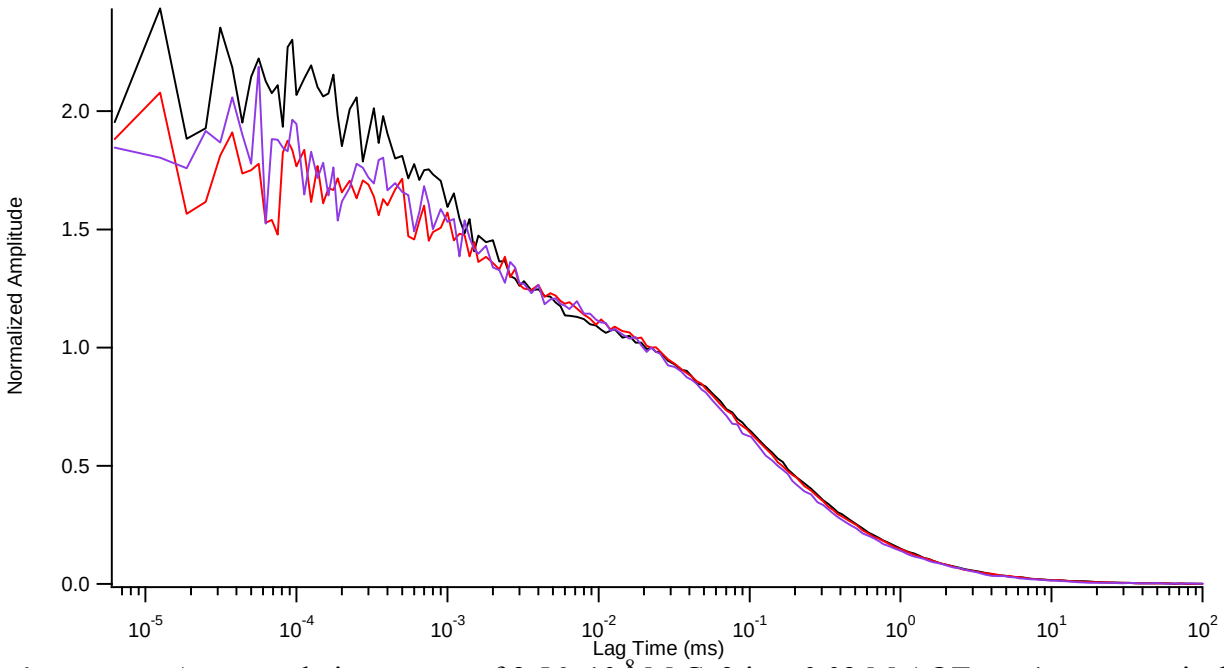

Figure 4.4: Autocorrelation curves of 3.56×10^{-8} M Cy3 in a 0.02 M AOT w_0=1 reverse micelle sample. The fluorescence emission was detected by cross-correlating the detectors using different emission filters; Detector 1 650 ± 15 nm band pass-Detector 2 600 ± 15 nm band pass (black), Detector 1 570 ± 15 nm band pass -Detector 2 600 ± 15 nm band pass (red), Detector 1 570 ± 15 nm band pass -Detector 2 650 ± 15 nm band pass (purple).

To further investigate the dynamics of Cy3 in the w_0=1 reverse micelles and the anomalous diffusion behavior, autocorrelation functions at two different excitation wavelengths, 514 nm and 532 nm, were measured (Figure 4.5). The previous chapter demonstrated that 514 nm radiation primarily excites the aggregate form of Cy3 while 532 nm primarily excites the monomer form of the dye in w_0=1[32]. Interestingly, the autocorrelation function for Cy3 in w_0=1 reverse micelles excited at 532 nm appears similar to the autocorrelation function for Cy3 in larger reverse micelles, particularly with respect to the process occurring at shorter timescales. Using the FCS data and equations 3, 4, and 5, the hydrodynamic radius for the w_0=1 excited at 532 nm was determined. The results of this analysis reveal reverse micelles with sizes commensurate with the dynamic light scattering measurement for w_0=1, as shown in Table 4.1. Thus, the anomalous diffusion behavior is no longer observed when exciting at 532 nm suggesting that the anomaly may relate to Cy3 aggregation.

If aggregation is responsible for the anomalous diffusion, then a dependence on Cy3 concentration should be observed. Autocorrelation functions from FCS measurements on samples containing varying concentrations of Cy3 dye while holding the concentration of reverse micelles constant and exciting at 514 nm appear in Figure 4.6. The autocorrelation function for the lowest concentration of Cy3 is qualitatively similar to the results for larger size reverse micelles as well as results for Cy3 in w_0=1 excited at 532 nm. However, as the concentration increases, the amplitude of the short timescale process and the width of the autocorrelation function both increase. Despite the exceedingly low overall Cy3 concentrations probed, the increased amplitude of the short time process and the increased width of the autocorrelation function supports the hypothesis that Cy3 aggregation leads to the features observed in the FCS results.

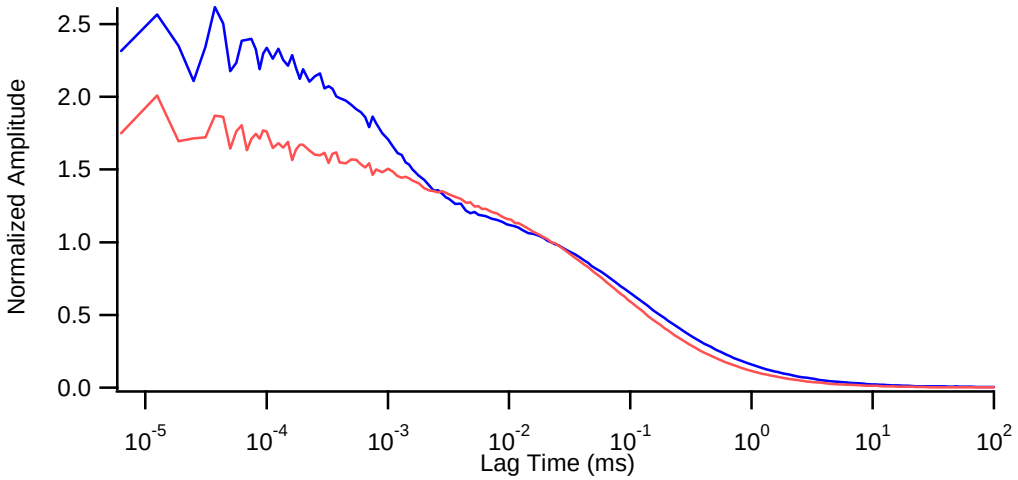

Figure 4.5: Autocorrelation curves of Cy3 in a w_0=1 reverse micelle sample from fluorescence correlation spectroscopy experiments at two different excitation wavelengths: 514 nm (blue) and 532 nm (red). The concentration of Cy3 is 3.56×10^{-8} M and the concentration of AOT is 0.02 M AOT.

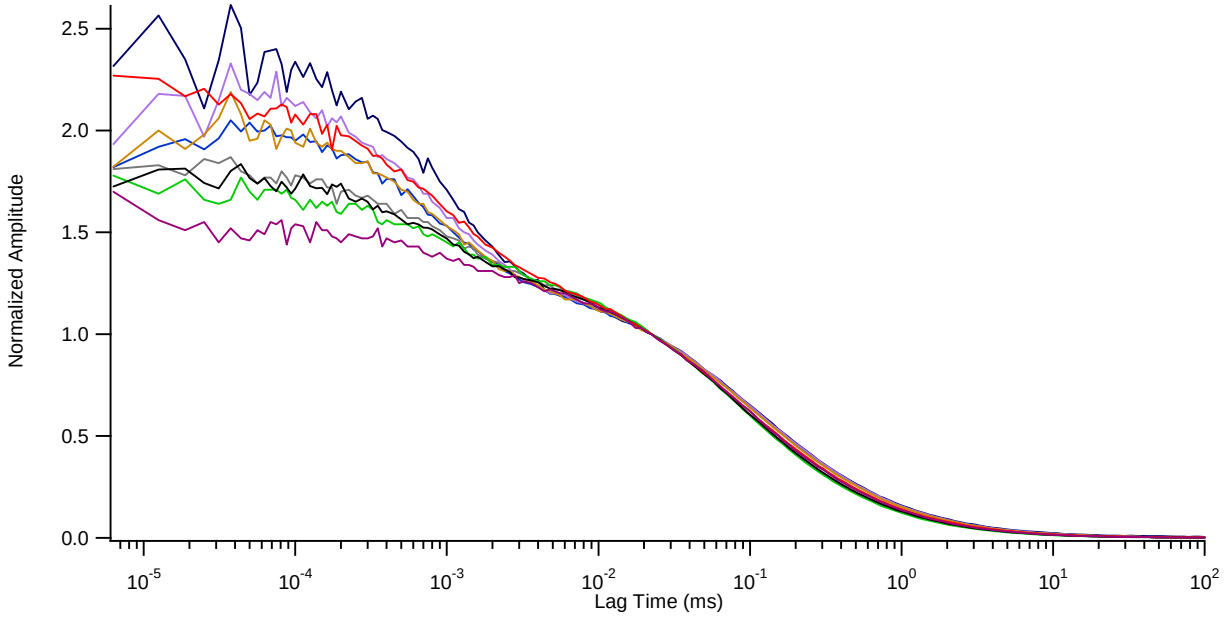

Figure 4.6: Autocorrelation curves of Cy3 in a w_0=1 reverse micelle sample from fluorescence correlation spectroscopy experiments at different overall Cy3 concentrations: 8.93×10^{-10} M (dark purple), 1.78×10^{-9} M (green), 3.56×10^{-9} M (grey), 5.4×10^{-9} M (black), 7.93×10^{-9} M (red), 8.93×10^{-9} M (light blue), 1.78×10^{-8} M (gold), 2.67×10^{-8} M (purple), 3.56×10^{-8} M (dark blue). The concentration of AOT in all samples is 0.02 M.

4.3 Discussion

The results and analysis from the DLS and FCS experiments performed on the reverse micelles ranging in size from w_0=30 to w_0=2 are consistent with the expectation that the Cy3 exists primarily as monomer and that the reverse micelles diffuse as independent particles. This behavior is also observed for the w_0=1 reverse micelles when exciting the sample at 532 nm, which is consistent with the previous chapter in which it was deduced that 532 nm light primarily excites the monomer form of Cy3 inside the w_0=1 reverse micelles[32]. However, when Cy3 in w_0=1 reverse micelles are analyzed with 514 nm excitation, anomalous diffusion is observed that occurs more slowly than independent, isolated w_0=1 reverse micelles as observed by DLS or FCS with 532 nm excitation. The FCS experiments probe only reverse micelles labeled with Cy3 dye molecules whereas the DLS experiments probe the bulk reverse micelle sample. The fraction of reverse micelles labeled with dye is approximately 45 parts per million. Thus, this anomalous diffusion behavior is only observed in the minuscule fraction of dye labeled reverse micelles and only when excited at 514 nm, which is thought to be due to a Cy3 aggregate.

The observation that anomalous diffusion occurs only with 514 nm excitation and not at 532 nm excitation further suggests there are two sub-populations of dye labeled reverse micelles when w_0=1, those that contain Cy3 aggregates with longer diffusion times and those that contain Cy3 monomers and have a shorter diffusion time. Furthermore, these observations suggest that not only are the Cy3 molecules aggregated but that aggregation of Cy3 results in the aggregation of the reverse micelles, hence the slower diffusion time.

In the previous chapter, significant changes in the fluorescence emission spectra of Cy3 in w_0=1 as the concentration of Cy3 increased were observed, indicating an increase in the amount of aggregation[32]. The changes in the autocorrelation function of Cy3 in w_0=1 as the concentration of Cy3 increases suggests that these changes are associated with the aggregate form of the Cy3

dye. At the lowest concentration, the autocorrelation function is qualitatively similar to those measured for the larger reverse micelles and the w_0=1 excited at 532 nm (Figures 1 and 5). This suggests that the Cy3 exists as a monomer at the lowest concentration. However, at the higher concentrations, the increased amplitude in the shorter timescale process and the increased width of the autocorrelation function suggest that a different form of the dye is being probed and that this form of the dye is diffusing more slowly. To verify these results, dynamic light scattering measurements were performed on samples of varying Cy3 concentration. Given the low Cy3 concentration leading to very low occupation numbers, fewer than one in 20,000, it is not surprising that no change in the bulk diffusion properties as a function of Cy3 concentration was observed in these measurements. This confirms that the changes observed in the FCS autocorrelation function are due to the small fraction of reverse micelles that have Cy3 molecules associated with them.

The spectroscopy and dynamics in the data presented thus far and in the previous chapter shows that in the w_0=1 reverse micelle the presence of Cy3 induces the aggregation of the dye and the reverse micelles. A mechanism consistent with these observations was suggested by the kinetic study described previously.[22] This study suggests the formation of a transient dimer with a ≈ 25 μs lifetime. Based on our experiments and this previous study, it is proposed that when Cy3 dimers form, they occur in environments that transiently conjoin two reverse micelles containing the dyes.

Figure 4.7 shows a proposed mechanism for aggregation of Cy3 in w_0=1 reverse micelles, where individual Cy3 molecules are encapsulated by the individual reverse micelles. Upon colliding, the reverse micelles fuse together to create a transient dimer structure. This reverse

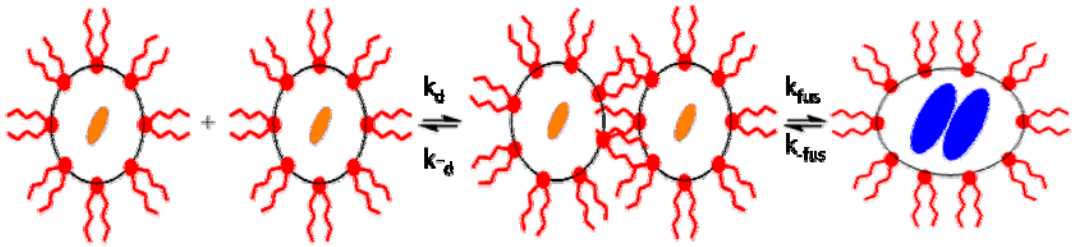

Figure 4.7: Proposed mechanism for the formation of the reverse micelle transient dimer.

micelle dimer adopts a prolate ellipsoidal form rather than the typical spherical reverse micelle structure, which results in a longer diffusion time than would be observed for a spherical particle of the same volume. This mechanism explains the spectroscopic changes as well as the longer diffusion time measured by FCS. It also explains why only a small fraction of the reverse micelles exhibit this behavior. Since the dye is present at such low concentrations, these transient dimers do not affect the entire bulk sample and are only observed in situations probing a select population of dye molecules. To describe this mechanism, the autocorrelation analysis in equation 4.3 has been generalized to include contributions from both monomers and dimers, as well as additional dynamic components, using the following equation:

$$G(\tau) = \left(\frac{A}{1 + \frac{\tau}{\tau_{d1}}} \right) + \left(\frac{B}{1 + \frac{\tau}{\tau_{d2}}} \right) * \left(1 + C \exp\left(\frac{-\tau}{\tau_{rxn1}} \right) \right) * \left(1 + D \exp\left(\frac{-\tau}{\tau_{rxn2}} \right) \right) \qquad (4.6)$$

Here, A is the fraction of molecules in the monomer form, τ_{d1} is the diffusion time of the monomer, B is the fraction of molecules existing as dimers, τ_{d2} is the diffusion time of the transient reverse micelle dimer. In addition, equation 6 includes τ_{rxn1}, a fast decay in the autocorrelation function and τ_{rxn2}, an intermediate decay discussed below. Moreover, the constants C and D relate to the fraction of molecules undergoing dynamics defined as τ_{rxn1} and τ_{rxn2}, respectively. When fitting the data to this equation, the value of τ_{d1} was fixed to that of individual w_0=1 reverse micelles determined by DLS. The value of τ_{d2} was determined using the highest concentration of Cy3 in w_0=1 (Figure 4.3), which has minimal contribution from τ_{d1} (A≈0). Measurement of τ_{d2} in this sample is consistent with a particle with roughly twice the volume of an individual reverse micelle with a prolate ellipsoidal form and thus has a smaller

diffusion coefficient (longer diffusion time) than a spherical particle of the same volume. The results of fitting the concentration dependent autocorrelation functions to equation 4.6 are shown in Table 4.2. Notice that the fast time component is fit with two exponential decays, τ_{rxn1} and τ_{rxn2}. The timescale of τ_{rxn1} is independent of Cy3 concentration. However, the amplitude of this component increases with increasing concentration, suggesting that the reaction being probed at this timescale occurs in the dimer. In the analysis above, the possibility that triplet blinking or the association/dissociation of the Cy3 aggregate causes this process is eliminated. Likewise, because the rotational correlation time for the transient dimer should be ~15 ns, which is much faster than the fluctuation observed on this 1 μs timescale, rotational correlation of the transient dimer as the source of this fluctuation is also ruled out. Although the exact process responsible for this fluctuation remains unclear, it is thought to be due to a conformational fluctuation of the Cy3 dimer that causes an intensity fluctuation in the autocorrelation function, consistent with the cross-correlation analysis of 600 and 650 nm, described previously.

The second time constant, τ_{rxn2}, was measured to be on the order of 10 to 20 μs. This time constant was also independent of Cy3 concentration. Based on indirect analysis, Fletcher and co-workers.[22] deduced the transient micelle dimer has a lifetime on the order of tens of μs, which is consistent with the measured value for τ_{rxn2}. It is hypothesized that τ_{rxn2} is the relaxation time for the formation of the transient dimer ellipsoid. With this assumption, the following discusses the calculation of the kinetic rate constants associated with our proposed mechanism.

The data presented here and in the previous chapter suggests that both the Cy3 dye and the reverse micelles interact to form aggregates. Recall the mechanism shown in Figure 4.7,

Table 4.2: Results of fitting the Cy3 concentration dependent autocorrelation functions to equation 8. The concentration of AOT is 0.02 M in all the samples.

Overall Cy3 Concentration (M)	A	τ_{d1} (μs) fixed	B	τ_{d2} (μs) fixed	C	τ_{rxn1} (μs)	D	τ_{rxn2} (μs)
1.78 e-9	0.34±0.02	70	0.33±0.02	145	0.45±0.02	0.9±0.04	0.26±0.01	11±2
3.56 e-9	0.14±0.02	70	0.25±0.01	145	0.51±0.03	1±0.03	0.24±0.01	15±3
5.4 e-9	0.13±0.03	70	0.28±0.02	145	0.48±0.04	1±0.03	0.23±0.02	18±4
7.13 e-9	0.02±0.005	70	0.09±0.004	145	0.62±0.03	0.9±0.03	0.3±0.01	10±1
8.93 e-9	N/A	N/A	0.11±0.003	145	0.56±0.01	0.9±0.02	0.19±0.01	13±1
1.78 e-8	N/A	N/A	0.04±0.001	145	0.56±0.01	0.9±0.02	0.19±0.01	15±2
2.67 e-8	N/A	N/A	0.03±0.001	145	0.66±0.02	0.9±0.03	0.19±0.02	11±2
3.56 e-8	N/A	N/A	0.015±0.001	145	0.77±0.04	1±0.04	0.21±0.03	9±2

which is consistent with this hypothesis. Here, two reverse micelles, each containing a Cy3 monomeric dye molecule, collide. Following this collision, the reverse micelles conjoin promoting the interaction and dimerization of the Cy3 molecules. The overall equilibrium for the process shown in Figure 4.6 is given by:

$$K_{overall} = K_d K_{fus} = \frac{k_d}{k_{-d}} \frac{k_{fus}}{k_{-fus}} \tag{4.7}$$

where k_d and k_{-d} are the forward and reverse rate constants for reverse micelle encounter and k_{fus} and k_{-fus} are the forward and reverse rate constants for reverse micelle fusion and Cy3 dimerization. Using data from FCS and DLS presented here, as well as results from steady-state and time-resolved spectroscopies[32], a detailed analysis of each step in the process is presented to obtain kinetic parameters that govern each process.

The initial step of the mechanism depicted in Figure 4.6 involves the collision of two Cy3 labeled reverse micelles. Translational diffusion of the reverse micelles limits the maximum forward rate for this process and can be described by[22]

$$k_d = \frac{8k_b T}{3\eta} \quad . \tag{4.8}$$

where k_b is the Boltzmann constant, T is temperature, and η is the solution viscosity. The conditions used yields k_d=1.4 x 10^{10} L mol^{-1} s^{-1}. Based on this value and the Cy3 concentration, we predict an upper limit for the collision rate of two Cy3 labeled reverse micelles to be 5.0 x 10^2 s^{-1} ($\tau \approx$ 2ms). Although this rate is too slow to be measured by our FCS experiment, it provides a value that can be used to explore the rest of the steps in the mechanism.

To determine K_d, it is necessary to obtain the rate constant for the separation of the encounter pair back to isolated reverse micelles, k_{-d}, which is defined by the equation[22]:

$$k_{-d} = \frac{6D}{(2r)^2} \quad . \tag{4.9}$$

Here, r is the radius of an individual reverse micelle, consistent with hard sphere droplet behavior. Using 2.4 x 10^{-10} m^2s^{-1} for D and 1.8 x 10^{-9} m for r, k_{-d} is calculated to be 1.1 x 10^8 s^{-1}, which yields K_d = 124 M^{-1}.

The second step in the mechanism involves the coalescence of two reverse micelles to form a transient dimer. The equilibrium constant, K_{fus}, associated with this step can be shown to be

$$K_{fus} = \frac{c_d}{K_d c_m^2} \tag{4.10}$$

where, K_d is the equilibrium constant governing the diffusion controlled reaction shown in the first step of our mechanism, c_m is the concentration of monomer and c_d is the concentration of dimer. Values for c_m and c_d begin with the mass balance equation for the association/dissociation of the Cy3 dimer, given by:

$$c_{total} = c_m + 2c_d \tag{4.11}$$

where, c_{total} is the overall concentration of Cy3. Considering the overall reaction occurring, c_d can be written as:

$$c_d = K_{overall} c_m^2 \quad . \tag{4.12}$$

Substituting equation 12 into equation 11 and solving for c_m gives:

$$c_m = \frac{-1 + \sqrt{1 + 8K_{overall} c_{total}}}{4K_{overall}} \quad . \tag{4.13}$$

Results from our previous work provide the value for $K_{overall} \approx (1.4 \pm 0.7)$ x 10^8 M^{-1} [32], hence a value for c_m. Using the overall Cy3 concentration, and equations 11 and 13 allows us to obtain a value for $K_{fus} \approx (1.1 \pm 0.5)$ x 10^6.

Furthermore, using equation $\tau_{rxn2}=1/(k_{fus}+k_{-fus})$ and the definition for K_{fus}, a relationship for the reverse rate constant, k_{-fus}, was derived to be:

$$k_{-fus} = \frac{1}{\tau_{rxn2}(1+K_{fus})} \tag{4.14}$$

where, τ_{rxn2} is the time constant for the fusion of two reverse micelles. Using our experimentally measured value for τ_{rxn2}, $k_{-fus} \approx (5.9 \pm 3.3) \times 10^{-2}$ s^{-1}. This rate constant and the associated equilibrium constant permits determination of $k_{fus} \approx (6.7 \pm 4.8) \times 10^{4}$ s^{-1}.

Fletcher and co-workers. suggested that the rate constant for reverse micelles to exchange their contents, k_{ex}, is given by the equation[22]:

$$k_{ex} = K_d k_{fus} \tag{4.15}$$

which leads to $k_{ex} \approx (8.3 \pm 5.9) \times 10^{6}$ $M^{-1}s^{-1}$. This value is consistent with k_{ex} values inferred by Fletcher and co-workers. for a similar system[22]. Thus, the FCS measurements show that as the transient dimeric reverse micelle species diffuses through the probe volume, it fluctuates between the intermediate encounter pair and the fused transient dimer. The FCS technique is sensitive to this conversion revealed by the ≈ 10 to 20 μs fluctuation in the FCS measurements.

The data presented demonstrates that the smallest reverse micelles, w_0=1, form transient dimers that are stable on the timescale of the FCS experiment. It is hypothesized that the reverse micelles undergo interactions that allow their contents to be exchanged. During this process, the reverse micelles form the transient dimer accompanied by the formation of a Cy3 dimer, which is observed in the FCS measurements and other spectroscopic studies[32]. However, this behavior is not observed in the larger reverse micelles which may be due to the slower rate of fusion of two micelles in these larger systems. The kinetic analysis above shows that the rate of fusion of the encounter pair is inversely proportional to the equilibrium constant for the first step in the

proposed mechanism (equation 4.15). This parameter, K_d, is proportional to the hydrodynamic radius of the reverse micelle raised to the third power. Therefore, as the particles become larger, the value of K_d increases, resulting in a decrease in the rate of fusion for the encounter pair and reducing the likelihood that the dimer will form in larger reverse micelles.

4.5 Conclusion

The work described in this chapter reports the direct observation of a transient reverse micelle dimer. The use of two different excitation wavelengths, 514 and 532 nm, allows the dynamics of both the Cy3 monomer labeled reverse micelles and those reverse micelles containing the Cy3 H-aggregate to be probed, which is consistent with the previous chapter. Moreover, the reverse micelles containing the Cy3 H-aggregate exhibit anomalous diffusion behavior that is not seen in the isolated reverse micelles and in our dynamic light scattering experiments. Furthermore, the kinetics of this reaction have been characterized and provide insight into the nature of intermicellar interactions, which is important to understanding processes occurring within reverse micelles such as reaction kinetics and diffusion properties. The results show that reverse micelles are dynamic, constantly undergoing collisions and exchanging contents. Although these systems can be made up of discrete individual droplets, aggregates and bicontinuous structures like the transient dimer observed here can exist, thus altering the diffusion properties of the system. The results presented here suggest that reverse micelles can be used as a nanocatalyst to cause reactions to occur that would otherwise not occur, as seen by the formation of the Cy3 H-aggregate at concentrations so dilute as to preclude aggregation in bulk aqueous solution.

1. De, T. K.; Maitra, A., Solution Behavior of Aerosol OT In Nonpolar-Solvents. *Advances in Colloid and Interface Science* **1995,** 59, 95-193.

2. Abuin, E.; Lissi, E.; Solar, C., Effect of Urea on the Enzymatic Activity of a Lipase Entrapped in AOT-Heptane-Water Reverse Micellar Solutions. *Journal Of Colloid And Interface Science* **2005,** 283, (1), 87-93.

3. Correa, N. M.; Durantini, E. N.; Silber, J. J., Catalysis in Micellar Media. Kinetics and Mechanism for the Reaction of 1-Fluoro-2,4-Dinitrobenzene With N-Butylamine and Piperidine in N-Hexane and AOT/N-Hexane/Water Reverse Micelles. *Journal of Organic Chemistry* **1999,** 64, (16), 5757-5763.

4. Martinek, K.; Levashov, A. V.; Klyachko, N.; Khmelnitski, Y. L.; Berezin, I. V., Micellar Enzymology. *European Journal of Biochemistry* **1986,** 155, (3), 453-468.

5. Menger, F. M.; Yamada, K., Enzyme Catalysis in Water Pools. *Journal of the American Chemical Society* **1979,** 101, (22), 6731-6734.

6. Novaira, M.; Moyano, F.; Biasutti, M. A.; Silber, J. J.; Correa, N. M., An Example of How to Use AOT Reverse Micelle Interfaces to Control a Photoinduced Intramolecular Charge-Transfer Process. *Langmuir* **2008,** 24, (9), 4637-4646.

7. Correa, N. M.; Zorzan, D. H.; Chiarini, M.; Cerichelli, G., Reverse Micellar Aggregates: Effect on Ketone Reduction. I. Substrate Role. *Journal of Organic Chemistry* **2004,** 69, (24), 8224-8230.

8. Correa, N. M.; Zorzan, D. H.; D'Anteo, L.; Lasta, E.; Chiarini, M.; Cerichelli, G., Reverse Micellar Aggregates: Effect On Ketone Reduction. 2. Surfactant Role. *Journal of Organic Chemistry* **2004,** 69, (24), 8231-8238.

9. Baruah, B.; Crans, D. C.; Levinger, N. E., Simple Oxovanadates As Multiparameter Probes of Reverse Micelles. *Langmuir* **2007,** 23, (12), 6510-6518.

10. Baruah, B.; Roden, J. M.; Sedgwick, M.; Correa, N. M.; Crans, D. C.; Levinger, N. E., When Is Water Not Water? Exploring Water Confined In Large Reverse Micelles Using a Highly Charged Inorganic Molecular Probe. *Journal of the American Chemical Society* **2006,** 128, (39), 12758-12765.

11. Baruah, B.; Swafford, L. A.; Crans, D. C.; Levinger, N. E., Do Probe Molecules Influence Water In Confinement? *Journal Of Physical Chemistry B* **2008,** 112, (33), 10158-10164.

12. Correa, N. M.; Levinger, N. E., What Can You Learn From A Molecular Probe? New Insights On The Behavior Of C343 In Homogeneous Solutions And AOT Reverse Micelles. *Journal Of Physical Chemistry B* **2006,** 110, (26), 13050-13061.

13. Crans, D. C.; Baruah, B.; Levinger, N. E., Oxovanadates: A Novel Probe For Studying Lipid-Water Interfaces. *Biomedicine & Pharmacotherapy* **2006,** 60, (4), 174-181.

14. Crans, D. C.; Rithner, C. D.; Baruah, B.; Gourley, B. L.; Levinger, N. E., Molecular Probe Location In Reverse Micelles Determined By NMR Dipolar Interactions. *Journal of the American Chemical Society* **2006,** 128, (13), 4437-4445.

15. Crans, D. C.; Trujillo, A. M.; Bonetti, S.; Rithner, C. D.; Baruah, B.; Levinger, N. E., Penetration Of Negatively Charged Lipid Interfaces By The Doubly Deprotonated Dipicolinate. *Journal Of Organic Chemistry* **2008,** 73, (24), 9633-9640.

16. Falcone, R. D.; Correa, N. M.; Biasutti, M. A.; Silber, J. J., Properties Of AOT Aqueous And Nonaqueous Microemulsions Sensed By Optical Molecular Probes. *Langmuir* **2000,** 16, (7), 3070-3076.

17. Harpham, M. R.; Ladanyi, B. M.; Levinger, N. E., The Effect Of The Counterion On Water Mobility In Reverse Micelles Studied By Molecular Dynamics Simulations. *Journal Of Physical Chemistry B* **2005,** 109, (35), 16891-16900.

18. Harpham, M. R.; Levinger, N. E.; Ladanyi, B. M., An Investigation Of Water Dynamics In Binary Mixtures Of Water And Dimethyl Sulfoxide. *Journal Of Physical Chemistry B* **2008,** 112, (2), 283-293.

19. Moilanen, D. E.; Levinger, N. E.; Spry, D. B.; Fayer, M. D., Confinement Or The Nature Of The Interface? Dynamics Of Nanoscopic Water. *Journal of the American Chemical Society* **2007,** 129, (46), 14311-14318.

20. Roess, D. A.; Smith, S. M. L.; Winter, P.; Zhou, J.; Dou, P.; Baruah, B.; Trujillo, A. M.; Levinger, N. E.; Yang, X. D.; Barisas, B. G.; Crans, D. C., Effects Of Vanadium-Containing Compounds On Membrane Lipids And On Microdomains Used In Receptor-Mediated Signaling. *Chemistry & Biodiversity* **2008,** 5, (8), 1558-1570.

21. Tan, H. S.; Piletic, I. R.; Riter, R. E.; Levinger, N. E.; Fayer, M. D., Dynamics Of Water Confined On A Nanometer Length Scale In Reverse Micelles: Ultrafast Infrared Vibrational Echo Spectroscopy. *Physical Review Letters* **2005,** 94, (5).

22. Fletcher, P. D. I.; Howe, A. M.; Robinson, B. H., The Kinetics Of Solubilisate Exchange Between Water Droplets Of A Water-In-Oil Microemulsion. *Journal Of The Chemical Society-Faraday Transactions I* **1987,** 83, 985-1006.

23. Zulauf, M.; Eicke, H. F., Inverted Micelles And Microemulsions In The Ternary-System H_2O-Aerosol-Ot-Isooctane As Studied By Photon Correlation Spectroscopy. *Journal of Physical Chemistry* **1979,** 83, (4), 480-486.

24. Fogarty, K.; McPhee, J. T.; Scott, E.; Van Orden, A., Probing The Ionic Atmosphere Of Single-Stranded DNA Using Continuous Flow Capillary Electrophoresis And Fluorescence Correlation Spectroscopy. *Analytical Chemistry* **2009,** 81, (1), 465-472.

25. Van Orden, A.; Fogarty, K.; Jung, J., Fluorescence Fluctuation Spectroscopy: A Coming Of Age Story. *Applied Spectroscopy* **2004,** 58, (5), 122A-137A.

26. Van Orden, A.; Jung, J., Fluorescence Correlation Spectroscopy For Probing The Kinetics And Mechanisms Of DNA Hairpin Formation. *Biopolymers* **2008,** 89, (1), 1-16.

27. Widengren, J.; Mets, U.; Rigler, R., Fluorescence Correlation Spectroscopy Of Triplet-States In Solution - A Theoretical And Experimental-Study. *Journal Of Physical Chemistry* **1995,** 99, (36), 13368-13379.

28. Widengren, J.; Rigler, R., Review - Fluorescence Correlation Spectroscopy As A Tool To Investigate Chemical Reactions In Solutions And On Cell Surfaces. *Cellular And Molecular Biology* **1998,** 44, (5), 857-879.

29. Widengren, J.; Schwille, P., Characterization Of Photoinduced Isomerization and Back-Isomerization Of The Cyanine Dye Cy5 By Fluorescence Correlation Spectroscopy. *Journal Of Physical Chemistry A* **2000,** 104, (27), 6416-6428.

30. Widengren, J.; Schwille, P.; Rigler, R., Photophysical Characterization Of The Dye Cy-5 By Fluorescence Correlation Spectroscopy *Biophysical Journal* **1997,** 72, (2), TU419-TU419.

31. Widengren, J.; Seidel, C. A. M., Manipulation And Characterization Of Photo-Induced Transient States Of Merocyanine 540 By Fluorescence Correlation Spectroscopy. *Physical Chemistry Chemical Physics* **2000,** 2, (15), 3435-3441.

32. McPhee, J. T. S., E.; Levinger, N.E.; Van Orden, A., *Journal of Physical Chemistry B* **2010**.

33. Stahla, M. L.; Baruah, B.; James, D. M.; Johnson, M. D.; Levinger, N. E.; Crans, D. C., H-1 NMR Studies Of Aerosol-OT Reverse Micelles With Alkali And Magnesium Counterions: Preparation And Analysis Of MAOTs. *Langmuir* **2008,** 24, (12), 6027-6035.

34. Jung, J.; Ihly, R.; Scott, E.; Yu, M.; Van Orden, A., Probing The Complete Folding Trajectory Of A DNA Hairpin Using Dual Beam Fluorescence Fluctuation Spectroscopy. *Journal Of Physical Chemistry B* **2008,** 112, (1), 127-133.

35. Jung, J. Y.; Van Orden, A., A Three-State Mechanism For DNA Hairpin Folding Characterized By Multiparameter Fluorescence Fluctuation Spectroscopy. *Journal of the American Chemical Society* **2006,** 128, (4), 1240-1249.

36. Elson, E. L.; Magde, D., Fluorescence Correlation Spectroscopy .1. Conceptual Basis And Theory. *Biopolymers* **1974,** 13, (1), 1-27.

Chapter 5

Preliminary Experiments Investigating the Fluorescence Properties of Rhodamine 6G and Cyanine-3/Cyanine-5 Fluorescence Resonance Energy Transfer inside AOT/*Iso*-octane Reverse Micelles

The first part of this chapter describes preliminary absorption and fluorescence correlation spectroscopy experiments that were carried out on samples containing aqueous Rhodamine 6G inside AOT/*iso*-octane reverse micelles. The absorption measurements were performed by Dr. Laura Swafford of the Levinger group at Colorado State University. The experiments are included with the permission of Professor Nancy Levinger. The fluorescence correlation spectroscopy (FCS) experiments were performed by myself and Eric Scott.

The second part of the chapter described preliminary experiments I carried out on reverse micelle samples containing both aqueous Cyanine-3 (Cy3) and Cyanine-5 (Cy5). These two dye molecules are a commonly used FRET pair and the goal of these experiments was to investigate, albeit preliminary, whether FRET was occurring inside the reverse micelle samples. The experiments included are steady-state fluorescence emission measurements, fluorescence correlation spectroscopy and time-resolved fluorescence lifetime measurements.

5.1 Experimental (R6G in AOT/*Iso*-octane Reverse Micelles):

5.1.1 *Sample Preparation*: Rhodamine 6G was purchased from Sigma-Aldrich (St. Louis, MO, USA). The solid dye was dissolved in Millipore water and the resulting solution stored under refrigeration. The reverse micelle solutions were prepared from AOT (sodium di-2-ethylhexyl sulfosuccinate, 99%, Sigma-Aldrich, St. Louis, MO), *iso*-octane (99.8%, Sigma-Aldrich, St. Louis, MO), and aqueous dye solution. The AOT undergoes a purification process, which has been described elsewhere[1]. Reverse micelles were prepared by dissolving AOT in *iso*-octane to

form a 0.3 M stock solution to which aqueous dye solution and water were added. All samples were prepared using 2 ml of a 0.3 M AOT in *iso*-octane solution, 10.8 μL of an aqueous R6G solution, for which the concentration varied from 1.7 x 10^{-5} M to 3.0 x 10^{-5} M. The size (w_0) and concentration of the reverse micelles was then adjusted by adding an appropriate amount of *iso*-octane and water, totaling 1 ml, resulting in a reverse micelle sample with an overall AOT concentration of 0.2 M. For the experiments performed herein, the concentration of AOT in the final solution was 0.02 M, unless otherwise noted. To make these final samples, a 100 μL aliquot of a 0.2 M AOT sample was diluted into 900 μL of isooctane. The final dye concentration ranged from 1.1 x 10^{-8} M to 6.1 x 10^{-8} M. This yield occupation numbers for R6G molecules in the reverse micelles that range from 1 R6G molecule per 1.1 to 6.1 x 10^4 reverse micelles.

5.1.2 *Steady-State and Time Resolved Measurements*: UV-Vis absorption spectroscopy was used to identify the absorption spectra of R6G in different sized reverse micelles. This was accomplished using a Cary 500 UV/Vis-NIR Spectrophotometer (Varian Inc., Walnut Creek, CA, USA). Spectra were collected using a 1 cm pathlength cuvette. Spectra were referenced to the spectrum of neat isooctane in the sample cuvette. Each sample was scanned a minimum of three times and the resulting spectra were averaged.

5.1.3 Fluorescence Correlation Spectroscopy Measurements: Fluorescence correlation spectroscopy (FCS) was used to probe the dynamics occurring within the reverse micelles. The experimental procedure and setup for the FCS experiments have been reported previously[2-4]. Briefly, the sample was placed into a well-slide and covered with a microscope cover slide, which sealed to the well-slide to prevent evaporation. The well-slide was treated with Sigmacote (Sigma-Aldrich, St. Louis, MO, USA) to prevent the R6G molecules from sticking to the glass

cover slide. Prior to FCS experiments, well-slides were stored overnight in Piranha solution to ensure cleanliness. Before use, the well-slides were rinsed with water and placed into an oven for 10 minutes and then cooled to room temperature. The sample was placed on the stage of a Nikon Eclipse TE-2000-U microscope (Nikon Inc., Melville, NY, USA) and irradiated with a CW laser beam at either 514 nm (Ar ion laser, Melles-Griot, Carlsbad, CA, USA) or 532 nm (Nd:YAG laser, B & W Tek, Newark, DE, USA) using a 100× 1.3 numerical aperture microscope objective. The laser power was 0.05 mW, before entering the microscope. The resulting fluorescence and laser light were transmitted back through the microscope. Fluorescence was separated from the incident laser light with a dichroic mirror, which transmitted the fluorescent light out of the microscope at a 90 degree angle. Upon exiting the microscope, the fluorescence was split by a 50/50 beam splitter and imaged onto two 50 μm confocal pinholes. The resulting light was band-pass filtered and focused onto two single-photon-counting avalanche photodiode detectors (PerkinElmer Inc., Waltham, MA, USA). The resulting output of the detectors was recorded using the two channels of an ALV-5000E/EPP card (ALV, Langen, Germany) interfaced to a computer. Samples underwent ten, 200-hundred second scans. For data analysis, the scans were averaged and plotted in a graphical analysis program (Igor Pro version 5.03). The fitting routine was performed using this same data analysis program.

5.2 Results and Discussion

Figure 5.1 shows the steady-state absorption of varying sizes of 0.02 M AOT reverse micelles containing aqueous R6G with an overall concentration of 1.2 x 10^{8} M. The reverse micelles ranging in size from w_0=2 to w_0=4 are consistent with the dye molecules being solvated within the water pool of the reverse micelles. The absorbance peak is shifted slightly to the red

consistent with the dye experience a more nonpolar environment due to the AOT surfactant and is-octane than in pure aqueous solution. Moreover, there is a slight growth in the blue-shifted absorbance shoulder for the w_0=2 sample. However, drastic changes occur in the w_0=1 reverse micelles. Here, the main absorbance peak at approximately 549 nm decreases and the shoulder at approximately 514 nm becomes as intense as the peak at the longer wavelength. This is consistent with the R6G molecules forming H-aggregates or H-dimers. Recall from the previous discussion above that J-aggregates are red-shifted from the monomer peak. The spectra are consistent with those observed for Cy3 inside w_0=1 reverse micelles as described previously. Thus, this data suggests that the extremely confined environment of the w_0=1 reverse micelle induces aggregation of the R6G dye molecules.

Figure 5.2 shows the autocorrelation function for two w_0=1 reverse micelle sample with differing overall concentrations of R6G, which are 1.1 x 10^{-8} M to 6.1 x 10^{-8} M. The autocorrelation functions are consistent with diffusion being the main dynamic process occurring within the sample. Interestingly, the width of the autocorrelation function differs between the two samples. This behavior is consistent with the results presented previously for aqueous Cy3 at differing overall concentration inside w_0=1 reverse micelles. The increased width of the more concentrated R6G sample suggests that there is aggregation occurring between the dye molecules that is also inducing two reverse micelles to conjoin and for an elliptical structure as described previously. These two pieces of data combine provide further evidence that an aggregated form of the dye exists and the reverse micelles have conjoined to form an ellipsoidal structure, i.e. the transient dimer discussed previously. Thus, the data is consistent with the

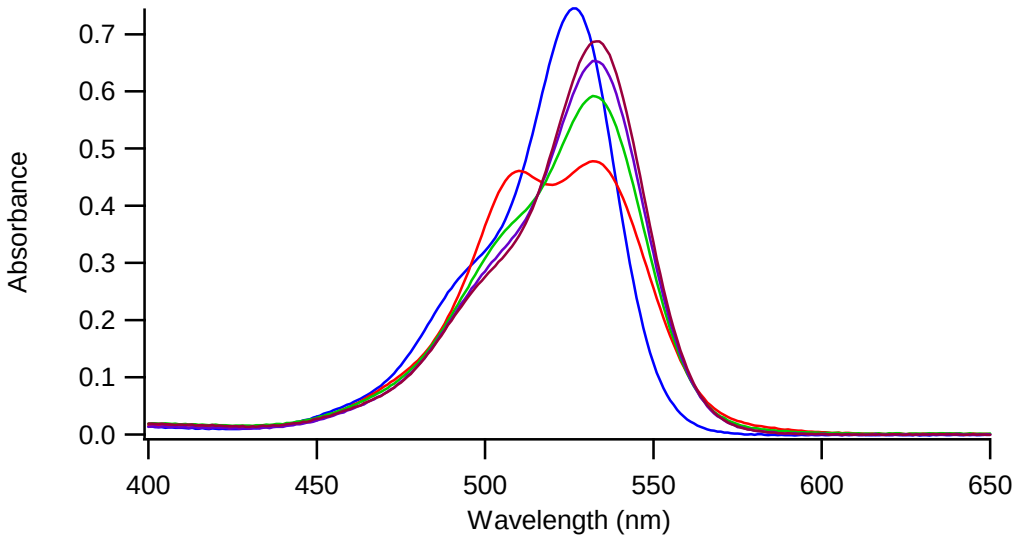

Figure 5.1: Normalized absorption spectra of R6G in water (blue) and four different sized reverse micelles; w_0=1 (red), w_0=2 (green), w_0=3 (purple), w_0=4 (brown). The concentration of AOT in all samples is 0.02M AOT and the overall R6G concentration is 1.2×10^{-8} M.

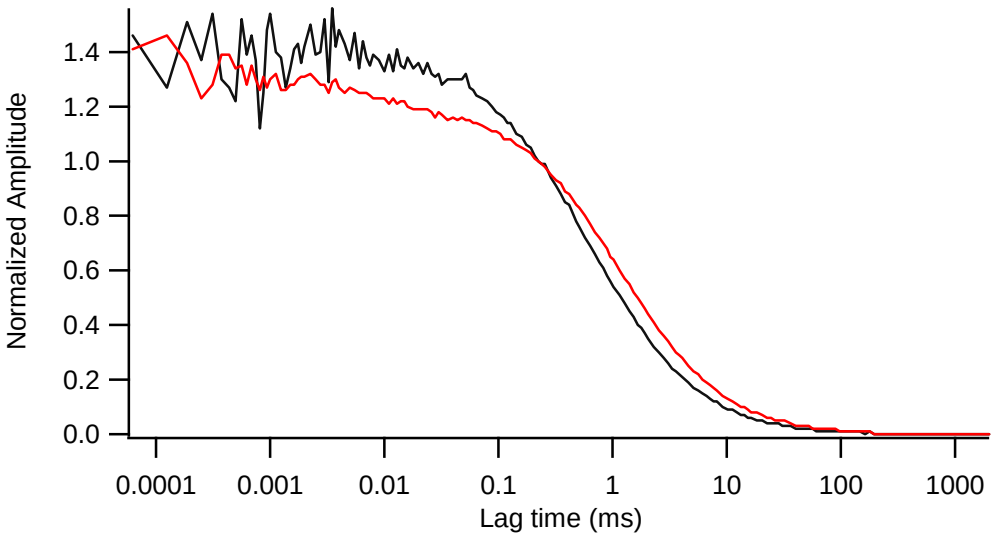

Figure 5.2: Autocorrelation functions of R6G in 0.02M AOT w_0=1 reverse micelles. The concentrations of the two samples are 1.1 x 10^{-8} M (black) and 6.1 x 10^{-8} M 9 (red).

mechanism and previous model described. With this information, the autocorrelation functions were fit to a similar model as that applied to the Cy3 reverse micelle data, as shown in the equation:

$$G(\tau) = \left(\frac{A}{1 + \frac{\tau}{\tau_d}} \right) * \left(1 + B \exp\left(\frac{-\tau}{\tau_{rxn}} \right) \right) \tag{5.1}$$

where, A is the amplitude of the autocorrelation function, B is the fraction of molecules undergoing dynamics on the shorter timescale, τ_{rxn} is proposed to be the reaction time for the association/dissociation of the transient dimer complex (as described in the previous chapter) and τ_d is the diffusion time. Analyzing the autocorrelation functions to equation 5.1 reveals that the reverse micelle sample with the higher concentration of R6G (6.1 x 10^{-8} M) contains a longer diffusion time than what is observed for the sample with the lower concentration of R6G (1.1 x 10^{-8} M). This interesting behavior is consistent with that observed in the reverse micelles labeled with Cy3, as described previously. The diffusion time of 121 ± 10 μs corresponds to a species with a diffusion coefficient of 1.2 x 10^{-10} m^2/s, consistent with the transient dimer of the reverse micelles. The longer diffusion component is not observed for the other sample. However, the diffusion time is consistent with isolated spherical reverse micelles containing individual R6G molecules. This behavior is consistent with that observed for the Cy3 labeled reverse micelles in which lower concentrations of Cy3 inside the reverse micelles did not exhibit the anomalous diffusion behavior.

The analysis of the autocorrelation functions to equation 5.1 also reveals a reaction time of approximately 17 μs for the more concentrated R6G labeled reverse micelle sample,

consistent with the results reported in the previous chapter for Cy3 molecules in the same reverse micelle system.

The interesting behavior observed within this system suggests that dye dimerization is not limited to the cyanine group and specifically Cy3. The observation of aggregation within the R6G labeled reverse micelles indicates that even at very low overall concentrations the dye starts to aggregate, which likely induces the transient dimer formation of the reverse micelles. Further experiments are needed to better understand the nature of the R6G labeled reverse micelles. Additional experiments could investigate changes in the steady-state fluorescence of the Rhodamine molecules as a function of both the reverse micelle size and the overall dye concentration. Dimerization (or aggregation) of the dye molecules should cause changes to the dye's spectroscopy. This could be seen through the appearance of new spectroscopic features within the spectra, an enhancement of total fluorescence or a decrease in the fluorescence and/or quantum yield. Recall that H-aggregates tend to be weakly fluorescent but that instances have been reported in which H-aggregates were highly fluorescent have been reported, albeit in the case of cyanine dyes and not rhodamines. Thus, the rigid environment of the reverse micelle could enhance the fluorescence intensity of these aggregates.

Further steady-state absorption measurements could investigate the nature of the peak growth that is observed in the w_0=1 reverse micelles. The growth of the blue-shifted peak is likely due to dimerization. This hypothesis could be tested by altering the overall concentration of R6G within the w_0=1 reverse micelles. If this were aggregation, it would be expected that the peak would become more intense as the overall concentration of R6G increased. Furthermore, due the low cost and high availability of R6G, the upper limit for the overall concentration of R6G could easily approach the upper limit for solubility of the dye in water. In contrast to the

Cy3 experiments, in which the dye is expensive and not available in large quantities, the absorption measurements for R6G labeled reverse micelles could yield quantitative information including the equilibrium constant for the association/dissociation of the dimer. For example, a large concentration range will produce spectra that show a change in the absorption of the monomer and dimer peak. Selwyn and co-workers.[5] proposed the following analysis in order to obtain equilibrium constant for both aqueous Rhodamine B and aqueous R6G and the same (or similar) could be applied to the aggregation of R6G in AOT reverse micelles. Assuming the reaction is strictly conversion of monomers to dimers, the following is true[5]:

$$a(\lambda, c_j) = a_m(\lambda)X + a_d(\lambda)\frac{(1-X)}{2} \tag{5.2}$$

where, a (λ, c_j) is the effective solution extinction coefficient for a solution of total concentration c_j at a given wavelength λ, $a_m(\lambda)$ and $a_d(\lambda)$ are the extinction coefficients for the pure monomer and pure dimer at a given wavelength and X is the mole fraction of the monomer. The mass action expression can be written as[5]:

$$K = \frac{2X^2 c}{1-X} \tag{5.3}$$

where, K is the equilibrium constant and c is the total concentration of dye in the solution. Using initial guess values for K a corresponding value of X for a given concentration can be obtained. With this information, equation 5.2 can be solved using a least linear squares fitting routine to determine the values of $a_m(\lambda)$ and $a_d(\lambda)$. If the value of K is appropriate, the experimentally measured values of $a_m(\lambda)$ and $a_d(\lambda)$ should fall on a straight line defined by the conditions[5]:

$$\begin{aligned} a(\lambda, c_j) &= a_m\lambda \\ a(\lambda, c_j) &= a_d(\lambda/2) \end{aligned} \tag{5.4}$$

The top part of equation 5.4 is true when X=1 (i.e. all monomer is present) and the bottom part is true when X=0 (i.e. all dimer is present in the sample). Thus, using equations 5.2-5.4 it would be possible to approximate the value of K for the association/dissociation reaction. This approach could complement the method described in Chapter 3 to determine the equilibrium constant for the dimerization reaction of Cy3 in which fluorescence measurements were used. With this information, the kinetics of the intermicellar interactions of the R6G labeled reverse micelles could be investigated using FCS to determine if the rate constants are similar to those determined in the Cy3 labeled reverse micelle system.

As mentioned, more FCS experiments on varying overall concentrations of R6G could investigate the nature of the intermicellar interactions within this system. The preliminary results show an increased diffusion time at the higher R6G concentration (Figure 5.2) consistent with the mechanism described in Chapter 4. To further test this hypothesis, more experiments are needed as a function of varying overall R6G concentration in w_0=1 reverse micelles. Analyzing the data to equation A.1 would yield information about the diffusion time of the reverse micelles. Thus, it would be possible to determine at what point the diffusion time changes to the longer time that is consistent with the transient dimer species observed in Chapter 4.

Further FCS experiments could measure the autocorrelation function of R6G labeled reverse micelles with varying concentrations of AOT. It is expected that the autocorrelation function would change as a function of AOT. Recall in Chapter 4 in which the amount of dimerization decreased with increasing concentration of AOT while holding the overall concentration of Cy3 constant. This was attributed to the fact that as the concentration of surfactant increases the number of reverse micelles within the sample increases. Thus, if

aggregation is in fact present in the R6G labeled reverse micelles than changes in the autocorrelation function should be apparent as the concentration of AOT changes.

To determine the kinetics of the R6G labeled reverse micelles, the same mechanism and equations described in Chapter 4 could be used. Recall the mechanism, which involved two steps to from the transient dimer (Figure 5.3). It can be assumed that the equilibrium constant calculated via the absorption measurements described above governs the entire reaction and includes both steps within the mechanism. Thus, using this value and the method described in Chapter 4 the kinetics of this particular system can be determined. It is expected that the rate constants would be similar to those determined for the Cy3 labeled reverse micelles. Thus, the use of this second dye-reverse micelle system could proved further evidence to the existence of the transient dimer as well as the associated kinetics.

Lastly, independent dynamic light scattering measurements would be needed to corroborate that the anomalous diffusion behavior is only present in those reverse micelles containing a R6G dimer. Since the DLS measurements are sensitive to the bulk sample, the diffusion coefficient and hydrodynamic radius for w_0=1 reverse micelles containing R6G dye molecules would be expected to show isolated, individual reverse micelles with the expected values for the two properties. This would ensure that the reverse micelles samples were made properly and that the anomalous diffusion behavior is in fact only seen in the small subset of R6G labeled reverse micelles that have taken on the transient dimer shape. This measurement would confirm that the reverse micelles are present in their isolated, spherical shape, as expected. This measurement would be done over a range of overall R6G concentrations.

The preliminary experiments suggest that the R6G labeled reverse micelles behave similarly to the Cy3 reverse micelle system described in previous chapters. The increased

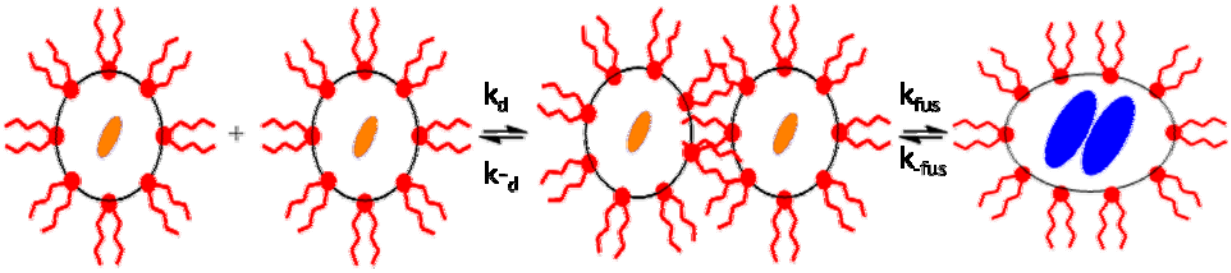

Figure 5.3: Proposed mechanism for Cy3 in AOT reverse micelles (chapter 4), which is consistent with the data for R6G in AOT reverse micelles.

absorbance of the blue shifted band in the absorption measurements suggests that dimerization is occurring in the smallest reverse micelle w_0=1. Furthermore, the increased width of the autocorrelation function also suggests that the reverse micelles are forming the transient dimer species described in Chapter 4. The extremely high local concentration when two R6G monomers come in contact makes the dimer the more favorable form of the dye. The results are interesting as this system contains a dye from the xanthene group and not the cyanine group. Thus, the interesting behavior seems to be more universal than simply due to the structure of cyanines. Therefore, it would be interesting to further study this system as well as some other classes of dyes to see if this interesting behavior is in fact occurring in a wide variety of systems.

5.3 Fluorescence Resonance Energy Transfer:

The process known as fluorescence (or forster) resonance energy transfer (FRET) was first observed in 1948 by the German scientist Theodore Forster[6, 7]. FRET involves the transfer of energy between two chromophores, one acting as the acceptor and the other as the donor. In order for FRET to be observed, the distance between the acceptor and donor chromophore has to be less than 10 nm[6, 7]. FRET is typically quantified in terms of the efficiency of the energy transfer, which is described by the equation:

$$E = \frac{k_{ET}}{k_f + k_{ET} + \sum k_i} \tag{5.5}$$

where, k_{ET} is the rate constant associated with the transfer of energy between the donor and acceptor chromophore, k_f is the rate of radiative decay and k_i refers to the various non-radiative decay pathways present in the system. Furthermore, equation 5.1 can be expressed in terms of the separation between the donor and acceptor chromophore as follows:

$$E = \frac{1}{1 + r/R_0} \tag{5.6}$$

Where, r is the separation distance and R_0 is the forster distance. The term R_0 is the distance at which the FRET efficiency is ≈ 50%. Equation 5.2 illustrates the inverse power law that is observed for FRET efficiency of a donor-acceptor pair. The FRET efficiency can also be calculated by using the fluorescence intensity of the donor in the presence and absence of the acceptor molecules by using the equation:

$$E = 1 - F_{D'} / F_D \tag{5.7}$$

where, $F_{D'}$ and F_D are the relative fluorescence intensities in the presence and absence of the acceptor molecule, respectively. Furthermore, the fluorescence lifetime of the donor molecule can provide information about the FRET efficiency from the equation:

$$E = 1 - \tau_{D'} / \tau_D \tag{5.8}$$

where, $\tau_{D'}$ and τ_D is the fluorescence lifetime of the donor in the presence and absence of the acceptor. Thus, measuring the fluorescence properties of donor-acceptor pair provides information about the FRET efficiency of the system. Moreover, knowledge of the FRET efficiency can provide information about various chemical and biological process occurring within complex systems if FRET pairs are used to monitor these reactions, as will be discussed more fully in the following section.

5.4 Experimental (Cy3-Cy5 in AOT/*Iso*-octane Reverse Micelles):

5.4.1 *Sample Preparation:* Cy3 and Cy5 monoreactive dye packs were purchased from GE Life Science (Piscataway, NJ, USA). The solid dye was dissolved in Millipore water and the resulting solution stored under refrigeration. The reverse micelle solutions were prepared from AOT (sodium di-2-ethylhexyl sulfosuccinate, 99%, Sigma-Aldrich, St. Louis, MO), *iso*-octane (99.8%, Sigma-Aldrich, St. Louis, MO), and aqueous dye solution. The AOT undergoes a

purification process, which has been described elsewhere[1]. Reverse micelles were prepared by dissolving AOT in *iso*-octane to form a 0.3 M stock solution to which aqueous dye solution and water were added. All samples were prepared using 2 ml of a 0.3 M AOT in *iso*-octane solution, 10.8 μL of an aqueous Cy3 or Cy5 solution, for which the concentration varied from 9.9×10^{-5} M to 9.9×10^{-6} M. The size (w_0) and concentration of the reverse micelles was then adjusted by adding an appropriate amount of *iso*-octane and water, totaling 1 ml, resulting in a reverse micelle sample with an overall AOT concentration of 0.2 M. For the experiments performed herein, the concentration of AOT in the final solution was 0.02 M, unless otherwise noted. To make these final samples, a 100 μL aliquot of a 0.2 M AOT sample was diluted into 900 μL of isooctane. The final dye concentration ranged was set at 3.6×10^{-8} M for all samples. This yields an occupation number for Cy3 and Cy5 molecules in the reverse micelles of 1 Cy3 or Cy5 molecule per 2.0×10^{4} reverse micelles. After each sample was prepared separately, the two solutions were mixed together for analysis.

5.4.2 *Steady-State and Time Resolved Measurements*: Steady-state fluorescence spectra were collected to identify changes in the emission wavelengths due to FRET between Cy3 and Cy5 within the different size reverse micelles. The spectra were collected using a SPEX steady-state spectrofluorometer (HORIBA Jobin Yvon, Edison, NJ, USA) using a 1 cm pathlength cuvette. Spectra were collected by exciting at 514 and 532 nm, to capture emission characteristics of various features observed in absorption spectra.

Fluorescent lifetime measurements were performed to monitor any change in the fluorescence lifetime of Cy3 due to FRET. To do so, a Fluorocube instrument (HORIBA Jobin Yvon, Edison, NJ, USA), which provides time-correlated single photon counting data, was used. The instrument response function was measured and the sample was subsequently loaded into

the instrument. All samples were excited at a 514 nm wavelength of an Argon flash lamp selected by a monochromator. Subsequent fluorescence was detected at 560, 600 and 650 nm.

5.5 Results and Discussion (Cy3-Cy5):

Figure 5.4 shows the absorption and emission spectra of Cy3 and Cy5[8]. The spectral overlap between the emission of Cy3 and the absorbance of Cy5 makes these two dyes a suitable FRET pair. In a typical FRET experiment using these two dyes, Cy3 is excited and transfers its energy from the excited state to the Cy5 molecule without emitting radiatively. On the other hand, Cy5 will absorb this energy and fluorescence will be emitted and thus can be detected suing conventional fluoresce spectroscopy methods.

Figure 5.5 shows the steady-state fluorescence emission spectra of different sized reverse micelles containing both aqueous Cy3 and Cy5 excited at the 514 nm wavelength. The spectra for the w_0=1 is consistent with the previously reported results in chapter 3 and resembles that of only Cy3 molecules being excited and emitting fluorescence. The spectrum contains three peaks at 570 nm, 600 nm and 650 nm, which is consistent with the dimer form of Cy3 being excited at the 514 nm wavelength. The results for each excitation wavelength are consistent with those reported in Chapter 3. Furthermore, the spectrum for w_0=3 is also consistent with the monomer form of Cy3 being excited as it only contains the two peaks at 570 nm and 600 nm. This is true

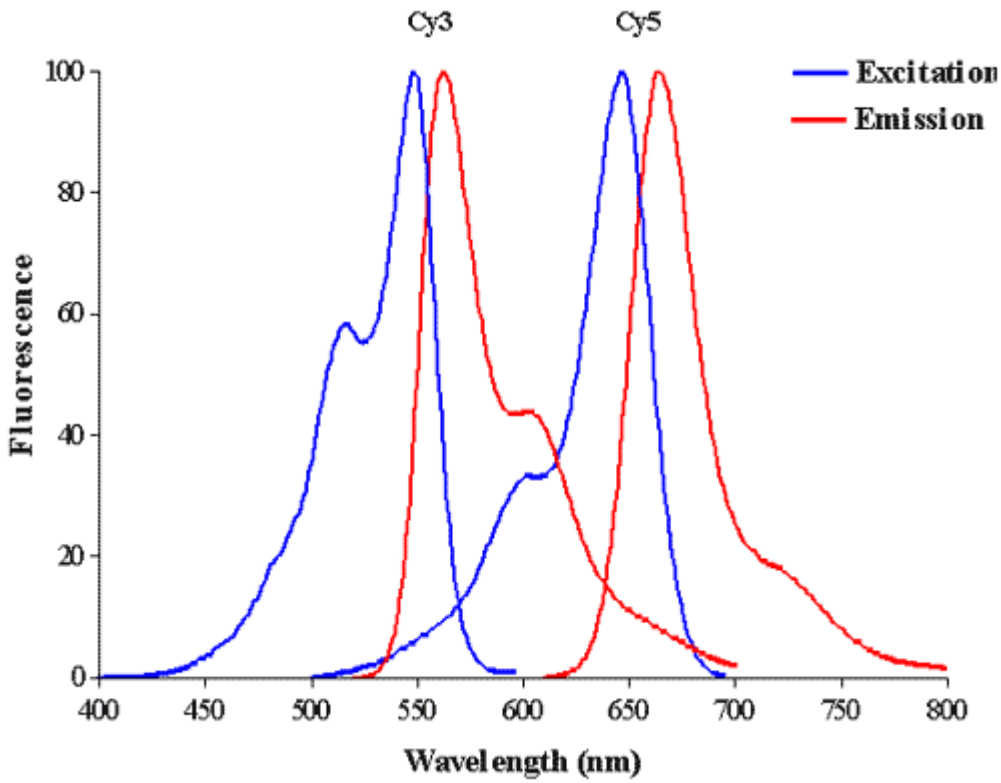

Figure 5.4: Absorption and Emission spectra for Cy3 and Cy5. Note the spectral overlap between the emission of Cy3 and the absorbance of Cy5 making these molecules a suitable FRET pair.

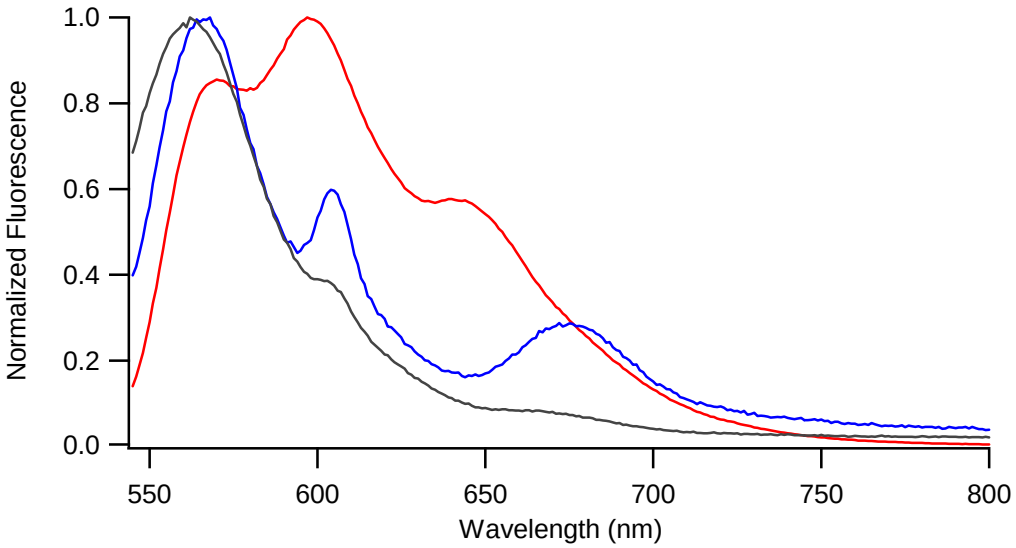

Figure 5.5: Normalized fluorescence of Cy3-Cy5 dye molecules in three different sized reverse micelles; w_0=1 (red), w_0=2 (blue), w_0=3 (black). The concentration of AOT in all samples is 0.02M AOT and the overall Cy3-Cy5 concentration is 3.6 x 10^{-8} M.

for all three excitation wavelengths used in these experiments. The spectrum for w_0=2 shows interesting changes from the spectra for w_0=1 and w_0=3. The spectrum shows a peak at 670 nm upon excitation at the 514 nm wavelength. Recall that the absorption spectrum of Cy5 shows minimal absorbance below 520 nm and thus the 514 nm should minimally excite the Cy5 molecules. Moreover, Cy5 emits maximally at 670 nm in aqueous solution, which is consistent with the peak observed in this sample. Furthermore, Figure 5.6 shows the unnormalized fluorescence emission. It can be seen that the relative intensity of the peak at 570 nm, which is attributed to Cy3, is greatly reduced compared to the w_0=3 sample (Note: The unnormalized emission for w_0=1 is not shown due to the extremely high intensity compared to the other two samples). This behavior suggests that FRET is occurring within the w_0=2 reverse micelles between the Cy3 and Cy5 molecules.

Figure 5.7 shows the fluorescence lifetime decays for the same w_0=2 and w_0=3 samples described above. The samples were excited with a 491 nm LED and the fluorescence was detected at 570 nm. The collection wavelength was chosen at 570 nm since this is where Cy3 emits maximally and the fluorescence lifetime would be expected to change if FRET were occurring[9-12]. Interestingly, the decay shows a qualitatively shorter lifetime for w_0=2 than in w_0=3, consistent with FRET occurring the sample. The decays for the two samples have not been analyzed quantitatively at this point in time.

The preliminary results suggest that FRET is occurring between Cy3 and Cy5 within the w_0=2 reverse micelles. However, further experiments are needed to verify that this is the process that is occurring within this system. One experiment that could provide more insight into whether FRET is in fact occurring is two-color fluorescence cross-correlation spectroscopy. The

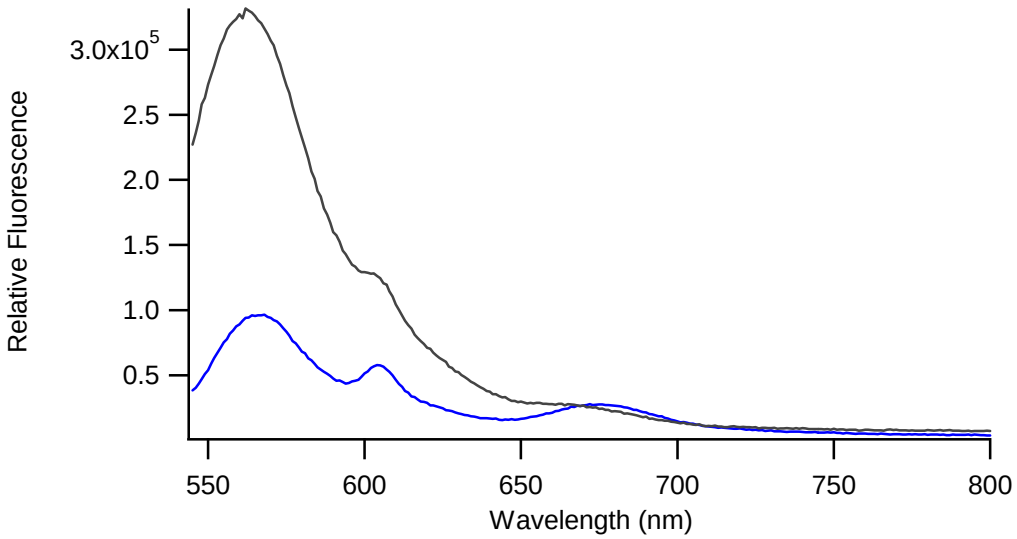

Figure 5.6: Relative fluorescence of Cy3-Cy5 dye molecules in w_0=2 (blue) and w_0=3 (black) AOT reverse micelles. The concentration of AOT in all samples is 0.02M AOT and the overall Cy3-Cy5 concentration is 3.6 x 10^{-8} M.

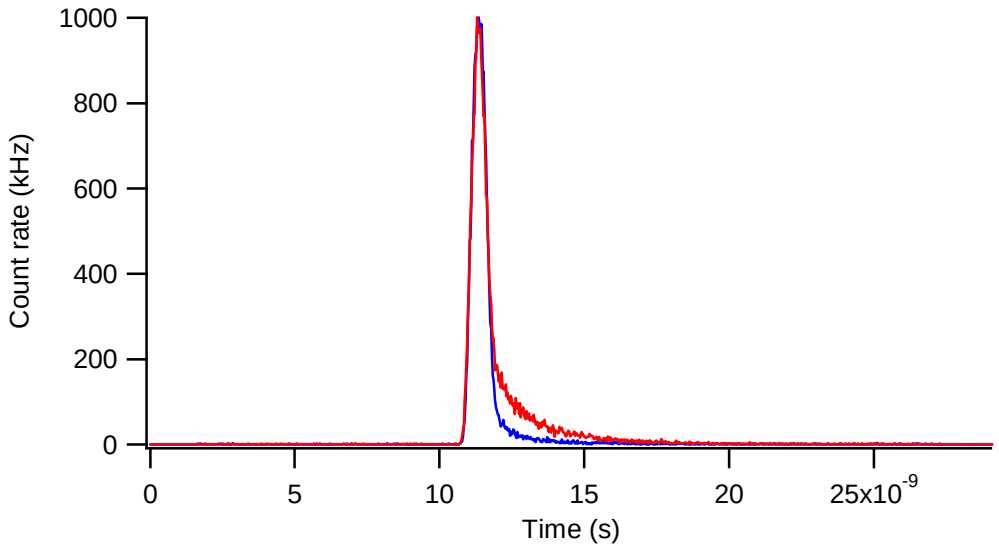

Figure 5.7: Fluorescence lifetime decays of Cy3-Cy5 dye molecules in w_0=2 (blue) and w_0=3 (red) AOT reverse micelles. The concentration of AOT in all samples is 0.02M AOT and the overall Cy3-Cy5 concentration is 3.6 x 10^{-8} M.

experiment could be setup such that one detector is monitoring the emission wavelengths corresponding to the Cy3 molecules and the other detector is monitoring the emission wavelengths of the Cy5 molecules. For the reverse micelles where FRET is thought to be

occurring, i.e. w_0=2, the experiments should show considerable cross-correlation between the two emission wavelengths. In contrast, the larger reverse micelles should show very little correlation as at this point in time it is believed that FRET is not occurring within these samples. This could provide interesting insight into the nature of the different systems. Moreover, information about the timescales of different process occurring within the system could be determined.

:

1. Stahla, M. L.; Baruah, B.; James, D. M.; Johnson, M. D.; Levinger, N. E.; Crans, D. C., H-1 NMR Studies of Aerosol-OT Reverse Micelles with Alkali and Magnesium Counterions: Preparation And Analysis Of Maots. *Langmuir* **2008,** 24, (12), 6027-6035.

2. Fogarty, K.; McPhee, J. T.; Scott, E.; Van Orden, A., Probing the Ionic Atmosphere of Single-Stranded DNA Using Continuous Flow Capillary Electrophoresis and Fluorescence Correlation Spectroscopy. *Analytical Chemistry* **2009,** 81, (1), 465-472.

3. Jung, J.; Ihly, R.; Scott, E.; Yu, M.; Van Orden, A., Probing the Complete Folding Trajectory of a DNA Hairpin Using Dual Beam Fluorescence Fluctuation Spectroscopy. *Journal Of Physical Chemistry B* **2008,** 112, (1), 127-133.

4. Jung, J. Y.; Van Orden, A., A Three-State Mechanism for DNA Hairpin Folding Characterized By Multiparameter Fluorescence Fluctuation Spectroscopy. *Journal Of The American Chemical Society* **2006,** 128, (4), 1240-1249.

5. Selwyn, J. E.; Steinfel.Ji., *Journal Of Physical Chemistry* **1972,** 76, (5), 762-&.

6. Guilbault, G. G., *Practical fluorescence; theory, methods, and techniques*. ed.; M. Dekker: New York, 1973.

7. Lakowicz, J. R., *Principles of fluorescence spectroscopy*. ed.; Kluwer Academic/Plenum: New York, 1999.

8. Lifesciences, G., Cy3 and Cy5 Absorption and Emission Properties. In ed..

9. Iqbal, A.; Arslan, S.; Okumus, B.; Wilson, T. J.; Giraud, G.; Norman, D. G.; Ha, T.; Lilley, D. M. J., Orientation Dependence in Fluorescent Energy Transfer Between Cy3 and Cy5 Terminally Attached to Double-Stranded Nuclelic Acids. *Proceedings Of The National Academy Of Sciences Of The United States Of America* **2008,** 105, (32), 11176-11181.

10. Iqbal, A.; Wang, L.; Thompson, K. C.; Lilley, D. M. J.; Norman, D. G., The Structure of Cyanine 5 Terminally Attached to Double-Stranded DNA: Implications for FRET Studies. *Biochemistry* **2008,** 47, (30), 7857-7862.

11. Massey, M.; Algar, W. R.; Krull, U. J., Fluorescence Resonance Energy Transfer (FRET) for DNA Biosensors: FRET Pairs and Forster Distances for Various Dye-DNA Conjugates. *Analytica Chimica Acta* **2006,** 568, (1-2), 181-189.

12. Gruber, H. J.; Hahn, C. D.; Kada, G.; Riener, C. K.; Harms, G. S.; Ahrer, W.; Dax, T. G.; Knaus, H. G., Anomalous Fluorescence Enhancement of Cy3 and Cy3.5 Versus Anomalous Fluorescence Loss of Cy5 And Cy7 Upon Covalent Linking to Igg and Noncovalent Binding to Avidin. *Bioconjugate Chemistry* **2000,** 11, (5), 696-704.

Chapter 6

Photon Counting Histogram Analysis on Single-Stranded DNA Using Fluorescence Correlation Spectroscopy and Capillary Electrophoresis

This chapter presents work that was performed on a 40 base pair single stranded DNA (ssDNA) sequence labeled with Tetramethyl Rhodamine (TMR) as a function of both the applied voltage and the Magnesium Chloride ($MgCl_2$) concentration in the sample. The goal of the experiments was to determine if the applied voltage, and subsequent Joule heating, was significant enough to alter the molecular brightness of TMR attached the DNA. The experiments were carried out by combining fluorescence correlation spectroscopy with photon counting histogram analysis. These experiments contributed to a paper in *Analytical Chemistry*, in January, 2009[1].

6.1 Introduction

6.1.1 Photon Counting Histogram Analysis

Photon counting histogram analysis (PCH) is a valuable technique to supplement the previously described advantages of fluorescence correlation spectroscopy (chapter 2). If multiple fluorescent species exist within a sample and their diffusion coefficients do not differ significantly, the autocorrelation function obtained via FCS measurements cannot resolve each species. However, PCH analysis can resolve the molecular brightness of more than one fluorophore within a system. Moreover, this technique yields information about the number of fluorophores being probed. PCH relies on the difference in molecular brightness whereas autocorrelation analysis relies on the temporal processes that cause fluorescence intensity fluctuations, e.g. diffusion.

PCH was developed simultaneously in 1999 by borh Chen[2] and co-workers and Kask[3] and co-workers. Prior to this time, little attention was given to the probability of detecting a certain number of photons in a given sampling time in FCS measurements, except for experiments carried out in 1989-1990 by Qian and Elson[4, 5]. In their work, they proposed a method to determine the fluorescence intensity distribution in macroscopic probe volumes. In essence, PCH is a variation of Qian and Elson's work. The main difference being that PCH uses confocal microscopy[2, 3]. PCH works because each fluorescent molecule has a characteristic molecular brightness, ε_i, which is defined as the average emission rate of a single molecule of species *i*. Thus, while molecules may have similar diffusion coefficients, they will likely have different values of ε and therefore PCH can be used to resolve multiple species within a sample.

Experimentally, PCH analysis is carried out by collecting the number of photons detected and placing them into successive time bins of identical length. Subsequently, if the diffusion time of the analyte molecule is longer than the sampling time of each bin then each bin represents a snapshot of the molecules fluorescence at a given moment in time. From this data, a histogram is generated that shows the probability of detecting a certain number of photons, *k*, in a given sampling time. An example of what a photon counting histogram might look like is shown in Figure 6.1[2]. The photon counting histogram is dependent on a variety of factors including the detection volume of the particular experimental setup, the concentration of the fluorescent molecules and their molecular brightness. For one photon excitation, the probability of detecting k photons (k>0) from one molecule is defined as[2]:

$$p^{(1)}(k;V_e,\varepsilon) = \frac{1}{V_0}\int Poisson\left[k,\varepsilon\cdot W(\vec{r})\right]d\vec{r} \qquad (6.1)$$

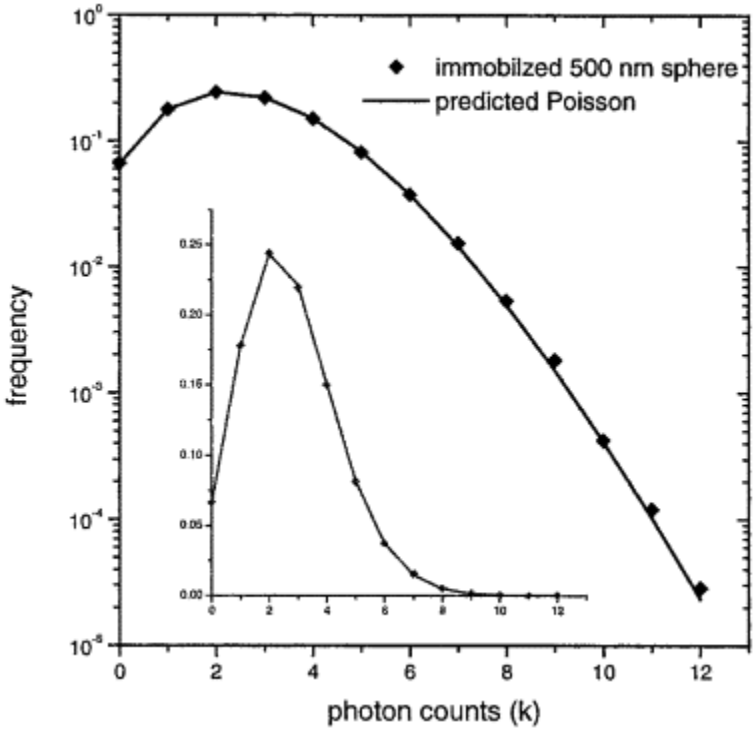

Figure 6.1: Photon counting histogram taken for an immobilized fluorescent sphere. The probability (frequency) is shown on the y-axis and the photon counts are shown on the x-axis. Figure adopted from Chen, Y.; Muller, J. D.; So, P. T. C.; Gratton, E., The Photon Counting Histogram in Fluorescence Fluctuation Spectroscopy. *Biophysical Journal* **1999,** 77, (1), 553-567.

where, V_0 is the reference volume. Furthermore, the Poisson distribution for the probability of detecting k photons when the number of photons detected is x, can be defined as[2]:

$$Poisson(k,x) = \frac{x^k e^{-x}}{k!} \tag{6.2}$$

Chen and co-workers[2] proposed integrating the PCH function to a three dimensional Gaussian approximation for the term W(r). This results in the expression[2]:

$$p_G^{(1)}(k;V_0,\varepsilon) = \frac{\pi\omega_0^2 z_0}{V_0 k!}\int_0^\infty \gamma(k,\varepsilon e^{-2x^2})dx \tag{6.3}$$

here, γ(k,x) is the incomplete gamma function, which in this case is defined as[2]:

$$\gamma(k,x) = \int_0^X \frac{t^{k-1}e^{-t}dt}{(k-1)!} \tag{6.4}$$

In the case of N number of particles, the N probability function can be derived by convoluting the one particle probability function N number of times, giving the equation[2]:

$$p^{(N)}(k;V_0,\varepsilon) = \underbrace{(p^{(1)} \otimes p^{(1)} \otimes ... p^{(1)})}_{N} \tag{6.5}$$

The technique of PCH revolves around the probability of detecting photon counts, which for a one species system is given as[2]:

$$P(k;\overline{N},\varepsilon) = \sum_{N=0}^{\infty} p^{(N)}(k;q,\varepsilon)\cdot Poisson(N,\overline{N}) \tag{6.6}$$

Recalling the convolution approach from equation 3.5, for the case of multiple species, the probability of detecting photon counts can be written as[2]:

$$P(k;\overline{N}_1,\varepsilon_1,\overline{N}_2,\varepsilon_2 ... \overline{N}_N,\varepsilon_N = P(k,\overline{N}_1,\varepsilon_1)\otimes P(k,\overline{N}_2,\varepsilon_2)\otimes ... \otimes P(k,\overline{N}_N,\varepsilon_N) \tag{6.7}$$

Using this analysis, PCH can resolve multiple species within a particular system based on the differences in molecular brightness.

After the initial development of PCH, further research has been devoted to this type of analysis. In particular, groups have looked at ways to make this technique more chemically selective. As a result, several variations of PCH have been developed. One alternative is dual-color PCH[6], which is similar to two dimensional fluorescence intensity distribution analysis (2d-FIDA)[7]. In traditional PCH, each detector monitors the same emission band. In dual-color PCH and 2d-FIDA, two different emission filters are used making each detector sensitive to different wavelengths of emission. Alternatively, polarization methods can be used in which each detector monitors a different polarization of the fluorescence, e.g. parallel or perpendicular. As a result, the photon counting histogram is not only selective to the molecular brightness and analyte concentrations, but it also depends on the emission wavelength or the polarization of the emitted light.

Another variation is photon counting multiple histogram analysis (PCMH)[6] or fluorescence intensity multiple distribution analysis (FIMDA)[8]. In traditional PCH, only one bin size is used and is usually on the order of microseconds. Moreover, the bin time and is typically shorter than the time the molecule diffuses out of the probe volume. In contrast, both PCMH and FIMDA require that the bin times are varied. Varying the bin time over a large time scale, such as microseconds to milliseconds, yields information about the diffusion rates of the molecules in the sample as well as their molecular brightness can be obtained. This is because the diffusion of the molecules affects the shape of the histogram, which is not the case in traditional PCH, where the sampling time is short compared to the diffusion time.

Another variation allows for the determination of both molecular brightness values and fluorescence lifetimes of molecules in the sample. This is known as fluorescent intensity and lifetime distribution analysis (FILDA)[9, 10]. In this method, a pulsed laser source is used, allowing

for both the number of photons detected per bin and the elapsed time between the excitation pulse and the arrival of a photon at the detector to be acquired. A histogram is generated based on the number of photons in the given bin time and the sum of the elapsed time between the excitation pulse and the arrival of a photon at the detector.

In short, PCH and the variations described above have proven to be useful techniques with a variety of applications. Although typically used in experiments in which there is a drastic change in the molecular brightness of the species of interest, such as when a ligand binds to a receptor, this chapter shows the technique's application to ascertain the effects of Joule heating inside a capillary used in capillary electrophoresis coupled with fluorescence correlation spectroscopy.

6.1.2 Effect of Temperature on Fluorescent Molecules

The effect of temperature on the fluorescence emission of molecules has been studied extensively[11, 12]. It has been shown that the fluorescence decreases (as well as the quantum yield) with increasing temperature. One reason for this is the degradation of the fluorescence species at high temperatures. On the other hand, increases in fluorescence due to decreasing temperature can be rationalized by the fact that cooling down a solution can increase the viscosity of the medium, thereby decreasing the rate of collisions. Thus, as the rate of collisions decreases, the propensity for energy to be dissipated via collisional deactivation is reduced. Moreover, other processes involving the excited singlet state, such as intermolecular bonding, tend to occur more faster as the temperature increases[11].

6.1.3 Joule Heating

First described in 1841 by James Prescott Joule, Joule heating is the phenomenon that occurs when a voltage is applied to a conducting material. The current that passes through the

conductor releases heat. In capillary electrophoresis, this process is defined mathematically by the equation[13]:

$$Q = \frac{VI}{\pi r^2 L} \tag{6.8}$$

where Q is the rate of heat generation in units of Watts, V is the applied voltage, I is the current in units of Amperes, L is the length of the capillary and r is the radius of the capillary. Assuming the capillary is cylindrical, the volume is given by the equation[13]:

$$V = \pi r^2 L \tag{6.9}$$

Joule heating can have a significant and unwanted effect in capillary electrophoresis experiments by introducing variance in the peaks. Thus, error is introduced into the experiment. Specifically, heat that is produced can affect the sample solution by altering its viscosity. Moreover, the change in viscosity alters the diffusion rate of the molecules, making them diffuse faster as they become heated. Also, the heat produced can affect the flow profile through the capillary. Instead of having the desired electroosmotic flow, the flow profile resembles laminar flow, This occurs because the temperature at the center of the capillary is different from the temperature at its walls. The walls of the capillary can dissipate heat to the surrounding environment whereas the center of the capillary cannot.

The motivation behind the experiments presented in this chapter is that a significant amount of Joule heating within the capillary would alter the diffusion properties of the sample since the Stokes-Einstein equation contains a temperature parameter[14]. Thus, observed changes in the diffusion properties thought to arise from real events instead result from the error introduced into the experiment by Joule heating. Since diffusion analysis was one a main goal of the overall investigation, it was important to determine what contribution Joule heating has on the results.

6.2 Experimental

6.2.1 Preparing the Capillary

The capillary used in these experiments was a square fused-silica capillary, with an inner diameter of 50 μm and an outer diameter of 375 μm and was approximately 25 cm in length. A square capillary was used to minimize lensing effects on the laser beam, which cause distortions to the shape of the beam. Lensing effects are typically seen with cylindrical capillaries. Moreover, the flat, rectangular shape of the capillary makes it easier to focus the laser onto the surface of the capillary. The capillary is covered with a polyimide coating, which make the capillary stronger and less likely to break. Unfortunately, for laser applications, it makes it impossible to image the laser into the capillary. Therefore, the coating on the capillary was removed. To do so, one of two methods was employed; either a lighter can be used to burn off the coating with a flame, or sulfuric acid can be heated to 75 °C, which will dissolve the coating. The size of the burned window was on the order of 1 cm. The capillary was mounted to a glass slide and affixed onto a stage, allowing for the laser foci to be aligned inside the capillary.

It was important to minimize wall interactions between the sample solutions and the walls of the capillary. To do so, a coating procedure developed by Belder and co-workers. was used[15]. They determined that using poly(vinyl alcohol) (Sigma, St. Louis, MO, USA) to coat the inside walls of the capillary reduced sample-wall interactions. Procedurally, the approximately 25 cm capillary, with a window burned into the coating, as described before, was filled with an acidic aqueous glutaraldehyde solution. The solution was prepared by taking 200 μl of a 50 wt% aqueous glutaraldehyde solution (Fisher, Houston, TX, USA) and adding it to 800 μl of 1M Hydrochloric acid (Mallinckrodt, Hazelwood, MO, USA). After filling the capillary with this solution, a 2.5 wt% solution of poly(vinyl alcohol) (Sigma, St. Louis, MO, USA) in 0.6 M

hydrochloric acid was injected into the capillary for ≈ 10 seconds. The sample was driven into the capillary using 0.5 MPA of N_2 gas. The capillary was allowed to dry using continuous flow of N_2 gas for ≈ 4 hours.. The gluteraldehyde reacts with the poly(vinyl alcohol) molecules to form a coating on the interior walls of the capillary. Prior to collecting data, the capillary was flushed with the appropriate buffer solution.

6.2.2 Sample Preparation

40-oligo poly(dT) single stranded DNA (ssDNA) labeled at the 5' end with Tetramethyl Rhodamine (TMR-ssDNA, Operon Biotechnologies, Huntsville, AL, USA) was diluted to a concentration of approximately 10 nM in a tris-glycine buffer solution, which had a pH of 8.3 (3mM Tris-HCl, 3 mM Glycine, Sigma, St. Louis, MO, USA). Magnesium Chloride (Fisher Scientific, Houston, TX, USA) was added to the buffer solutions in concentrations ranging from 0 to 3 mM. The permanent coating procedure described above was supplemented with a dynamic coating, which involved adding a 0.125 wt% solution of poly(vinylpyrrolidone) (PVP, Sigma, St. Louis, MO, USA) to the sample solutions. This dynamic coating further reduced sample interactions with the interior walls of the capillary. To prevent contamination, all centrifuge tubes and glass bottles holding buffer solutions were autoclaved prior to use.

6.2.3 Instrumentation

The optical setup for these experiments started with an air cooled, continuous wave, Argon-ion laser. The wavelength was set to 514.5 nm. The beam was expanded and then collimated using two telescoping lenses. After being re-collimated, the beam was split using a 50/50 beam splitter (Newport Inc., Irvine, CA, USA). The power of each beam was attenuated using the appropriate absorptive neutral density filters. The nearly parallel beams were then passed through a focusing lens with a focal length of 150 mm. Upon exiting the focusing lens,

the beams hit a 530 nm dichroic mirror, which directs them into a 100x, 1.25 numerical aperture oil immersion objective (Edmund Industrial Optics, Barrington, NJ, USA). The objective focuses the beam into a glass window that has been burned into the fused silica capillary (Polymicrotechnologies, Phoenix, AZ, USA) used to deliver the sample. The size of the laser foci was controlled by carefully position the focusing lens such that it was 300 mm from the back of the microscope objective. The focusing lens was on a stage that can be adjusted in three directions, allowing for the beam size to be minimized ensuring a near ideal Gaussian beam profile. Pressure flow was used to rinse the capillaries, coat the capillaries and introduce the sample prior to taking measurements. To do so, a micro-centrifuge tube containing the appropriate solution was placed into a custom built pressure chamber that was attached to a tank of nitrogen gas. One end of the capillary, which is sealed inside the pressure chamber, was placed into the tube containing the solution. The pressure of nitrogen in the chamber was controlled by a pneumatic pressure regulator (Fairchild Model 81, Winston-Salem, NC, USA), which drove the solution through the capillary. For the experiments discussed in chapter 3, the capillary was filled with the sample and the microcentrifuge tubes containing the sample solution were placed at equal heights on each end of the capillary. A platinum wire, connected to a high voltage power supply (Spellman, Plainview, NY, USA) was inserted into the sealed chamber and placed into the sample. At the other end of the capillary, a grounded platinum wire was placed into the sample. A voltage was applied across the capillary resulting in electrophoretic migration of the target molecules. The resulting fluorescence was collected through the objective described previously and passed back through the dichroic mirror, which rejects the laser light, and was split by a 50/50 beamsplitter cube (Thorlabs, Newton, NJ, USA). After being split, the fluorescence was spatially filtered using two 50 um pinholes (Thorlabs, Newton, NJ, USA) and

subsequently filtered by two 535 long-pass filters, one for each detector. The filtered fluorescence was focused down onto the active area of two single photon counting avalanche photodiode detectors (PerkinElmer Optoelectronics, Wellesley, MA, USA) using aspheric lenses (Newport Inc., Irvine, CA, USA). The raw photon count data was digitized using a two channel, 800 MHz gated photon counter card (Becker and Hickl GmbH, Berlin, Germany) which was interfaced to a Pentium computer. Note that although the instrument was setup to do two beam cross-correlation analysis, only one beam was needed to perform the PCH measurements. After verifying that a cross-correlation peak was present, indicating electrophoretic flow and a voltage across the capillary, the second beam was blocked and the PCH measurements were taken.

6.3 Results and Discussion

The goal of these experiments was to determine the effect of Joule heating inside the capillary used in the FCS-capillary electrophoresis setup. If the temperature inside the capillary was significantly greater than the room temperature, it would impact the diffusion properties of the molecules. Recall the Stokes-Einstein equation, which shows that the diffusion coefficient of molecule is proportional to the temperature, given by the equation[14]:

$$D = \frac{k_B T}{6\pi\eta R_H} \tag{6.10}$$

where, k_B is the Boltzmann constant, T is the temperature, η is the viscosity and R_H is the hydrodynamic radius. The working hypothesis for this investigation is that if the temperature within the capillary was significantly greater than room temperature, the fluorescence properties of TMR would be altered to a measurable degree. Thus, by measuring the molecular brightness of TMR as a function of the applied voltage, it is possible to determine the extent of Joule heating on the experiment.

Figure 6.2 shows the fluorescence emission spectrum of TMR as a function of temperature. It is observed that intensity of the fluorescence emission decreases with increasing temperature. The spectrum indicates that temperature has a significant effect on the brightness of the fluorophore. This result is consistent with previous studies that showed a decrease in the fluorescence emission and quantum yield with increasing temperature[11, 12]. Thus, significant Joule heating should alter the brightness enough that it would be observed in the PCH measurements. Figure 6.3 shows the experimental data and fit line of a TMR-ssDNA sample with a $MgCl_2$ concentration of 2 mM and an applied voltage of 10 kV. Similar data was obtained for $MgCl_2$ concentrations of 0.005 mM, 1 mM, 2 mM and 3 mM and for applied voltages of 0 kV, 10 kV, 12.5 kV and 15 kV. The data for all these samples and the corresponding voltages were analyzed to determine the molecular brightness of the dye. The results of this analysis are shown in Figure 6.4, where the molecular brightness is plotted as a function of the applied voltage for the four samples studied in this experiment. The results suggest that there is not a systematic change in the molecular brightness as a function of either the salt concentration or the applied voltage. Moreover, any changes observed are not significant but rather are within the error of the measurements. If Joule heating was a factor, it would be expected that the molecular brightness values would decrease as a function of increasing voltage (equation 6.8, Figure 6.4).

The molecular brightness values were used to obtain a quantitative value for the temperature inside the capillary. This calculation assumes that the change in temperature is

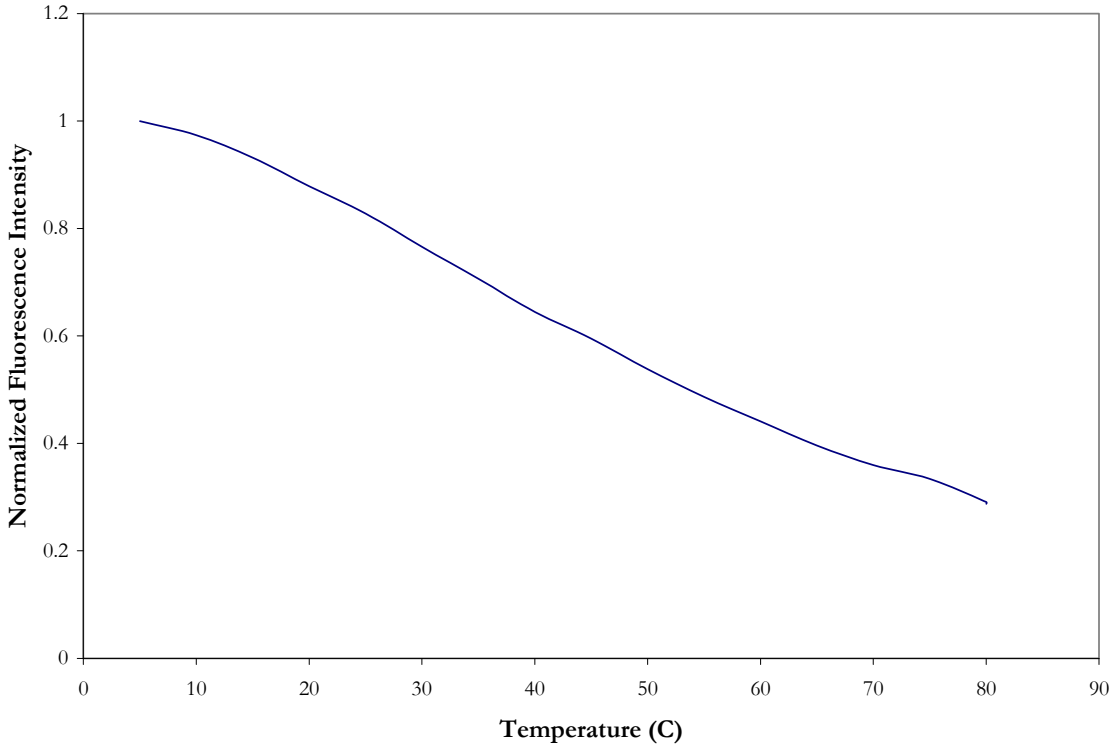

Figure 6.2: Fluorescence emission spectrum as a function of temperature of TMR-ssDNA used in these experiments.

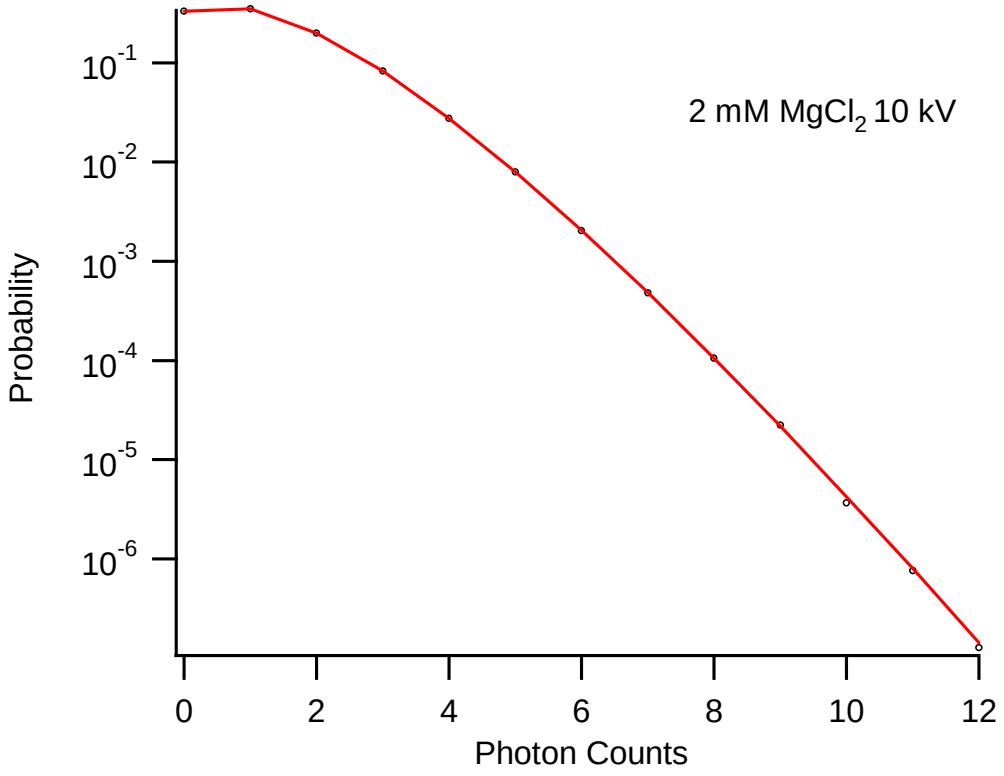

Figure 6.3: Experimental PCH data (dots) and resulting fit (solid red line) for a TMR-ssDNa sample with a $MgCl_2$ concentration of 2 mM and an applied voltage of 10 kV. Similar fits were obtained for other samples with varying Magnesium Chloride concentration, which provided a value for the molecular brightness of each sample.

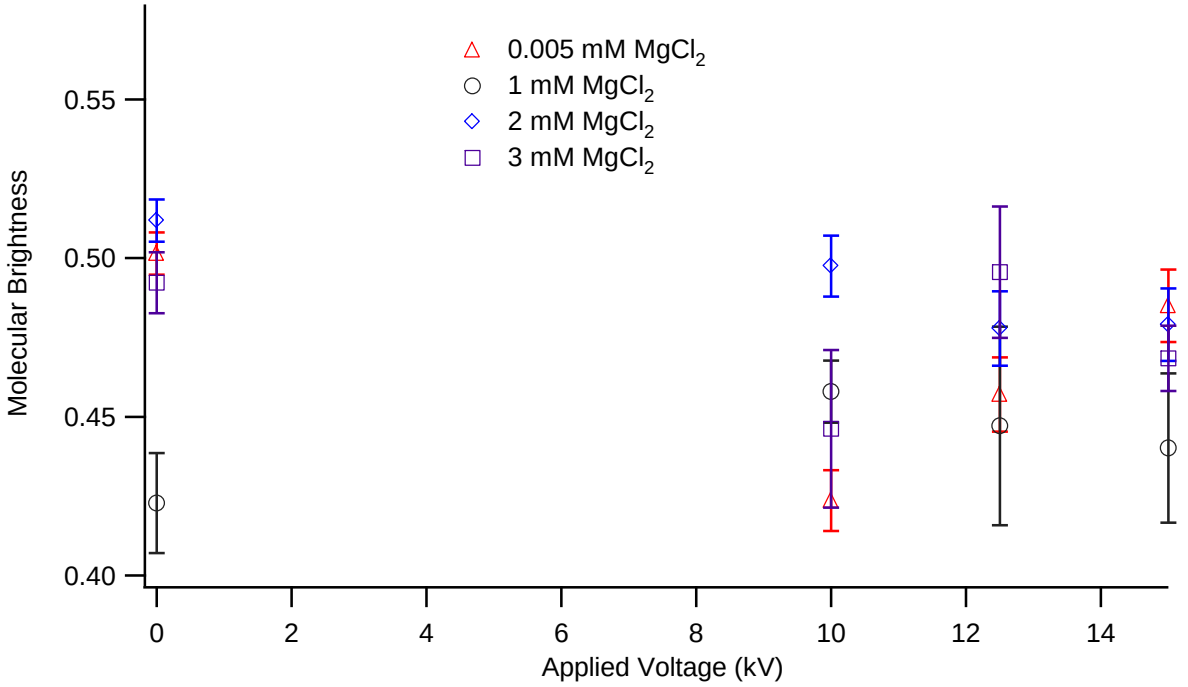

Figure 6.4: Results of the PCH analysis for four different Magnesium Chloride concentrations, 0.005, 1, 2 and 3 mM and four different electric fields, 0, 10, 12.5 and 15 kV. The symbols correspond to the different salt concentrations; triangle (0.005 mM), circle (1 mM), diamond (2mM), square (3mM). The molecular brightness, with error bars, is plotted as a function of the applied electric field.

proportional to the change in the molecular brightness of the dye. Based on this assumption, the average molecular brightness value for the four different $MgCl_2$ concentrations analyzed at 0 kV and 15 kV were calculated. It is assumed that at 0 kV the temperature of the capillary is that of room temperature. At 15 kV, which was the maximum applied voltage, it is assumed that the capillary experiences the greatest effect of Joule heating, as described by equation 6.8. Thus, the difference of these two average values gives the maximum change in the molecular brightness, as defined by the equation:

$$\Delta\varepsilon = \left|\varepsilon_{avg(15kV)} - \varepsilon_{avg(0kV)}\right| \tag{6.11}$$

where, $\varepsilon_{avg(15kV)}$ is the average molecular brightness value for the four $MgCl_2$ concentrations with an applied voltage of 15 kV and $\varepsilon_{avg(0kV)}$ is the average molecular brightness value of the four $MgCl_2$ concentrations with no voltage applied across the capillary. From here, the percentage change in the average molecular brightness, %Δε, at these two voltages is determined using the equation:

$$\%\Delta\varepsilon = \frac{\left|\varepsilon_{avg(15kV)} - \varepsilon_{avg(0kV)}\right|}{\varepsilon_{avg(0kV)}} * 100 \tag{3.12}$$

solving for equation 6.12 yields a seven percent change between the two voltages. If we assume that the change in the molecular brightness is proportional to the change in the temperature, the following equation can be used to determine the temperature change inside the capillary:

$$\Delta T = T_{(0kV)} * \frac{\left|\varepsilon_{avg(15kV)} - \varepsilon_{avg(0kV)}\right|}{\varepsilon_{avg(0kV)}} \tag{6.13}$$

where ,$T_{(0\ kV)}$ is the temperature inside the capillary with zero applied voltage. Solving for equation 6.13 gives a value of 1.4 ± 0.1 °C. With this information, the maximum temperature inside the capillary can be calculated using the equation:

$$T_{\max} = T_{(0kV)} + \Delta T \tag{6.14}$$

where, T_{max} is the maximum temperature inside the capillary. Solving for equation 6.14 gives a maximum temperature ≈ 21.4 ± 0.6 °C.

The results suggest that Joule heating has not played a significant role in the analysis of the diffusion properties of the ssDNA in various salt environments and different applied voltages. The lack of a significant change in the molecular brightness of the fluorophore and the minimal change in temperature calculated above support this conclusion. One plausible explanation for the lack of Joule heating playing a significant role in this experimental setup was the environment that surrounded the capillary. Recall the experimental setup, which has the capillary was mounted to a glass slide, which is in contact with a metal stage. On the other side, immersion oil was in contact with the capillary and the oil was in contact with a metal objective. The objective was connected to a metal stand, which is mounted to a metal laser table. This configuration provides ample opportunities for any heat generated to be quickly dissipated out for the capillary to an extent that it did not significantly impact the temperature of the sample inside the capillary.

6.4 Conclusion

The work presented here shows one of many application of PCH analysis in the realm of FCS experiments. Not only can it be used to determine the molecular brightness of one species, as shown here, or multiple species, as discussed previously, it can be applied to the field of capillary electrophoresis to better understand the affects of Joule heating. The advantages of this method are the chemical selectivity, due to the large dependence of the shape of the histogram ion the molecular brightness of the analyte molecules of interest and the relatively small sample requirements, on the order of ten nanomolar, as demonstrated here and elsewhere[2, 3, 6-10, 16].

1. Fogarty, K.; McPhee, J. T.; Scott, E.; Van Orden, A., Probing the Ionic Atmosphere of Single-Stranded DNA Using Continuous Flow Capillary Electrophoresis and Fluorescence Correlation Spectroscopy. *Analytical Chemistry* **2009,** 81, (1), 465-472.

2. Chen, Y.; Muller, J. D.; So, P. T. C.; Gratton, E., The Photon Counting Histogram in Fluorescence Fluctuation Spectroscopy. *Biophysical Journal* **1999,** 77, (1), 553-567.

3. Kask, P.; Palo, K.; Ullmann, D.; Gall, K., Fluorescence-Intensity Distribution Analysis and Its Application In Biomolecular Detection Technology. *Proceedings Of The National Academy Of Sciences Of The United States Of America* **1999,** 96, (24), 13756-13761.

4. Qian, H.; Elson, E. L., On the Analysis of High-Order Moments of Fluorescence Fluctuations. *Biophysical Journal* **1990,** 57, (2), 375-380.

5. Qian, H.; Elson, E. L., Distribution Of Molecular Aggregation By Analysis Of Fluctuation Moments. *Proceedings Of The National Academy Of Sciences Of The United States Of America* **1990,** 87, (14), 5479-5483.

6. Chen, Y.; Tekmen, M.; Hillesheim, L.; Skinner, J.; Wu, B.; Muller, J. D., Dual-Color Photon-Counting Histogram. *Biophysical Journal* **2005,** 88, (3), 2177-2192.

7. Kask, P.; Palo, K.; Fay, N.; Brand, L.; Mets, U.; Ullmann, D.; Jungmann, J.; Pschorr, J.; Gall, K., Two-Dimensional Fluorescence Intensity Distribution Analysis: Theory and Applications. *Biophysical Journal* **2000,** 78, (4), 1703-1713.

8. Palo, K.; Metz, U.; Jager, S.; Kask, P.; Gall, K., Fluorescence Intensity Multiple Distributions Analysis: Concurrent Determination of Diffusion Times and Molecular Brightness. *Biophysical Journal* **2000,** 79, (6), 2858-2866.

9. Palo, K.; Brand, L.; Eggeling, C.; Jager, S.; Kask, P.; Gall, K., Fluorescence Intensity and Lifetime Distribution Analysis: Toward Higher Accuracy in Fluorescence Fluctuation Spectroscopy. *Biophysical Journal* **2002,** 83, (2), 605-618.

10. Gall, K.; Palo, K.; Brand, L.; Eggeling, C.; Kask, P., Fluorescence Intensity and Lifetime Distribution Analysis: A New and Highly Sensitive Fluorescence Fluctuation Method. *Biophysical Journal* **2002,** 82, (1), 1728.

11. Guilbault, G. G., *Practical Fluorescence; Theory, Methods, and Techniques*. ed.; M. Dekker: New York, 1973.

12. Lakowicz, J. R., *Principles of Fluorescence Spectroscopy*. ed.; Kluwer Academic/Plenum: New York, 1999.

13. Landers, J. P., *Handbook of Capillary Electrophoresis*. 2nd ed.; CRC Press: Boca Raton, 1997.

14. Van Orden, A.; Fogarty, K.; Jung, J., Fluorescence Fluctuation Spectroscopy: A Coming of Age Story. *Applied Spectroscopy* **2004,** 58, (5), 122A-137A.

15. Belder, D.; Deege, A.; Husmann, H.; Kohler, F.; Ludwig, M., Cross-Linked Poly(Vinyl Alcohol) As Permanent Hydrophilic Column Coating For Capillary Electrophoresis. *Electrophoresis* **2001,** 22, (17), 3813-3818.

16. Perroud, T. D.; Huang, B.; Zare, R. N., Effect of Bin Time On the Photon Counting Histogram For One-Photon Excitation. *Chemphyschem* **2005,** 6, (5), 905-912.

Chapter 7: Conclusion and Future Work

This dissertation has illustrated the effectiveness of steady-state and time-resolved fluorescence spectroscopy and fluorescence correlation spectroscopy to extract meaningful information from a variety of systems. The work described has applied these types of fluorescence spectroscopy to multiple systems; fluorescently labeled single-stranded DNA, Cy3 labeled AOT reverse micelles, R6G labeled AOT reverse micelles and Cy3-Cy5 inside AOT reverse micelles. Moreover, the use of fluorescence spectroscopy has allowed for a better understanding of dynamic processes and associated kinetics of the Cy3 labeled reverse micelles.

In Chapter 3, steady-state and time resolved spectroscopy were used to probe the effects of confinement on the dye Cyanine-3 (Cy3). These measurements revealed a highly unexpected result in the smallest reverse micelle, w_0=1. Here, it was observed that the Cy3 was forming H-aggregates (or H-dimers) and concentrations so dilute, nM, as to preclude aggregation in bulk water. The steady-state spectroscopy showed dramatic changes in both the absorption and emission properties of the dye confined within the w_0=1consistent with the formation of H-aggregates. Furthermore, the time-resolved fluorescence lifetime experiment showed a significant change in the fluorescence lifetime of the aggregate compared to the monomer, which is also consistent with the formation of H-aggregates. Recall that the fluorescence emission properties and the fluorescence lifetime of Cy3 within w_0=1 reverse micelles was dependent on the excitation wavelength. Thus, it was concluded that both the aggregate form and the monomer form of the dye are present within these samples. This result was extremely unexpected as the occupation number of Cy3 in the w_0=1 ranged from one Cy3 molecule per 20,000 to 900,000 reverse micelles. However, it was concluded that the diffusion limited

reaction has a rate that implies a timescale of reverse micelle collisions to be on the order of milliseconds, thereby making the formation of the H-aggregate possible.

It was also observed that the Cy3 dye did not show the presence of the aggregate for the larger reverse micelles but rather showed that the dye was present as monomers and behaved more or less as if it were being solvated by the water molecules within the larger reverse micelles. There was some evidence of aggregation in the w_0=1 reverse micelles, where slight changes in the spectroscopy started to appear, thus indicating this may be a point where the formation of aggregates becomes possible. Lastly, the unique behavior of Cy3 in the extremely confined environment of the w_0=1reverse micelles provided the opportunity to actively probe the dynamics of the Cy3 labeled reverse micelles using fluorescence correlation spectroscopy, as discussed in Chapter 4.

The FCS measurements revealed a very interesting and dynamic Cy3 labeled reverse micelle system. The measurements showed that larger Cy3 labeled reverse micelles, w_0=2-30, behaved as expected. The diffusion properties were consistent with dynamic light scattering measurements and theoretical values. In other words, as w_0 decreased the diffusion coefficient increased (decreased diffusion time). However, anomalous diffusion behavior was observed in the Cy3 labeled reverse micelles measured by FCS. Recall that the autocorrelation function showed a longer diffusion component for w_0=1 reverse micelles compared to the w_0=1 reverse micelles. However, the dynamic light scattering measurements revealed a diffusion coefficient consistent with w_0=1 reverse micelles. In other words, the bulk diffusion properties of the w_0=1 reverse micelles are consistent with what is expected but differ from the small sub-population of reverse micelles that are labeled with a Cy3 molecule(s).

The FCS measurements revealed the anomalous diffusion at 514 nm excitation as well as two other dynamic processes, one occurring on ≈ 1 μs timescale and the other occurring on ≈ 13 μs timescale. A series of experiments were carried out to try and identify the process occurring at approximately 1 μs. Recall the experiments that were discussed in Chapter 5, in which dual-color cross-correlation data was obtained to determine if this fluctuation resulted from the association/dissociation of the Cy3 dimer. Also, recall the experiment in which the laser power was varied to determine if this fluctuation resulted from triplet blinking. Both of these hypotheses were eliminated based on the results of these two experiments. Moreover, the rotational diffusion of the transient dimer was calculated and determined to be too fast to be responsible for this observed fluctuation. It was concluded that this intensity fluctuation was due to the dimer undergoing a conformational fluctuation but to date the exact cause is unknown.

The intensity fluctuation occurring on the 10-20 μs timescale was identified as the transient dimer complex undergoing a fluctuation between the fused dimer and the encounter pair and is consistent with that inferred by Fletcher and co-workers. The result is important as it represents the first direct observation of the transient micelle dimer. Moreover, it provides direct evidence that reverse micelles are a dynamic system and have the ability to exchange their contents as has been previously inferred. The unique spectroscopic properties of the Cy3 aggregate allowed this investigation to take place.

The Cy3 labeled reverse micelle results are interesting in that the behavior is highly unexpected. It would be interesting to investigate the spectroscopy of different dyes within reverse micelles to see if the confined environment of the reverse micelles alters these properties. Preliminary work done in our group has shown evidence for the formation Rhodamine 6G

aggregates in the smaller reverse micelles based on observed changes in the absorption properties of the dye confined within.

The observation of the transient dimer structure revealed the timescale of this process was independent of the overall Cy3 concentration. However, Fletcher and co-workers inferred that the rate of exchange between two reverse micelles was dependent on the non-polar solvent used. It was suggested that longer chain hydrocarbons resulted in an increase in the rate of exchange. Thus, it would be interesting to perform FCS experiments in which the non-polar solvent used to make the reverse micelles was altered. Recall the kinetic analysis in Chapter 5 which showed that the rate of exchange was dependent on the rate of fusion and the equilibrium governing the diffusion controlled reaction of two individual reverse micelles. Thus, if the exchange rate changes as a function of the length of the non-polar solvent, one would expect to see a change in the time constant governing the fusion reaction, which was defined in Chapter 5 as τ_{rxn2}.

The R6G labeled reverse micelle systems showed interesting results throughout the preliminary experiments described in Chapter 5. The steady-state absorption data showed the growth a blue shifted peak relative the main peak in the absorption spectrum consistent with the formation of H-aggregates within the smallest reverse micelle system. This system provides another opportunity to probe the dynamics of the reverse micelles as well as the effects of molecular scale confinement. Since R6G is readily available, the experiments are very feasible and could be carried out in the manner presented in this work. The same experiments performed on the Cy3 labeled reverse micelle system could be carried out to create a global picture as to what may be occurring within the system. Moreover, the fact that R6G is readily available provides the opportunity to utilize UV-Vis spectroscopy to obtain quantitative information such

as the equilibrium constant governing the system. Recall that the Cy3 labeled reverse micelles required a few assumptions to obtain information about the equilibrium constant governing the dimerization reaction within the reverse micelle system. Thus, the R6G labeled reverse micelles provide an opportunity to confirm, or deny, those assumptions and resulting values.

The preliminary FRET experiments showed interesting results which indicate that FRET is occurring between Cy3 and Cy5 in the w_0=2 reverse micelles. The steady-state fluorescence showed the appearance of a peak at about 650 nm, consistent with the maximum emission of Cy5. Furthermore, this peak was not observed in the w_0=3 sample and thus is likely not due to direct excitation of the Cy5 molecules within the system. Moreover, the unnormalized fluoresce emission showed a dramatic decrease in the overall fluorescence in the w_0=2 sample. This is also consistent with FRET occurring, as the energy of the Cy3 molecules after excitation is transferred nonradiatively to the Cy5 molecules. The fluorescence lifetime decays for the w_0=2 and w_0=3 samples showed that the fluorescence lifetime of Cy3 was qualitatively shorter in the w_0=2 sample than that observed in the larger, w_0=3, sample, consistent with FRET. One experiment that could provide more insight into whether FRET is in fact occurring is two-color fluorescence cross-correlation spectroscopy. The experiment could be setup such that one detector is monitoring the emission wavelengths corresponding to the Cy3 molecules and the other detector is monitoring the emission wavelengths of the Cy5 molecules. For the reverse micelles where FRET is thought to be occurring, i.e. w_0=2, the experiments should show considerable cross-correlation between the two emission wavelengths. In contrast, the larger reverse micelles should show very little correlation as at this point in time it is believed that FRET is not occurring within these samples. This could provide interesting insight into the

nature of the different systems. Moreover, information about the timescales of different process occurring within the system could be determined.

Chapter 6 described how fluorescence correlation spectroscopy coupled with capillary electrophoresis, photon counting histogram (PCH) analysis and steady-state fluorescence spectroscopy were used to better understand the nature of Joule heating within a capillary electrophoresis experiment. The steady-state fluorescence showed that the fluorescence intensity of the fluorescent label decreased with increasing temperature. With this information, the changes in the fluorescence intensity were monitored by measuring PCH of the fluorescently labeled single-stranded DNA. The PCH experiments provided an opportunity to monitor any changes in the fluorescence intensity as a function of both $MgCl_2$ concentration, ranging from 0 mM to 3mM, and the applied voltage, which ranged from 0 kV to 15 kV. Moreover, the use of the photon counting histogram allowed this information to be determined using the same experimental setup that was used to take other measurements on these samples. Recall that the diffusion properties of the DNA are sensitive to the local temperature and thus an increase in temperature due to an increase in the applied voltage could potentially skew the results in one direction. The PCH measurements and subsequent analysis reveal no systematic variation in the molecular brightness as a function of increasing $MgCl_2$ concentration or applied voltage. These experiments provided a unique opportunity to measure any changes to the fluorescent label throughout the course of the experiment. Thus, PCH has the ability to be applied to a variety of systems, such as resolving multi component systems or determining the effect of Joule heating inside a capillary.

The work as a whole has demonstrated the effectiveness of steady-state and time-resolved fluorescence spectroscopy to study different processes including the dynamics of reverse

micelles, the role of confinement on water soluble organic dyes , the occurrence of FRET within the reverse micelle environment and the role of Joule heating in capillary electrophoresis. The work presented here has laid a solid foundation for further experiments regarding water soluble dyes as well as other materials of interest within the reverse micelle environment as it has demonstrated the interesting, unexpected behavior that occurs when such materials are confined on the molecular level.